Studies on the food compounds showing anti-obesity effect and their mechanism to suppress obesity

Kana Ohyama

2016

Contents

INTRODUCTION

Recently, obesity is rapidly becoming a major global health problem (1) and is a major risk factor for several common diseases, including type 2 diabetes, cardiovascular diseases and cancer (2). Obesity develops when the energy intake chronically exceeds the total energy expenditure (3). Currently all the available anti-obesity medications act by limiting energy intake through suppression of appetite or inhibiting intestinal lipid absorption; however, chronic use of such medications is often associated with adverse effects, such as depression and steatorrhoea (4). Over the past few years, a growing body of evidence from studies on rodent models and adult humans indicate that activating thermogenesis in brown adipose tissue (BAT) is a plausible alternative approach to modulate whole body energy balance (5).

BAT is specialized to dissipate energy through uncoupling protein 1 (UCP1). Recent studies with ^{18}fluoro-labelled 2-deoxy-glucose positron emission tomography (^{18}FDG-PET) scanning demonstrated that adult humans have active BAT deposits (6-9) and that the amount of BAT inversely correlates with adiposity and body mass index (7, 8), indicating that it plays an important role in energy homeostasis in adult humans. Hence, a better understanding of the molecular control of BAT development may lead to an alternative approach to alter energy balance by increasing energy expenditure.

In this study, we demonstrated that EHMT1 was a key enzymatic component that controls the lineage specification and thermogenic function of BAT. Additionally, we focused on food components as daily supplements to suppress obesity. Hence, we evaluated the anti-obese effect of two food components, capsinoids and OmniVin. Capsinoids (CSNs) are capsaicin analogs found in a non-pungent type of chili pepper,

'CH-19 Sweet' (10, 11). CSNs differ from capsaicin in chemical structure only at the center linkage of an ester bond, resulting in reduced (<0.1%) pungency while maintaining the metabolic effect, which facilitates daily intake. OmniVin is a catechin rich grape seed extract (CGSE) manufactured using specially selected materials. In the preliminary analysis, CGSE was shown to be a 98% purified polyphenol product and was found to contain high concentrations of monomeric proanthocyanidins. We investigated their effect and mechanism by using diet induced obesity model mice.

REFERENCES

1. Batsis JA, Nieto-Martinez RE,Lopez-Jimenez F: Metabolic syndrome: from global epidemiology to individualized medicine. Clin Pharmacol Ther 82(5):509-524, 2007

2. Matsuzawa Y: The metabolic syndrome and adipocytokines. FEBS Lett 580(12):2917-2921, 2006

3. Spiegelman BM,Flier JS: Obesity and the regulation of energy balance. Cell 104(4):531-543, 2001

4. Cheung BM, Cheung TT,Samaranayake NR: Safety of antiobesity drugs. Therapeutic advances in drug safety 4(4):171-181, 2013

5. Kajimura S,Saito M: A new era in brown adipose tissue biology: molecular control of brown fat development and energy homeostasis. Annual review of physiology 76:225-249, 2014

6. Nedergaard J, Bengtsson T,Cannon B: Unexpected evidence for active brown adipose tissue in adult humans. Am J Physiol Endocrinol Metab 293(2):E444-452, 2007

7. Saito M, Okamatsu-Ogura Y, Matsushita M, Watanabe K, Yoneshiro T, Nio-Kobayashi J, Iwanaga T, Miyagawa M, Kameya T, Nakada K, Kawai Y,Tsujisaki M: High incidence of metabolically active brown adipose tissue in healthy adult humans: effects of cold exposure and adiposity. Diabetes 58(7):1526-1531, 2009

8. van Marken Lichtenbelt WD, Vanhommerig JW, Smulders NM, Drossaerts JM, Kemerink GJ, Bouvy ND, Schrauwen P,Teule GJ: Cold-activated brown adipose tissue in healthy men. N Engl J Med 360(15):1500-1508, 2009

9. Virtanen KA, Lidell ME, Orava J, Heglind M, Westergren R, Niemi T, Taittonen M, Laine J, Savisto NJ, Enerback S,Nuutila P: Functional brown adipose tissue in healthy adults. N Engl J Med 360(15):1518-1525, 2009

10. Kobata K, Sutoh K, Todo T, Yazawa S, Iwai K,Watanabe T: Nordihydrocapsiate, a new capsinoid from the fruits of a nonpungent pepper, capsicum annuum. J Nat Prod 62(2):335-336, 1999

11. Kobata K TT, Yazawa S, Iwai K, Watanabe T: Novel Capsaicinoid-like Substances, Capsiate and Dihydrocapsiate, from the Fruits of a Nonpungent Cultivar, CH-19 Sweet, of Pepper (Capsicum annuum L.). . J. Agric. Food Chem. 46:1695-1697., 1998

CHAPTER. I

EHMT1 controls brown adipose cell fate and thermogenesis through the PRDM16 complex

Chapter. I

EHMT1 controls brown adipose cell fate and thermogenesis through the PRDM16 complex

Obesity develops when energy intake chronically exceeds total energy expenditure. All anti-obesity medications currently approved by the FDA act to repress energy intake, either by suppressing appetite or by inhibiting intestinal fat absorption. However, because of their side effects including depression, oily bowel movements and steatorrhoea, there is an urgent need for alternative approaches. BAT is specialized to dissipate energy through uncoupling protein 1 (UCP1). Recent studies with ^{18}fluoro-labelled 2-deoxy-glucose positron emission tomography (^{18}FDG-PET) scanning demonstrated that adult humans have active BAT deposits (1-4) and that the amount of BAT inversely correlates with adiposity and body mass index (2, 3), indicating that it plays an important role in energy homeostasis in adult humans. Hence, a better understanding of the molecular control of BAT development may lead to an alternative approach to alter energy balance by increasing energy expenditure.

It has been reported that brown adipocytes in the interscapular and peri-renal BAT arise from Engrailed-1^{+} and Myf5^{+} dermotomal precursors (5-7). The PRDM16–C/EBP-β complex in the myogenic precursors activates the brown adipogenic gene program through inducing peroxisome proliferator-activated receptor (PPAR)-γ expression (6, 8, 9); however, the mechanism by which the PRDM16–C/EBP-β complex functions as a fate switch to control brown adipocyte versus myocyte lineage remains unexplored.

Previously we determined the essential domains of PRDM16 for converting

myoblasts into brown adipocytes by generating two deletion mutants of PRDM16: a mutant lacking the PR-domain (DPR), a domain that shares high homology with methyltransferase SET domains (10, 11), and a mutant lacking the zinc-finger domain-1 (DZF-1) (**Fig. 1a, top panel**). Wild type (WT) and the DPR mutant, but not the DZF-1 mutant, were able to convert myoblasts into brown adipocytes, suggesting that the ZF-1 domain is required (8). Consistent with the results, the PRDM16 complex purified from brown adipocytes expressing WT and DPR, but not DZF-1, had significant methyltransferase activities on H3 (**Fig. 1a, bottom panel**). Because this effect was independent of its SET domain, we searched for methyltransferases that were associated with differentiation-competent PRDM16 proteins (that is, WT and DPR), but not with differentiation-incompetentPRDM16 (DZF-1). By using high-resolution liquid chromatography coupled with tandem mass spectrometry (LC–MS/MS), we found EHMT1 as the only methyltransferase that was co-purified preferentially with the differentiation-competent PRDM16 complexes (8). EHMT1 has enzymatic activity on H3K9 mono- or di-Me (12). Notably, haploinsufficiency of the EHMT1 gene, because of 9q34.3 microdeletions or point mutations in humans (13), is associated with clinical phenotypes including mental retardation. Importantly, 40–50% of patients with EHMT1 mutations develop obesity (14, 15); however, the underlying mechanism remains completely unknown. Given the essential role of the PRDM16 complex for BAT development, we considered that EHMT1 is a key enzymatic component that controls the lineage specification and thermogenic function of BAT.

To test this hypothesis, we first confirmed the PRDM16-EHMT1 interaction by immunoprecipitation followed by western blotting in brown adipocytes (**Fig. 1b and Supplementary Fig. 1**). The purified ZF-1 (224–454) and ZF-2 (881–1038) domains of

glutathione S-transferase (GST)-PRDM16 protein bound to the in-vitro-translated EHMT1 protein, whereas the 680-1038 region of PRDM16 bound to CtBP1 as previously reported (16) (**Fig. 1c and Supplementary Fig. 2**). These results indicate that EHMT1 directly interacts with PRDM16. EHMT1 is the main methyltransferase of the PRDM16 complex in brown adipocytes, because the histone methyltransferase activity of the PRDM16 complex was largely lost when EHMT1 was depleted using two short hairpin RNAs (shRNAs) targeted to EHMT1 (**Fig. 1d and Supplementary Fig. 3**). Furthermore, expression of EHMT1 protein was highly enriched in BAT and in cultured brown adipocytes, correlating wellwithPRDM16 (**Fig. 1e and Supplementary Fig. 4**). In contrast, amounts of EHMT2 protein were higher in white adipose tissue (WAT) than in BAT. To test if EHMT1 modulates the PRDM16 transcriptional activity, we performed luciferase assays using a luciferase reporter gene containing PPAR-γ binding sites (17). As shown in **Fig. 1f**, co-expression of EHMT1 and PRDM16 synergistically increased the reporter gene activity, whereas this induction was completely lost when the DZF-1 mutant was expressed. These data indicate that EHMT1 forms a transcriptional complex with PRDM16 and regulates its activity through direct interaction.

Next, we investigated the genetic requirement for EHMT1 in BAT development in vivo. Because a whole-body knockout of the Ehmt1 gene causes embryonic lethality before the emergence of brown adipocytes (12), the *Ehmt1* gene was deleted in brown adipocyte precursors by crossing *Ehmt1*$^{flox/flox}$ mice (18) with *Myf5-Cre* mice (17). As shown in **Fig. 2a–c**, the interscapular BAT of Ehmt1^{myf5} knockout mice was substantially smaller than in WT mice at postnatal stage (P)1. Haematoxylin and eosin staining showed that brown adipocytes in Ehmt1^{myf5} knockout mice were significantly smaller and contained fewer lipids than in WT mice, whereas other tissues near the BAT including

skin seemed normal (**Fig. 2b and Supplementary Fig. 5**). Similar results were observed in embryos at embryonic day (E)18.5 (**Supplementary Fig. 6**). Subsequently, we analysed the global gene expression of BAT from the WT and *Ehmt1*^{myf5} knockout embryos by RNA-sequencing. The following gene ontology analysis found that the gene expression pattern in the *Ehmt1*^{myf5} knockout BAT showed a skeletal-muscle phenotype: that is, a broad activation of the skeletal muscle-selective genes, and a broad reduction of the BAT-selective genes. Strikingly, 78.7% of the differentially expressed genes (118 out of 150 genes) between WT and knockout mice were stratified into categories of skeletal muscle development, BAT development and BAT function (glucose/fatty-acid metabolism). Specifically, 77.5% of the ectopically activated genes in the knockout BAT were related to skeletal muscle development, including myogenin and myosin heavy chains. On the other hand, 80.0% of the reduced genes in the knockout BAT were involved in BAT development and fatty-acid/glucose metabolism, including *Ucp1*, *Pgc1α*, *Cebpb*, *Cpt1a* and *Elovl3* (**Fig. 2d and Supplementary Fig. 7**). These results indicate that EHMT1 is absolutely required for the cell-fate specification between BAT versus muscle.

To investigate the mechanisms by which EHMT1 determines BAT lineage, retroviruses expressing a scrambled controlRNA(scr) or shRNAs targeting EHMT1 (shEHMT1-1 and -2) were transduced into C2C12 myoblasts together with PRDM16 (**Supplementary Fig. 8a**). As shown in **Fig. 2e (upper panels)**, PRDM16 expression powerfully blocked myogenic differentiation in a dose-dependent fashion, as shown by immunohistochemistry using a pan-skeletal myosin heavy chain (MHC) antibody. In contrast, EHMT1 depletion significantly impaired the PRDM16-mediated repression on myogenesis (**Fig. 2e, lower panels**). Gene expression analysis showed that the repression on muscle-selective genes such as myogenin was near completely abolished when

EHMT1 was depleted (**Fig. 2f and Supplementary Fig. 8b**). This repressive effect was mediated through the methyltransferase activity of EHMT1, because ectopic expression of the EHMT1 mutant (N1198L; H1199E) that lacks methyltransferase activity (19) significantly blunted the PRDM16-mediated repression on myogenesis (**Supplementary Fig. 9a**). Additionally, two chemical inhibitors of EHMT1/2, BIX-01294 and UNC0638, blocked the repressive effects of PRDM16 (**Supplementary Fig. 9b, c**). BIX-01294 treatment in brown adipocytes also significantly reduced the expression of BAT-selective genes (**Supplementary Fig. 9d**). Consistent with these data, chromatin immunoprecipitation assays found that EHMT1 depletion robustly reduced amounts of H3K9me2 and me3 at the proximal region of the myogenin gene promoter on which EHMT1 was recruited (**Fig. 2g**). On the contrary, the amounts of H3K9/14ac were significantly increased by EHMT1 depletion without any effect on total H3 amounts. Similar changes were observed at the promoter regions of other muscle-selective genes including Acts, Ryr1 and Mylpf1, where EHMT1 was recruited (**Supplementary Fig. 10**). Conversely, under pro-adipogenic culture conditions, knockdown of EHMT1 largely blocked the PRDM16-induced brown adipogenesis in C2C12 cells (**Supplementary Fig. 11**). Together, these results indicate that EHMT1 determines BAT versus muscle cell lineage through PRDM16 by controlling H3K9methylation status of the muscle-selective gene promoters. To investigate the role of EHMT1 in BAT thermogenesis, EHMT1 was depleted in immortalized brown adipocytes by retrovirus-mediated shRNA knockdown (**Supplementary Fig. 12a, b**). Total and uncoupled (oligomycin-insensitive) oxygen consumption rate in the EHMT1-depleted brown adipocytes was significantly reduced both at the basal and cyclicAMP (cAMP)-stimulated states (**Fig. 3a**). Conversely, EHMT1 overexpression significantly increased messengerRNA (mRNA) amounts of BAT-

selective thermogenic genes, including *Ucp1*, *Pgc1α* and *Dio2* (**Fig. 3b**), and oxygen consumption rate (**Supplementary Fig. 12c**). To test further if this EHMT1 action requires PRDM16, EHMT1 was ectopically introduced into mouse embryonic fibroblasts that did not express endogenous PRDM16. As shown in **Fig. 3c**, mouse embryonic fibroblasts expressing PRDM16 and C/EBP-β uniformly differentiated into lipid-containing adipocytes as previously reported2. Although EHMT1 alone did not stimulate brown adipogenesis, the combination of EHMT1 with PRDM16 and C/EBP-β synergistically increased mRNA amounts of the BAT-selective genes, including *Ucp1*, *Cidea*, *Cox7a* and *Cox8b* (**Fig. 3d**). These data indicate that EHMT1 positively regulates the BAT-selective thermogenic gene program through PRDM16.

To determine which domains of EHMT1 are required for the induction of PRDM16 transcriptional activity, we tested a series of EHMT1 mutants for their ability to interact and co-localize with PRDM16 (**Supplementary Figs 13 and 14**). A deletion mutant of EHMT1 (772–1009), which failed to interact with PRDM16, was unable to increase PRDM16 reporter gene activity (**Fig. 3e**). EHMT1 with mutations in the SET domain (N1198L; H1199E) had no methyltransferase activity, but was still able to bind to and activate PRDM16. Even a mutant that lacked the SET-domain altogether (1–1009) interacted with and activated PRDM16. Thus an interaction between EHMT1 and PRDM16 seems to be required to activate PRDM16 transcriptional activity. Notably, expression of EHMT1 robustly increased the amount of PRDM16 protein, independently of its mRNA expression (**Fig. 3f and Supplementary Fig. 15**). This effect was due to changes in the rate of protein degradation, because cycloheximide chase experiments showed that expression of EHMT1 extended the half-life of PRDM16 protein from 8.5 to 16.5 h. The N1198L; H1199E mutant also extended the half-life of PRDM16 protein as

potently as the WT form (**Fig. 3g**). PRDM16 protein accumulation was induced only by the EHMT1 mutants that bind to PRDM16 (**Supplementary Fig. 16**). EHMT1 regulates endogenous PRDM16 protein amounts *in vivo* (**Extended Data 1**). EHMT1 protein stability was not affected by PRDM16 (**Supplementary Fig. 17**). These results collectively suggest that EHMT1 has dual functions: that is, repressive effects on the muscle-selective gene program through its methyltransferase activity, and activation of the BAT-selective gene program through stabilization of PRDM16 protein through direct association.

Next, we examined the requirement for EHMT1 in adaptive thermogenesis *in vivo*. To exclude potential defects in the skeletal muscle of *Ehmt1*^{myf5} knockout mice, we generated adipose tissue-specific *Ehmt1* knockout mice (*Ehmt1*^{adipo} knockout) using *Adiponectin-Cre* mice (20). Of note, 62.3% of the differentially expressed muscle/BAT-selective genes in the *Ehmt1*^{myf5} mice were similarly dysregulated in the *Ehmt1*^{adipo} knockout mice (**Extended Data 2**). Although *Adiponectin-Cre* is expressed both in BAT and WAT, expression of EHMT1 is highly enriched in BAT compared with WAT (**Fig. 1e**). Furthermore, lipolysis capacity in the WAT of *Ehmt1*^{adipo} knockout mice was indistinguishable from WT mice (**Supplementary Fig. 18**). EHMT1 is required for beige/brite cell development (**Extended Data 3**). Hence, the *Ehmt1*^{adipo} knockout mice allow us to examine the role of EHMT1 in BAT/beige fat mediated thermogenesis *in vivo*. As shown in **Fig. 3h**, rectal temperature of *Ehmt1*^{adipo} knockout mice strikingly dropped within 1 h after a cold challenge to 4 ^{o}C, whereas that of control mice remained constant. Expression of BAT-selective genes in skeletal muscle (21) was not altered in Ehmt1^{adipo} knockout mice (**Supplementary Fig. 19**). We subsequently measured oxygen consumption rate at thermoneutrality (29–30 ^{o}C) (22) in response to an activation of the

β3-adrenoceptor pathway. As shown in **Fig. 4a**, the oxygen consumption rate of WT mice was significantly increased after administering CL316,243 whereas this induction was completely lost in knockout mice. The impaired thermogenesis in knockout mice was accompanied by higher serum amounts of free fatty acids (FFAs) (**Fig. 4b**). This is consistent with previous findings that BAT serves as a major sink of FFAs for heat generation (23), and that reduced fatty-acid oxidation in BAT leads to an increase in amounts of serum FFA (24). Indeed, fatty-acid oxidation capacity in the knockout BAT was significantly lower than in WT mice at the basal state and after administering CL316,243 (**Fig. 4c**). Additionally, fatty acid uptake in the knockout BAT was reduced (**Supplementary Fig. 20**). These results indicate that EHMT1 is absolutely required for BAT mediated adaptive thermogenesis and fatty-acid metabolism *in vivo*.

Lastly, we tested whether EHMT1 deficiency in BAT affects the propensity for weight gain in response to an obesogenic diet at thermoneutrality (29–30 ^{o}C), because an obesity phenotype in *Ucp1* knockout mice was observed only at thermoneutrality (25). As shown in **Fig. 4d** and **Supplementary Fig. 21**, *Ehmt1*^{adipo} knockout mice gained significantly more body mass than WT mice without any change in food intake (**Supplementary Table 1**). Knockout mice had higher amounts of epididymal WAT and interscapular BAT that contained substantially larger lipid droplets than WT mice (**Fig. 4e, f**). A glucose tolerance test found that knockout mice showed significantly higher blood glucose concentrations than WT mice (**Fig. 4g**). Similarly, knockout mice showed impaired responses to insulin during an insulin tolerance test (**Fig. 4h**) and higher amounts of serum insulin at the fasted and glucose-stimulated states (**Fig. 4i**). Knockout mice showed an insulin-resistance phenotype even at ambient temperature, whereas no statistically significant difference was observed in body mass (**Supplementary Fig. 22**).

Notably, the liver from knockout mice contained higher amounts of lipids and triglyceride (**Fig. 4j, k**) and showed impaired insulin signalling as assessed by phosphorylation of Akt in response to insulin (**Fig. 4l and Supplementary Fig. 23**). Together, these results indicate that EHMT1 deficiency in BAT leads to obesity, systemic insulin resistance and hepatic steatosis under a high-fat diet.

In conclusion, we have identified EHMT1 as an essential BAT-enriched methyltransferase that controls brown adipose cell fate, adaptive thermogenesis and glucose homeostasis *in vivo*. Although presence of BAT in adult humans is now widely appreciated, no mutation that causes defects in human BAT development and thermogenesis had been described except polymorphisms in UCP1 and β3-adrenoceptor genes (26). Delineating the causal link between EHMT1 mutations and BAT thermogenesis will provide a new perspective in understanding the molecular control of energy homeostasis through the epigenetic pathways, which may lead to effective therapeutic interventions for obesity and metabolic diseases.

METHODS

Animals.

All animal experimentswereperformed according to procedures approved by University of California, San Francisco's Institutional Animal Care and Use Committee for animal care and handling. *Ehmt1*^{flox} mice and *Adiponectin*$^{Cre/+}$ mice were provided by A. Tarakhovsky and E. D. Rosen. *Myf5*$^{Cre/+}$ mice were obtained from the Jackson Laboratory (27). To analyse embryonic BAT development, *Ehmt1*$^{flox/flox}$ or *Myf5-Cre*$^{+/-}$*;Ehmt1*$^{flox/flox}$ embryos at E18.5 or newborn mice at P1 were collected and fixed in 4%

paraformaldehyde for histological analyses. The presumptive BAT depots in the interscapular region were micro-dissected for histological and RNA expression analyses. For cold exposure experiments, male *Ehmt1*^{adipo} knockout mice (*Adipo-Cre*$^{+/-}$*;Ehmt1*$^{flox/flox}$) and body-weight-matched control mice (*Ehmt1*$^{flox/flox}$) at 10 weeks of age were single-caged and exposed to 4 ^{o}C for 5 h. Rectal temperatures were monitored every hour using a TH-5 thermometer (Physitemp).

Metabolic studies.

Whole-body energy expenditure of *Ehmt1*^{adipo} knockout mice or control mice matched for body mass at 14 weeks of age was measured at thermoneutrality (29-30 ^{o}C) using a Comprehensive Lab Animal Monitoring System (Columbus Instruments). The mice were injected intraperitoneally with a β3-adrenergic receptor-specific agonist CL316,243 at a dose of 0.5 mg kg^{-1}. For diet-induced obesity studies, male mice at 6-7 weeks of age were fed a high-fat diet (D12492, Research Diet) for 4 weeks at thermoneutrality. At the end of the experiments, serum samples were collected. Amounts of serum insulin (Millipore), triglyceride (Thermo) and FFA (Wako) were measured using commercially available kits. For glucose tolerance test experiments, male mice were fed a high-fat diet for 9 weeks. After an overnight fast, the mice were injected intraperitoneally with glucose (1 g kg^{-1}). For insulin tolerance test experiments, male mice under a high-fat diet for 10 weeks were used. After an overnight fast, the mice were injected intraperitoneally with insulin (0.75 U kg^{-1}). Blood samples were collected at indicated time points and amounts of glucose were measured using blood glucose test strips (Abbott). To measure liver triglyceride contents, the liver tissue (25mg) was homogenized in 1.25 ml of Folch solution (chloroform/methanol, 2:1, v/v). Subsequently, equal amounts (0.4 ml) of chloroform and

water were added to the lysate. After centrifugation at 735g for 3 min, the chloroform phase was collected and dried. The pellet was dissolved in isopropanol. Amounts of triglycerides were determined by an Infinity Triglycerides kit (Thermo).

Fatty-acid oxidation assay.

WT and Ehmt1adipo knockout mice at 11 weeks old were intraperitoneally injected with saline or CL316,243. Five hours after the injection, the interscapular BAT depots were isolated. Fatty-acid oxidation assay was performed according to the protocol described by Mao et al (28). Briefly, the adipose tissues were minced to small pieces and incubated with DMEM supplemented with 1mM pyruvate, 1% FFA-free BSA and 0.5mM oleate. [^{14}C]oleic acid at 1 μCi μl^{-1} was added for 2 h at 37 ^{o}C. After adding 70% perchloric acid into each well, CO_2 was captured by Whatman paper soaked in 3M NaOH solution for 1 h. ^{14}C radioactivity was measured by liquid scintillation counter and normalized to tissue mass. To assess fatty-acid uptake, BAT (approximately 100mg) was isolated from WT and Ehmt1^{adipo} knockout mice and incubated in DMEM containing oleic acid (250 μM, Nu-Chek Prep) supplemented with [^{14}C]oleic acid (0.25 μCi μl^{-1}) and 10% FBS for 15 min. ^{14}C radioactivity in the BAT explants was measured by liquid scintillation counter and normalized to the total protein content.

Cell culture.

Immortalized brown fat cells were isolated from the interscapular BAT of WT mice at P1–P3. Mouse embryonic fibroblasts have been described previously (8). HEK293 cells and C2C12 cells were obtained from the American Type Culture Collection. Adipocyte differentiation in C2C12 cells was induced by treating confluent cells with DMEM

containing 10% FBS, 0.5 μM isobutylmethylxanthine, 125 mM indomethacin, 2 μg ml^{-1} dexamethasone, 850nM insulin, 1 nM T3 and 0.5 μM rosiglitazone. Two days after induction, cells were switched to the maintenance medium containing 10% FBS, 850nM insulin, 1 nM T3 and 0.5 μM rosiglitazone. For cAMP treatment, cells were incubated with 10 μM forskolin for 4 h. Myocyte differentiation in C2C12 myoblasts was induced by treating cells in DMEM containing 2% horse serum. For beige cell differentiation in culture, the stromal vascular (SV) fraction was isolated from $Ehmt1^{flox/flox}$ mice and plated in collagen-coated plates (BD Biosciences). Cells were differentiated in the absence or presence of rosiglitazone at 0.5 μM according to the previous paper (29).

DNA constructs and viruses production.

Deletion mutants of Flag-tagged PRDM16 and GST-fused PRDM16 fragments (1–223, 224–454, 455–680, 680–880, 881–1038 and 1039–1176) were described previously (16). EHMT1 expression constructs were gifts from Y. Shinkai (19) and E. Hara (30). EHMT1 was cloned to pMSCV-puro vector for retroviral expression. The sequences used for retroviral shRNA expression vectors targeting EHMT1 were 5'-CGC TAT GAT GAT GAT GAA TAA-3' (shEHMT1-1) and 5'-GAGGATAGTAGGACTTCTAAA-3' (shEHMT1-2). The corresponding double-stranded DNA sequences were ligated into pSUPER-Retro (GFP-Neo) (Oligoengine) for retroviral expression. For retrovirus production, Phoenix packaging cells were transfected at 70% confluence by calcium phosphate method with 10 mg retroviral vectors. After 48 h, the viral supernatant was collected and filtered. Cells were incubated overnight with the viral supernatant and supplemented with 6 μg ml^{-1} polybrene. Subsequently, puromycin (PRDM16 and EHMT1), hygromycin (C/EBP-β) or G418 (shRNAs) were used for selection.

Gene expression analysis.

Total RNA was isolated from tissues using Trizol (Invitrogen) or RiboZol reagents (AMRESCO) following the manufacturers' protocols. Quality of RNA from all the samples was checked by spectrophotometer. Reverse transcription reactions were performed using an IScript complementary DNA (cDNA) synthesis kit (Bio-Rad). The sequences of primers used in this study can be found in Supplementary Table 2. Quantitative reverse transcriptase PCR (qRT-PCR) was performed with SYBR green fluorescent dye using an ABI ViiA7 PCR machine. Relative mRNA expression was determined by the DD-Ct method using TATA-binding protein as an endogenous control to normalize samples.

RNA-sequencing and gene ontology analysis.

Total RNA was isolated from the presumptive interscapular BAT depots of WT and *Ehmt1*^{myf5} knockout mice at P1 or from the interscapular BAT depots of WT and *Ehmt1*^{adipo} knockout mice at 12 weeks old. RNA-sequencing libraries were constructed from 50 ng of total RNA from the *Ehmt1*^{adipo} knockout and *Ehmt1*^{myf5} knockout BAT using an Ovation RNA-sequencing system version 2 (NuGEN). mRNA was reverse transcribed to cDNAs using a combination of randomhexameric and a poly-T chimaeric primer. The cDNA libraries were subsequently amplified by single primer isothermal amplification (31) using an Ultralow DR library kit (NuGEN) according to the manufacturer's instructions. The qualities of the libraries were determined by Bioanalyzer (Agilent Technologies). Subsequently, high-throughput sequencing was performed using a HiSeq 2500 instrument (Illumina) at the University of California, San Francisco Genomics Core

Facility. RNA-sequencing reads for each library were mapped independently using TopHat version 2.0.8 against the University of California, Santa Cruz (UCSC) mouse genome build mm9 indexes, downloaded from the TopHat website (http://tophat.cbcb.umd.edu/igenomes.shtml). The mapped reads were converted to fragments per kilobase of exon permillion fragments mapped by running Cuffdiff 2 (32) on the alignments from TopHat and the UCSC coding genes to estimate amounts of gene and isoform expression. Based on the list of genes that showed significant difference (P,0.05, the delta-method-based hypothesis test) from the RNA-sequencing data, enrichment of the Gene Ontology biological process terms (GO FAT category) was analysed using the Gene Set Enrichment Analysis (GSEA) program, according to the method described by the previous paper (33). RNA-sequencing reads have been deposited in ArrayExpress (www.ebi.ac.uk) under accession number E-MTAB-1704.

Immunocytostaining.

Differentiated C2C12 myotubes or COS7 cells expressing green fluorescent protein (GFP)–PRDM16 and EHMT1 constructs were fixed with 4% paraformaldehyde for 10 min at room temperature (24 ºC), rinsed with PBS and then exposed to 0.2% Triton X-100 in PBS for 5 min. The cells were subsequently incubated with anti-MF20 mouse antibody (DSHB, 1:50) for MHC and with Flag antibody (M2, 1:200) for EHMT1. After washing with PBS, Alexa 594-labelled anti-mouse IgG (1:800) was added as a secondary antibody.

Protein interaction analyses.

Immortalized brown fat cells stably expressing Flag-tagged WT, PR-domain deletion

mutant and ZF-1 deletion mutant of PRDM16 or an empty vector were grown to confluence (8) . Nuclear extracts were isolated from these cells and incubated with Flag M2 agarose beads, washed in a binding buffer (180mM KCl) and subsequently eluted either by 3x or by 1x Flag peptides (0.2μg ml^{-1}). The eluted proteins were subjected to histonemethyltransferase assay or to reverse-phase LC–MS/MS for peptide sequencing using a high-resolution hybridmass spectrometer (LTQ-Orbitrap, Thermo Scientific) with TOP10 method. Data obtained was annotated using the IPI mouse database (34). Proteins were considered significantly identified with at least two unique valid peptides, and the false discovery rate was estimated to be 0% using the target-decoy approach (35). To confirm the interaction between PRDM16 and EHMT1 in brown adipocytes, the immunopurified complex was purified using anti-EHMT1 (R&D Systems) or Flag antibody (M2) and subjected to 4–12% SDS–PAGE. Rabbit polyclonal PRDM16 antibody (36) or EHMT1 antibody (R&D Systems) was used for western blotting. COS7 cells expressing haemagglutinin (HA)-tagged PRDM16 or deletion fragments of Flag-tagged EHMT1 (30) were collected 48 h after transfection. Total cell lysates were incubated overnight at 4 °C with Flag M2 agarose beads, washed and eluted by boiling. The immunoprecipitants were analysed by western blot analysis using HA antibody (Roche). For in vitro binding assays, various fragments of the GST-fusion PRDM16 fragments were purified as previously described (16). ^{35}S-labelled proteins (EHMT1, EHMT2, CtBP1, C/EBP-β) were prepared with a TNT reticulocyte lysate kit (Promega). Equal amounts of GST fusion proteins (2 mg) were incubated overnight at 4 °C with in vitro translated proteins in a binding buffer containing 20mM HEPES pH 7.7, 300mM KCl, 2.5mM $MgCl_2$, 0.05% NP40, 1mM DTT and 10% glycerol. The sepharose beads were then washed five times with the binding buffer. Bound proteins were separated by

SDS-PAGE and analysed by autoradiography.

Histone methylation assay.

The PRDM16 transcriptional complex was immunopurified from nuclear extracts of brown adipocytes using Flag M2 agarose or IgG (negative control). The immunoprecipitants were incubated with 2 mg of core histone (Millipore) with [^{3}H]S-adenosyl-methionine at 30 ^{o}C for 1 h. Subsequently, the reaction was stopped by addition of sample buffer. Core histone was resolved by 4-12% SDS-PAGE and detected by autoradiography or by scintillation counter.

Chromatin immunoprecipitation assay.

After cross-linking with 1% formaldehyde at room temperature (24 ^{o}C) for 10 min, total cell lysates from brown adipocytes were sonicated to shear the chromatin, and immunoprecipitated overnight at 4 ^{o}C using antibodies for H3 di-methyl and tri-methyl K9 (Abcam), acetyl-H3K9/K14 (Millipore), pan-H3 (Cell Signaling), EHMT1 (R&D Systems) or IgG (Santa Cruz). After extensive washing, the immunoprecipitants were eluted with 2% SDS in 0.1M NaH_2CO_3. Cross-linking was reversed by heating at 65 ^{o}C overnight. Input DNA and immunoprecipitated DNA were purified by a PCR purification kit (Qiagen) and analysed by qRT-PCR using SYBR green fluorescent dye (Bio-Rad). Enrichment of each protein was calculated as a ratio to input DNA. Primer sequences used in the chromatin immunoprecipitation assays are provided in Supplementary Table 2.

Protein stability assay.

COS7 cells expressing HA-tagged PRDM16 and EHMT1 or vector control were incubated with a medium containing 60 μg ml^{-1} cycloheximide for up to 24 h. Total cell lysates were isolated and separated by SDS-PAGE. Horseradish peroxidase-conjugated HA antibody (Sigma) and β-actin (Sigma) were used for western blotting. Image J software was used to quantify the intensity of signals. Half-life of the protein was estimated by regression analysis.

Reporter gene assay.

A luciferase reporter gene controlled by PPAR-γ binding sites (3xDR1-Luciferase) was transiently transfected with PPAR-γ/RXR-α, PRDM16 andEHMT1expression plasmids in COS7 cells using Lipofectamine 2000 (Invitrogen). Forty-eight hours after the transfection, cells were collected and reporter gene assays used the Dual Luciferase Kit (Promega). Transfection efficiency was normalized by measuring expression of Renilla luciferase.

Cellular respiration assay.

Immortalized brown adipocytes were transduced with retroviral shEHMT1 (shEHMT1-1) or scramble control and induced to differentiate. Brown adipocytes expressing EHMT1 or vector control were also differentiated under a pro-adipogenic condition. At day 6 of differentiation, oxygen consumption was measured as previously described (37). Oligomycin was used to determine uncoupled respiration. In addition, antimycin A was added at the end of experiments to determine non-mitochondrial cellular respiration. For cAMP-induced respiration assays, fully differentiated brown adipocytes were incubated with 0.5mM dibutyryl cyclic AMP for 12 h before measuring oxygen consumption.

Statistical analyses.

Statistical analysis used JMP version 9.0 (SAS Institute). Two-way repeated-measures analysis of variance was applied to determine the statistical difference in glucose tolerance test, insulin tolerance test, body mass gain and rectal temperatures between genotypes. Effect size and power analysis were done by the pwr.t.test function of the R statistics package. Other statistical comparisons were assessed by an unpaired Student's t-test. $P<0.05$ was considered significant throughout the study.

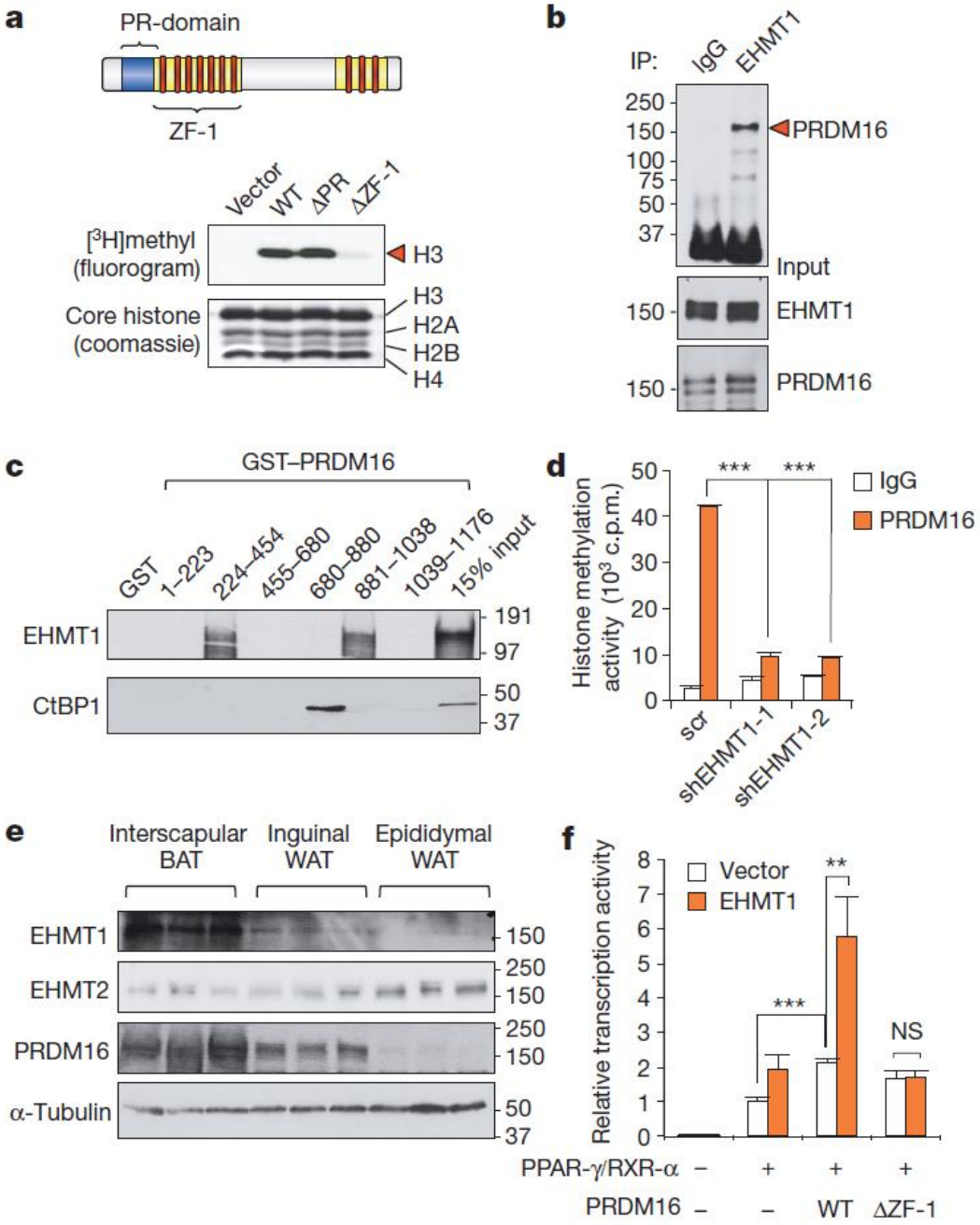

Figure 1 | Identification of EHMT1 in the PRDM16 transcriptional complex.
a, Top: schematic illustration of PRDM16. Bottom: PRDM16 complex purified from brown adipocytes were subjected to in vitro histone methylation assay. b, Immunoprecipitation of EHMT1 protein followed by western blotting to detect PRDM16. Input is shown in lower panels. c, In vitro binding assay of 35S-labelled EHMT1 or CtBP1 and purified PRDM16 fragments. d, Histone methylation assay of PRDM16 complex from brown adipocytes expressing indicated constructs (n=3 or 4). e, Western blotting for indicated proteins in adipose tissues. f, Transcriptional activities of PRDM16 using a PPAR-□-responsive luciferase reporter (n53). Error bars, s.e.m. **P<0.01, **P<0.001.

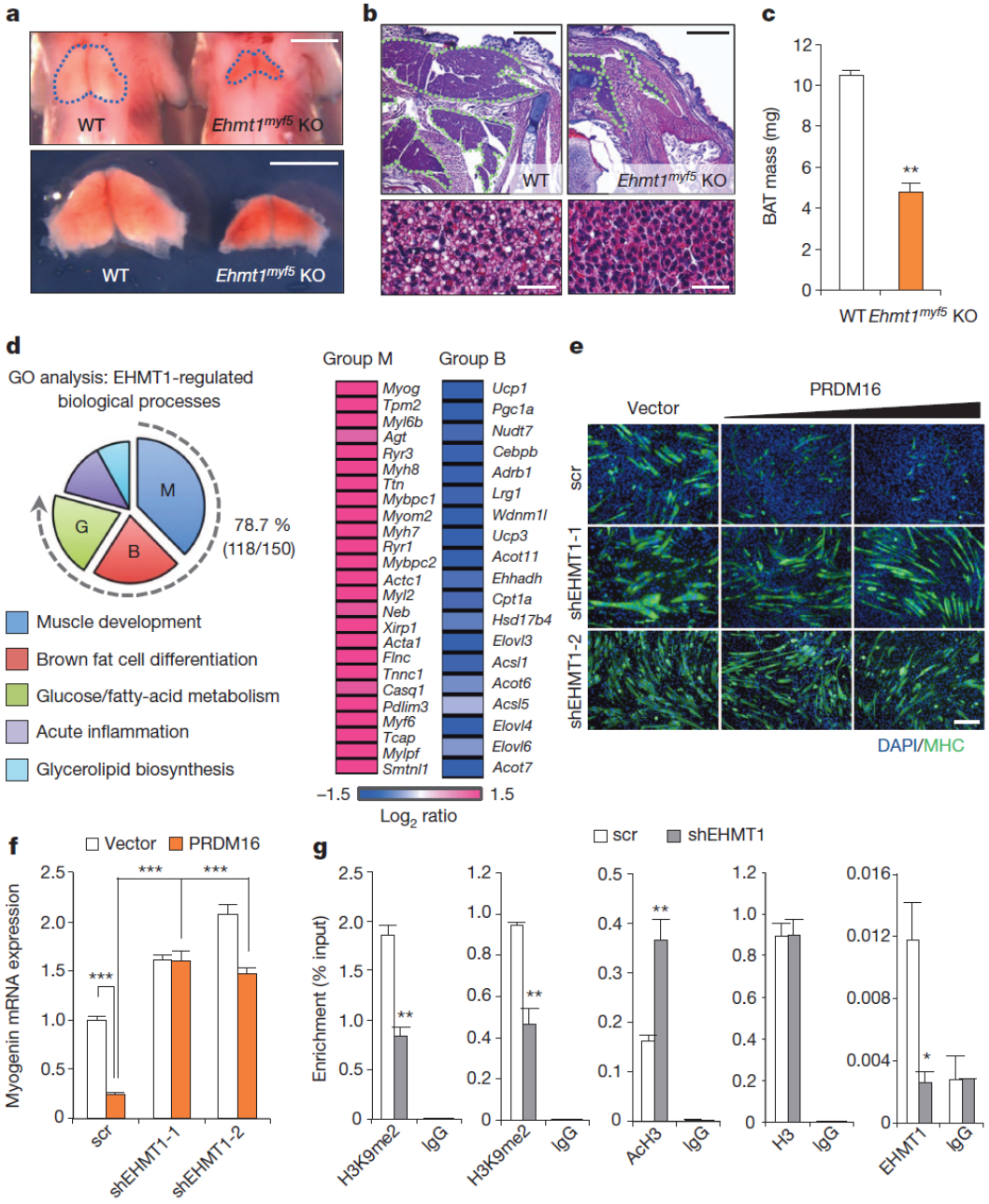

Figure 2 | EHMT1 is required for BAT versus muscle lineage specification.
a, Morphology of BAT from WT and Ehmt1^{myf5} knockout embryos at P1. Scale bar, 2.5mm. KO, knockout. b, Haematoxylin and eosin staining of WT and Ehmt1^{myf5} knockout (KO) BAT. Scale bar, 600 mm. Bottom: high-magnification images. Scale bar, 30 mm. c, BAT weight from WT (n=14) and knockout embryos (n=8). d, Gene ontology analyses of RNA-sequencing data. The log2-fold changes in the expression of skeletal muscle (group M) and BAT (group B) genes are shown. e, Immunocytochemistry for MHC in C2C12 cells expressing indicated constructs under pro-myogenic culture conditions. Scale bar, 200 mm. f, Myogenin mRNA expression in e (n=3). g, Chromatin immunoprecipitation assays using indicated antibodies (n=3). Error bars, s.e.m. *P<0.05, **P<0.01, ***P<0.001.

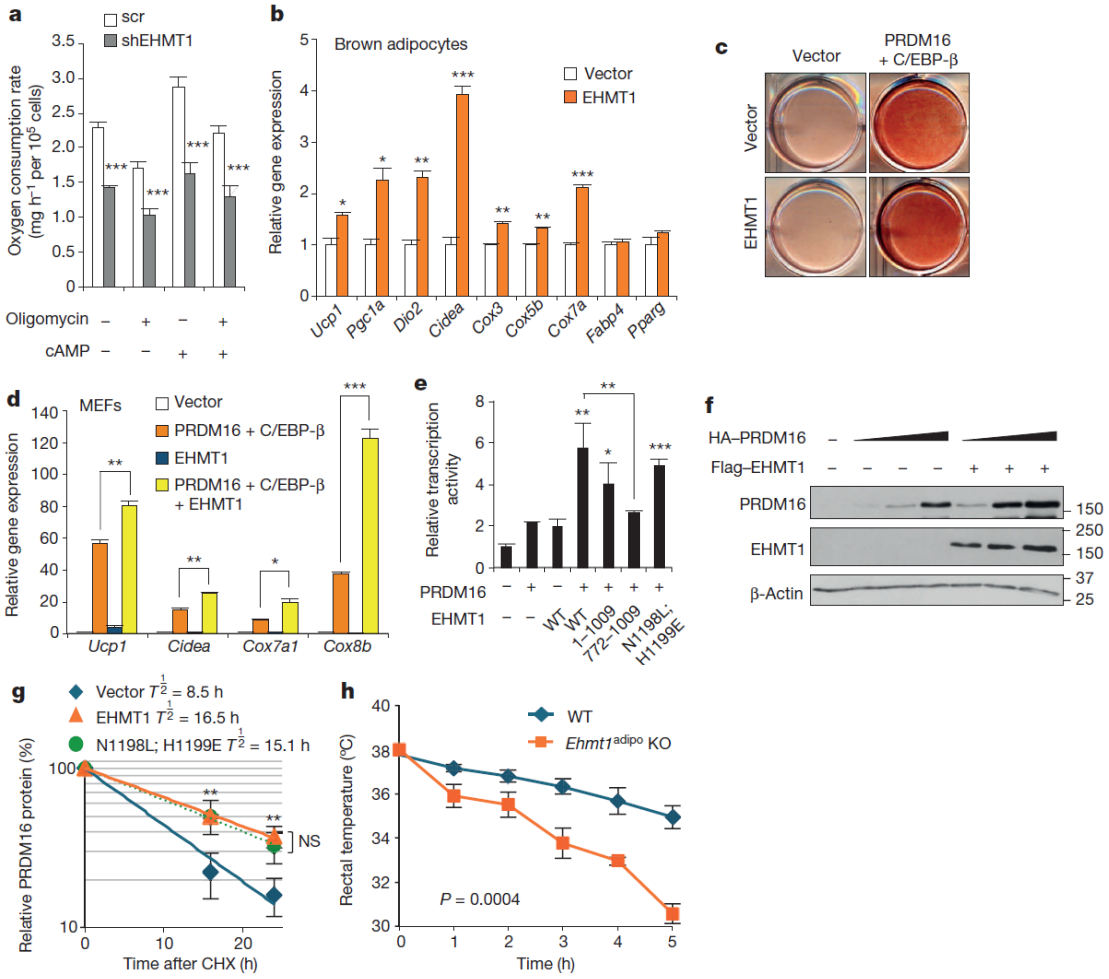

Figure 3 | EHMT1 controls BAT thermogenesis through stabilizing PRDM16 protein.
a, Cellular respiration in brown adipocytes expressing indicated constructs (n=6). b, BAT-selective gene expression in brown adipocytes expressing indicated constructs (n53). c, Oil-Red-O staining of mouse embryonic fibroblasts expressing indicated constructs under proadipogenic culture conditions. d, BAT-selective gene expression in c (n=3). e, Effects of EHMT1 mutants on PRDM16 transcriptional activities (n=3). f, Amounts of PRDM16 protein in COS7 cells expressing indicated constructs. g, Regression analysis of the PRDM16 protein stability (n=3). h, Changes in rectal temperature during a cold challenge (n=4 or 5). Error bars, s.e.m. *P<0.05, **P<0.01, ***P<0.001.

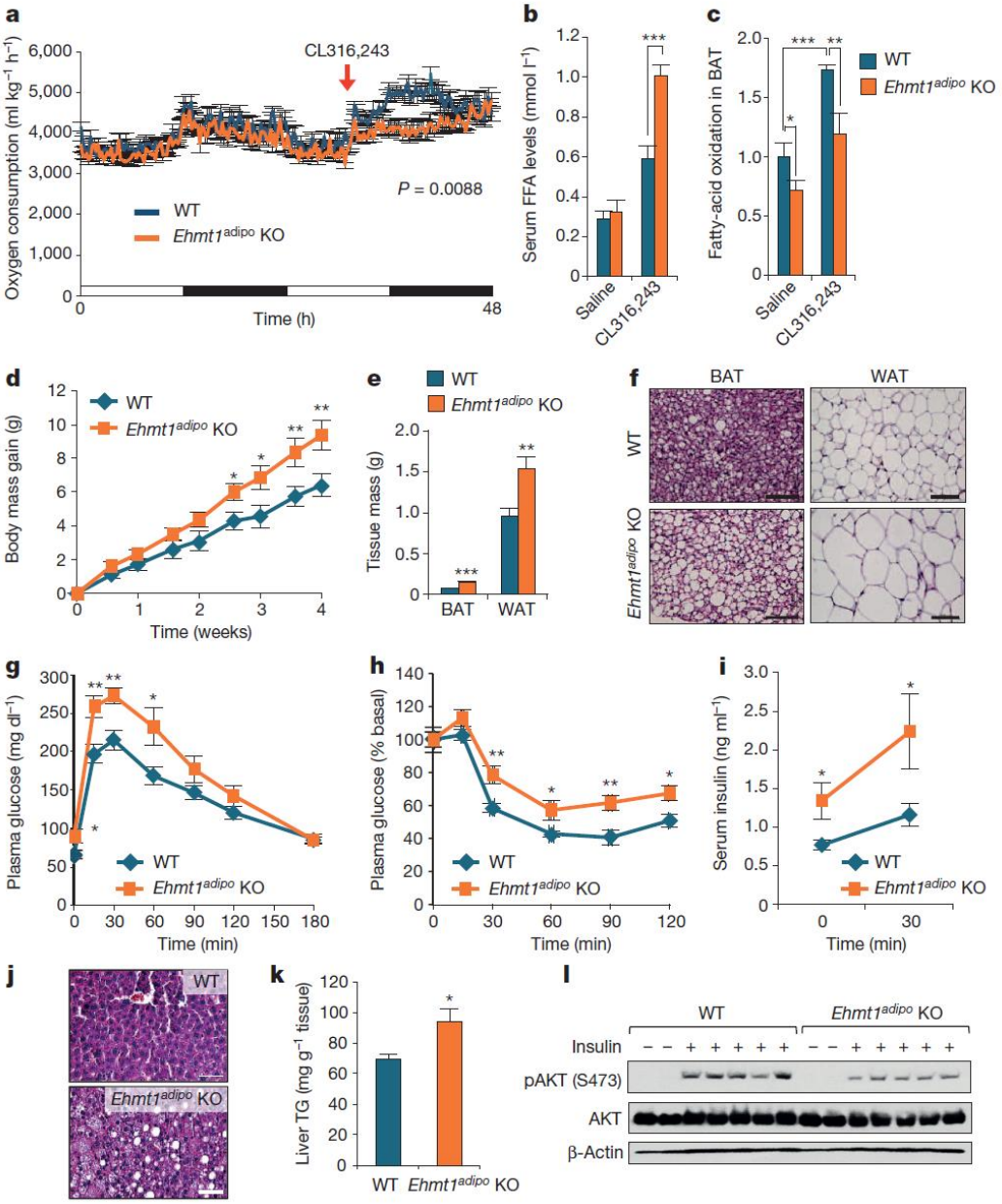

Figure 4 | EHMT1 deficiency in BAT causes obesity and insulin resistance.

a, Oxygen consumption rate of WT and Ehmt1^{adipo} knockout mice treated with CL316,243 (0.5mgkg^{-1}) at thermoneutrality (n=6). b, Amounts of serum FFA in mice treated with saline or CL316,243. c, Fatty-acid oxidation in BAT (n=6–10). d, Body mass change under a high-fat diet at thermoneutrality (n=16). e, Adipose tissue mass after 4-week high-fat diet (n=16). f, Haematoxylin and eosin staining of adipose tissues. Scale bar, 100 mm. g, Glucose tolerance test in 9-week high-fat diet-fed mice (n=9). h, Insulin tolerance test in 10-week high-fat diet-fed mice (n=9). i, Amounts of serum insulin at the fasted and glucose-stimulated states (n=9). j, Haematoxylin and eosin staining of liver in d. Scale bar, 50 mm. k, Amounts of liver triglyceride in j (n=9). l, Hepatic insulin signalling as assessed by phosphorylated (S473) and total Akt amounts. Error bars, s.e.m. *P<0.05, **P<0.01, ***P<0.001.

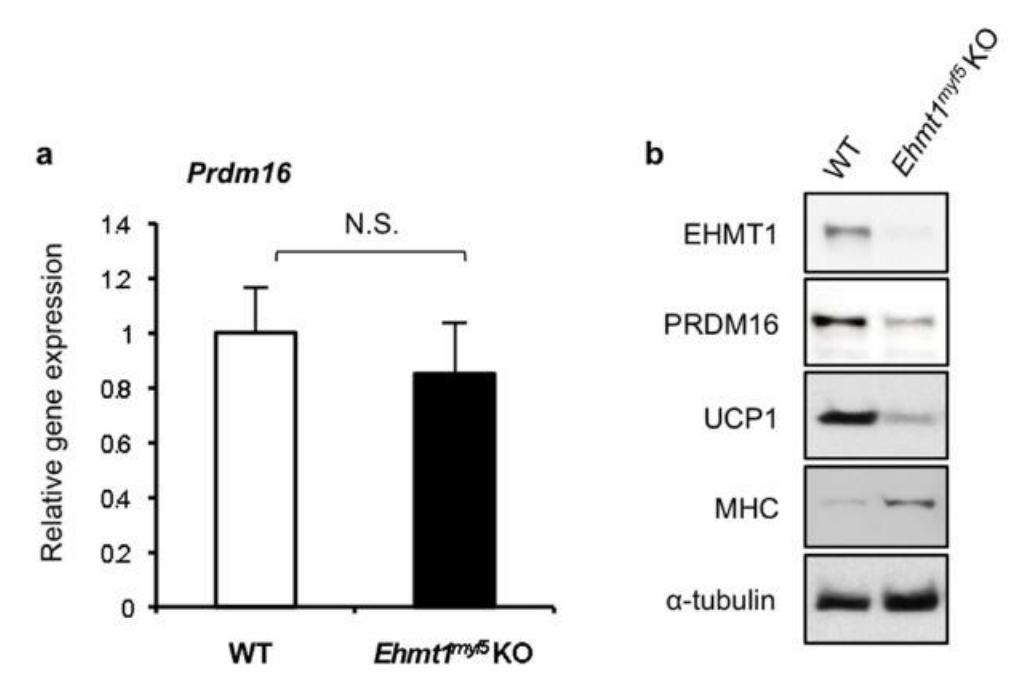

Extended Data Figure 1 | EHMT1 regulates endogenous PRDM16 protein expression in vivo.
a, The putative BAT was micro-dissected from WT and Ehmt1^{myf5} knockout embryos. mRNA expression of Prdm16 was measured by qRT–PCR. Data are presented as mean and s.e.m. (n=8–10). b, Western blotting to detect endogenous EHMT1, PRDM16, UCP1 and MHC in BAT from WT and Ehmt1^{myf5} knockout embryos. α-Tublin protein was shown as a loading control.

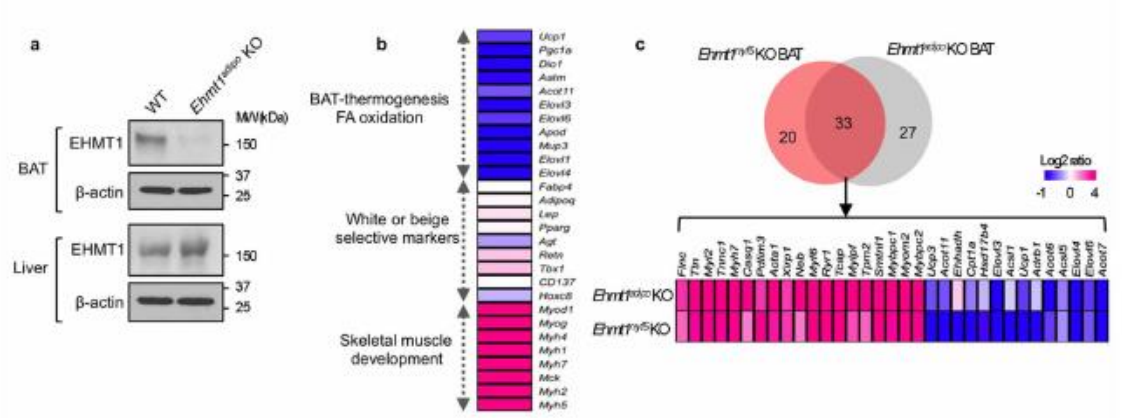

Extended Data Figure 2 | Ectopic activation of skeletal-muscle-selective genes and reduction of BAT-selective genes in the BAT from Ehmt1^{adipo} knockout mice.

a, Western blotting for endogenous EHMT1 in BAT and liver from WT and Ehmt1^{adipo} knockout mice. □-Actin protein was shown as a loading control. b, Amounts of mRNA expression of BAT, skeletal muscle, white fat and beige-fat selective genes in BAT from Ehmt1^{adipo} knockout mice. Values were normalized to those in WT mice. The amounts of mRNA were visualized by a heat-map using Multi Experiment Viewer. c, Venn diagram showing the overlapped genes between Ehmt1^{myf5} knockout and Ehmt1^{adipo} knockout mice. RNA-sequencing and gene ontology analyses identified 33 genes that were similarly dysregulated both in the Ehmt1^{myf5} knockout BAT and the Ehmt1^{adipo} knockout BAT. The mRNA expression values were normalized to WT mice for each knockout model and visualized by a heat-map using Multi Experiment Viewer. The colour scale shows the amounts of mRNA of the genes in a blue (low)–white (no change)–red (high) scheme.

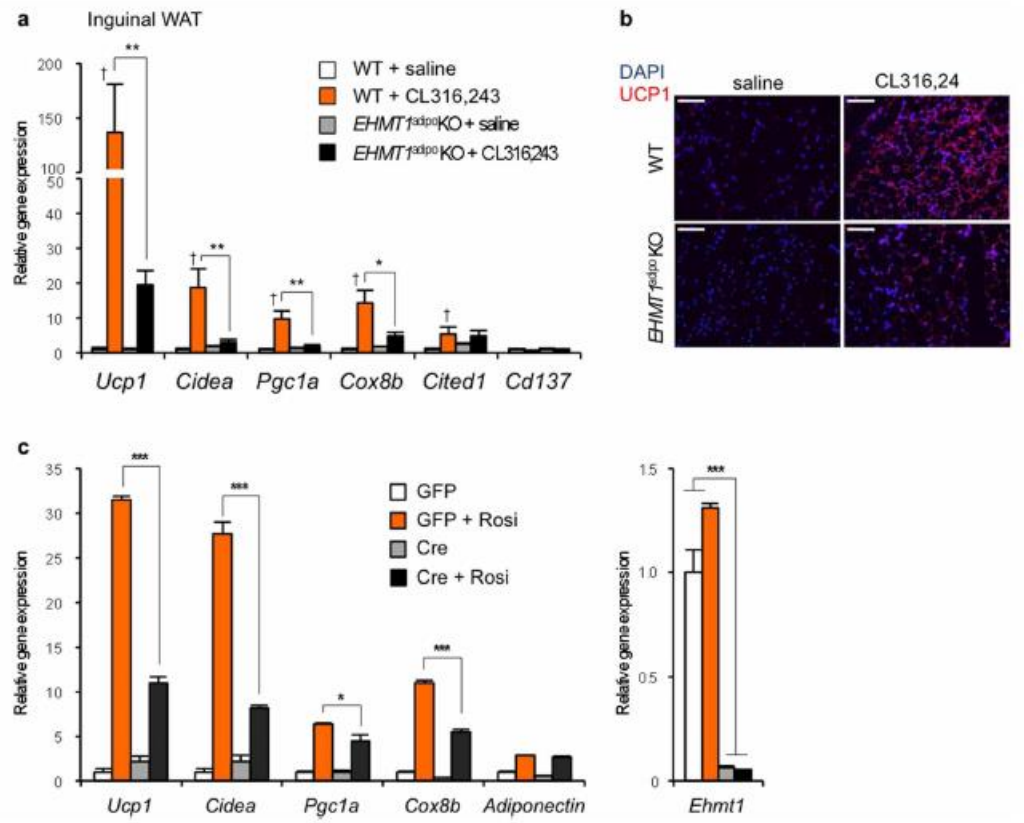

Extended Data Figure 3 | EHMT1 is required for beige/brite cell development.

a, The β3-AR agonist CL316,243 at a dose of 0.5mgkg^{-1} or saline were administered to WT or Ehmt1adipo knockout mice for 7 days. Inguinal WAT was collected for gene expression analysis. Amounts of mRNA expression of BAT and beige-fat selective genes (as indicated) were measured by qRT–PCR (n=3–6). {Significant between saline and CL316,243 in WT mice. b, Immunohistochemistry for UCP1 in a. Scale bar, 100 mm. Nuclei were stained with DAPI. c, To test a cell-autonomous requirement for EHMT1 in beige/brite cell development, the stromal vascular (SV) fractions were isolated from the inguinal WAT of Ehmt1$^{flox/flox}$ mice. Cells were infected with adenovirus expressing GFP or Cre. The SV cells were differentiated in the presence or absence of rosiglitazone (Rosi) at 0.5 μM. Amounts of mRNA expression of BAT-selective genes (as indicated) were measured by qRT–PCR. Deletion of Ehmt1 was confirmed by qRT–PCR (right graph) (n=3); data are presented as mean and s.e.m. *P<0.05, **P<0.01, ***P<0.001.

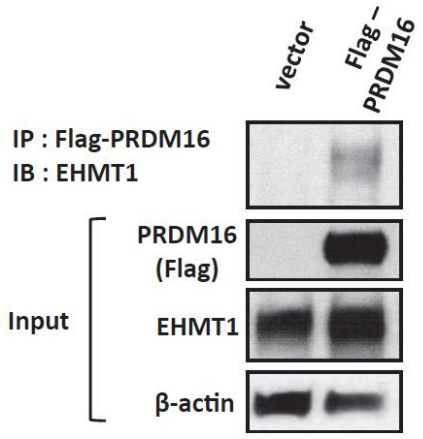

Supplementary Figure 1. PRDM16 interacts with endogenous EHMT1 in brown adipocytes.
Immunoprecipitation of PRDM16 complex by flag antibody (M2) followed by Western blot analysis to detect endogenous EHMT1 protein in brown adipocytes. Inputs are shown in lower panels.

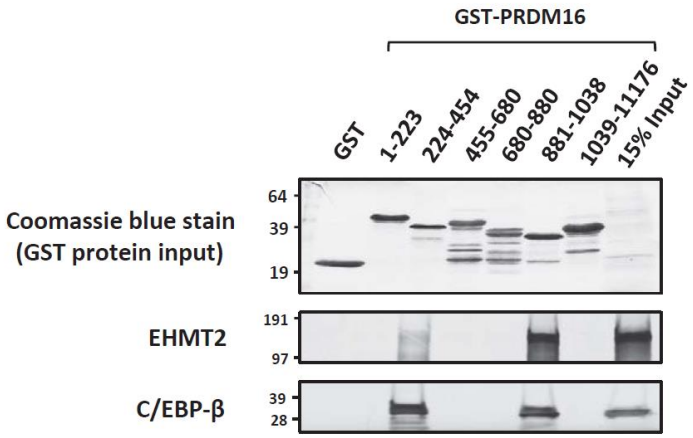

Supplementary Figure 2. Interaction between purified PRDM16 fragments and EHMT2 or C/EBP-β.
In vitro binding assay of 35S-labeled EHMT2 or C/EBP-β and purified GST-fusion fragments of PRDM16 (as indicated). GST-fusion proteins were separated by SDS-PAGE, and stained by Coomassie brilliant blue (top panel). EHMT2 and C/EBP-β proteins were detected by autoradiography.

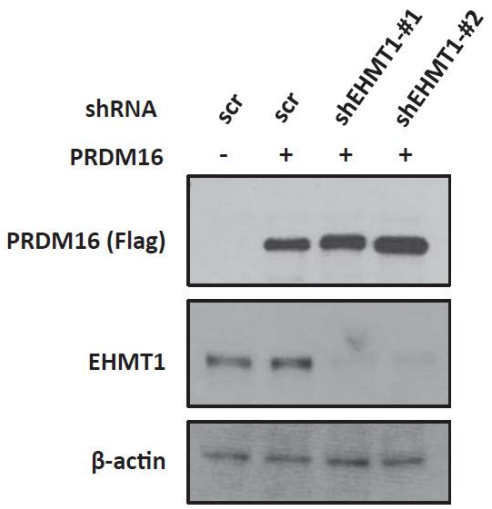

Supplementary Figure 3. Depletion of EHMT1 by two different shRNAs targeted to EHMT1 in brown adipocytes. Flag tagged PRDM16 was overexpressed in immortalized brown adipocytes by retrovirus. EHMT1 was depleted by retrovirus-mediated shRNAs for a scramble control (scr), shEHMT1-#1, and shEHMT1-#2. Flag tagged PRDM16 and endogenous EHMT1 protein were detected by Western blotting. β-actin protein was shown as a loading control.

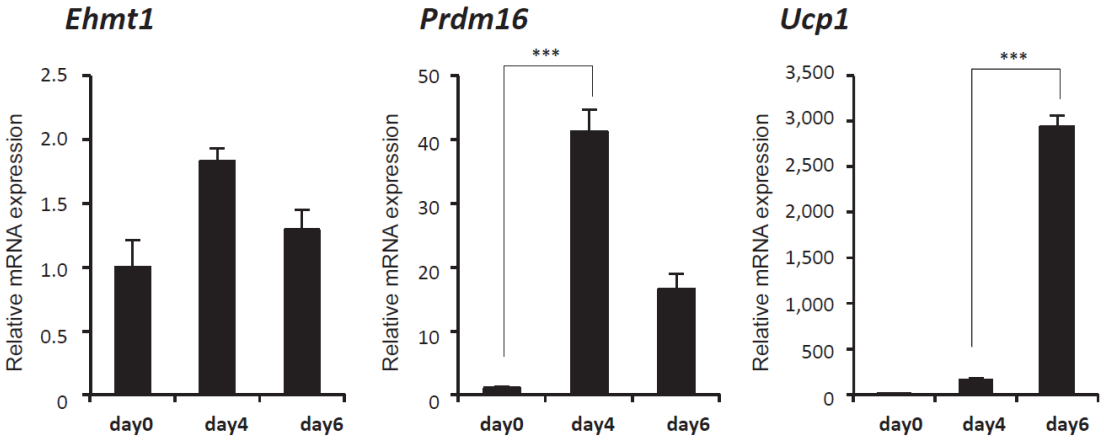

Supplementary Figure 4. Changes in EHMT1 expression during brown adipocyte differentiation.
mRNA levels of Ehmt1, Prdm16 and Ucp1 were measured during the differentiation of immortalized brown adipocytes by qRT-PCR. n=3; data are presented as mean and s.e.m. *** P <0.001.

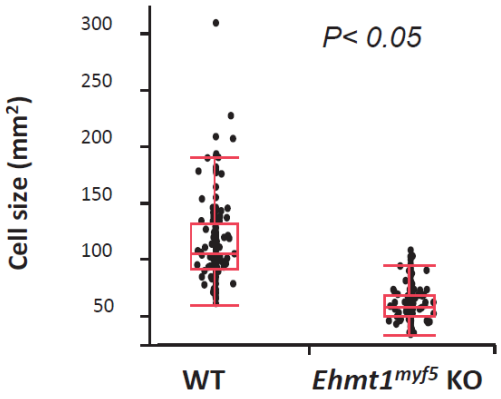

Supplementary Figure 5. Adipocyte cell size of the interscapular BAT from wild-type (WT) and Ehmt1^{myf5} KO embryos at P1 stage.
Brown adipocyte size was quantified in the BAT of wild-type (WT) and Ehmt1^{myf5} KO embryos at P1 using Image J software. n=145-154.

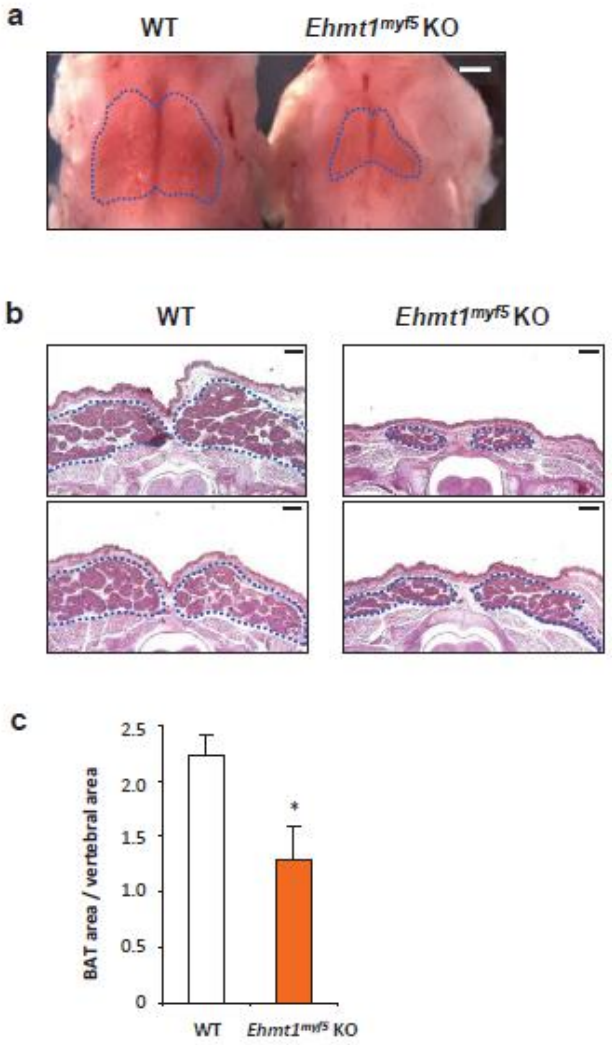

Supplementary Figure 6. Morphological characterization of Ehmt1^{myf5} KO embryos at E18.5.
a, Gross pictures of wild-type (WT) and Ehmt1^{myf5} KO embryos at E18.5. BAT is highlighted by dashed lines. Scale bar, 1 mm. b, Haematoxylin and eosin (H&E) staining of transverse sections of wild-type and Ehmt1^{myf5} KO embryos. Sections containing the largest area of BAT were shown. BAT is highlighted by dashed lines. Scale bar, 300 □m. c, Quantification of the BAT size of WT and Ehmt1^{myf5} KO embryos derived from multiple breeding pairs. The BAT size was normalized by vertebral size. n=4 per genotype. All error bars are s.e.m.; * P< 0.05.

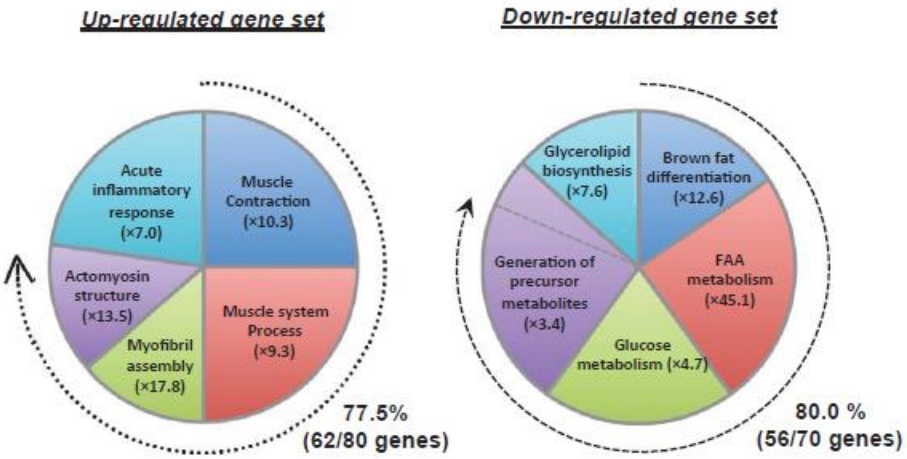

Supplementary Figure 7. EHMT1 controls cell fate determination between skeletal muscleversus brown fat.
RNA-sequencing and gene ontology (GO) analyses identified clusters of genes that were coordinately up-regulated (left) or down-regulated (right) in the BAT from Ehmt1^{myf5} KO mice as compared to that from wild-type mice. These clusters were annotated to the GO terms as shown in each pie slice. Fold enrichments of the each GO cluster are shown. Area of each pie slice are proportional to the number of genes.

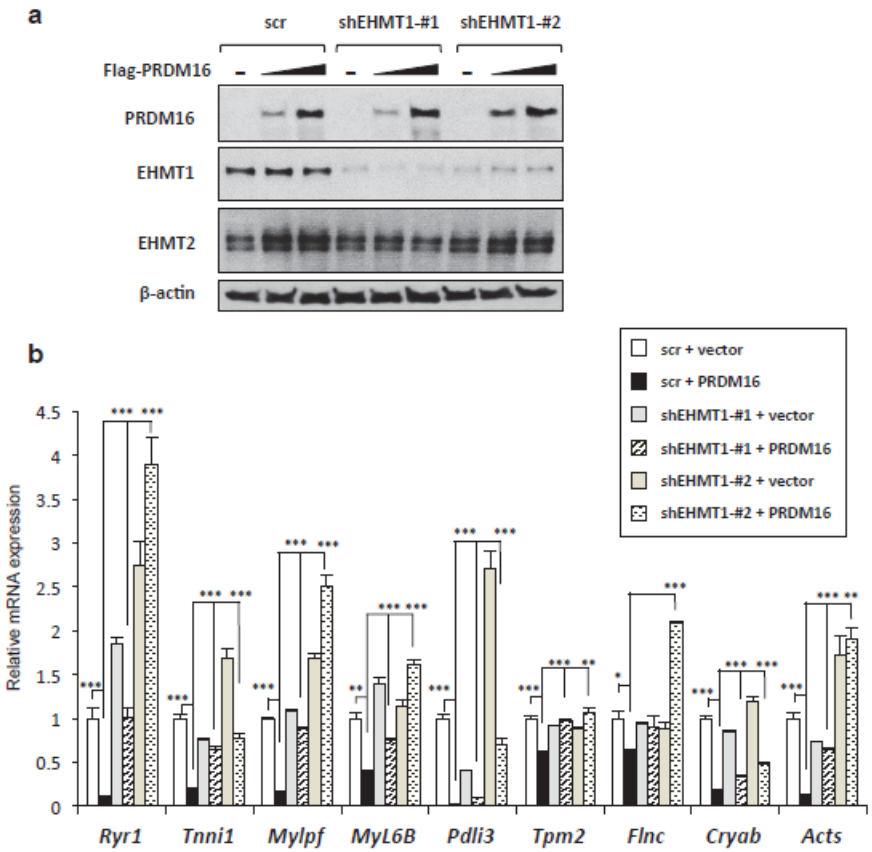

Supplementary Figure 8. EHMT1 is required for PRDM16-mediated repression on muscle-selective genes.
a, C2C12 myoblasts were transduced with scrambled control (scr) or shRNAs targeted to EHMT1 (shEHMT1-#1 and shEHMT1-#2) together with PRDM16 or vector control. Protein levels of PRDM16, EHMT1 and EHMT2 were detected by Western blotting. β-actin protein was shown as a loading control. b, mRNA expression of muscle-selective genes (as indicated) was measured by qRT-PCR. n=3; data are presented as mean and s.e.m.; * P< 0.05, ** P <0.01, *** P <0.001

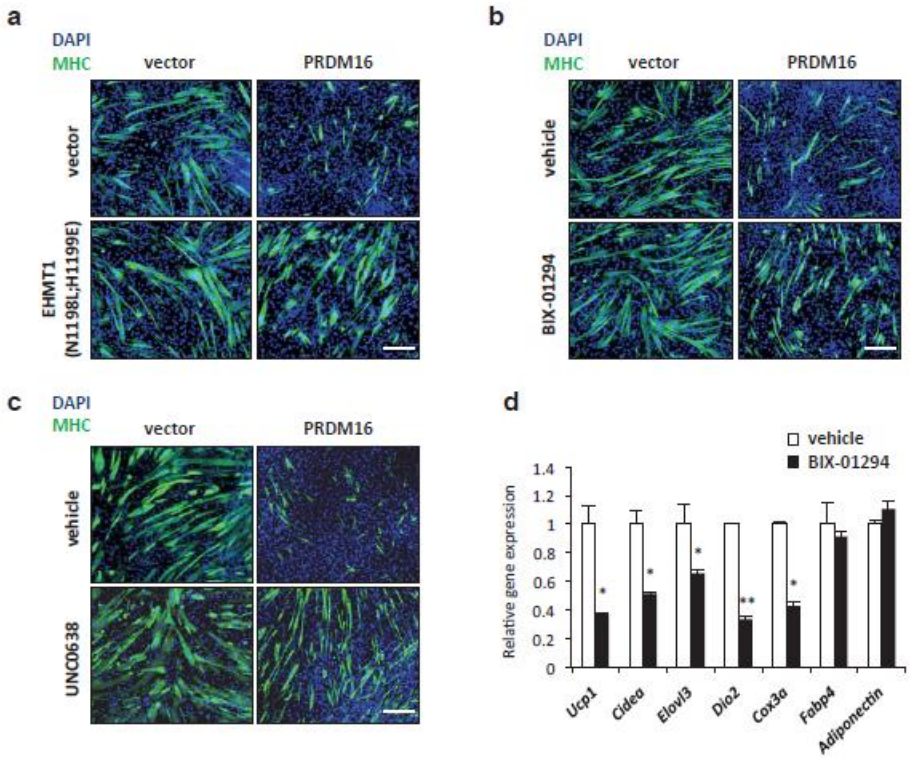

Supplementary Figure 9. Repressive effect of EHMT1 on myogenesis is mediated through its methyltransferase activity. a, The SET-domain mutant of EHMT1 (p. N1198L;H1199E) or vector was overexpressed in C2C12 myoblasts in the presence or absence of PRDM16. These cells were differentiated under pro-myogenic culture conditions. Differentiated myotubes were visualized by immunocytochemistry for skeletal myosin heavy chain (MHC). Nuclei were stained with DAPI (4′,6-diamidino-2-phenylindole). Scale bar, 200μm. b-c, C2C12 myoblasts expressing PRDM16 or vector control were differentiated under pro-myogenic culture conditions in the presence or absence of chemical inhibitors for EHMT1/2, BIX-01294 (b, 2.5 μM) or UNC0638 (c, 1.0 μM). Differentiated myotubes were stained with MHC antibody. Nuclei were counterstained with DAPI. Scale bar, 200μm. d, Brown adipocytes were treated with BIX-01294 under pro-adipogenic culture conditions. mRNA levels of BAT-selective genes (as indicated) were measured by qRT-PCR. n=3; data are presented as mean and s.e.m.; * P< 0.05, ** P <0.01.

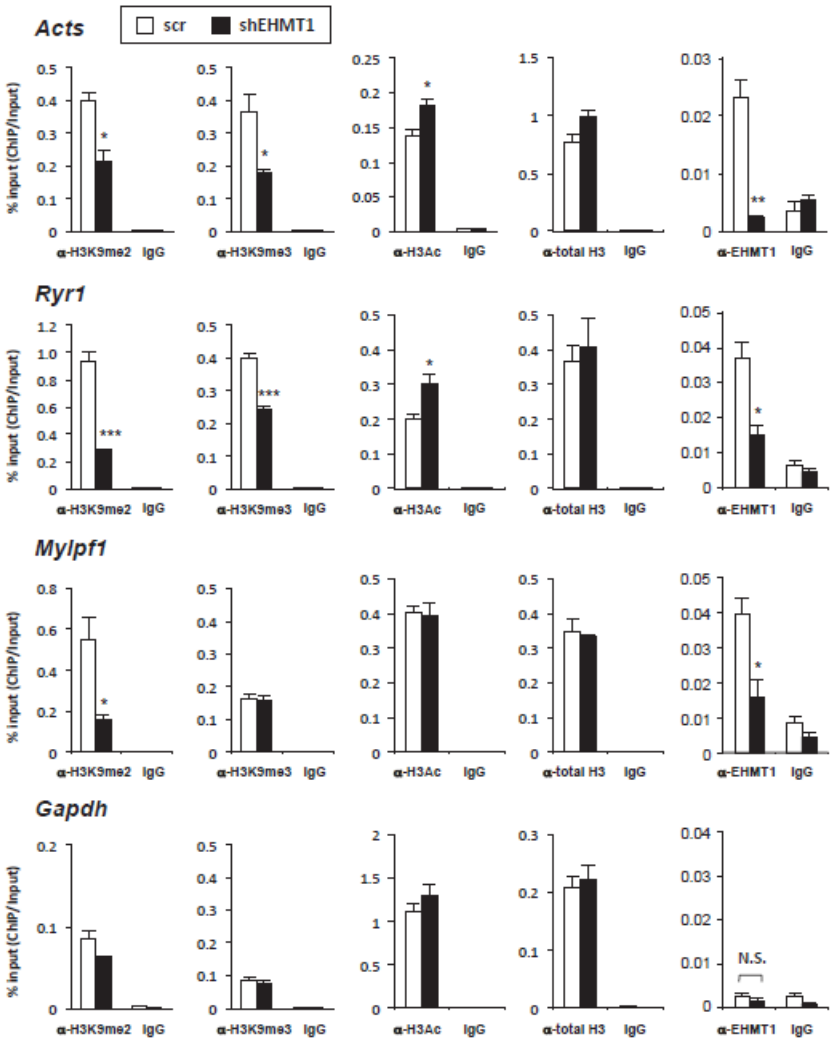

Supplementary Figure 10. EHMT1 controls H3K9 methylation status on the promoter regions of muscle-selective genes. ChIP assays were performed on the promoters of muscle-selective genes (as indicated) using antibodies against H3K9me2, H3K9me3, H3K9/K14ac, pan-H3, EHMT1, and IgG. White and black columns represent scr control and shEHMT1, respectively. ChIP assays were also performed on the promoter of Gapdh,a non-muscle related gene. n=3; data are presented as mean and s.e.m.; * P< 0.05, ** P <0.01, *** P <0.001.

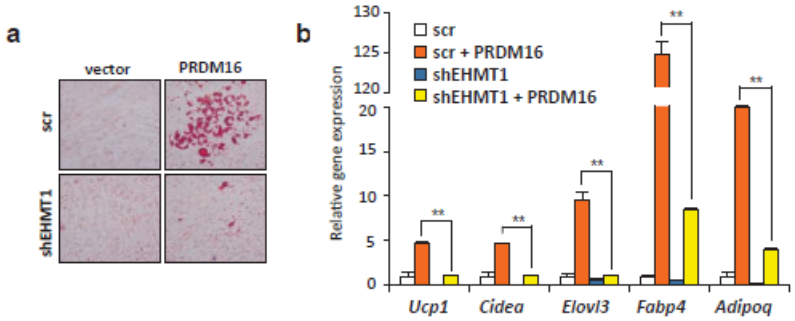

Supplementary Figure 11. Knockdown of EHMT1 blocked the PRDM16-induced brown adipogenesis.
a, Oil-Red-O staining of C2C12 cells expressing indicated constructs. C2C12 myoblasts were transduced with scrambled control (scr) or shRNA targeted to EHMT1 (shEHMT1-#1) together with PRDM16 or vector control, and differentiated under pro-adipogenic culture conditions for 8 days. b, mRNA expression of BAT-selective genes and adipogenic marker genes (as indicated) in a. n=3. All error bars are s.e.m.; ** P<0.01.

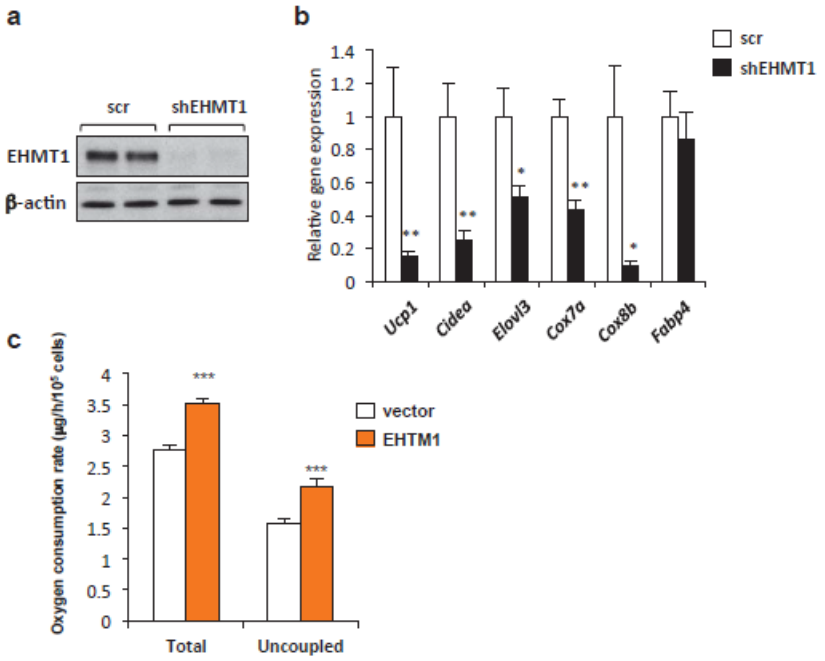

Supplementary Figure 12. EHMT1 controls the BAT-selective thermogenic program in brown adipocytes. a,EHMT1 was depleted in immortalized brown adipocytes by retrovirus-mediated shRNA knockdown (shEHMT1-#1). Endogenous EHMT1 protein was detected by Western blotting. □-actin protein was shown as a loading control. b, mRNA expression of BAT-selective genes (as indicated) was measured in differentiated brown adipocytes by qRT-PCR. n=3. c, Total and uncoupled (oligomycin-insensitive) cellular oxygen consumption rate was measured in differentiated brown adipocytes expressing vector or EHMT1. n=6. Data are presented as mean and s.e.m.; * P< 0.05, ** P <0.01, *** P<0.001.

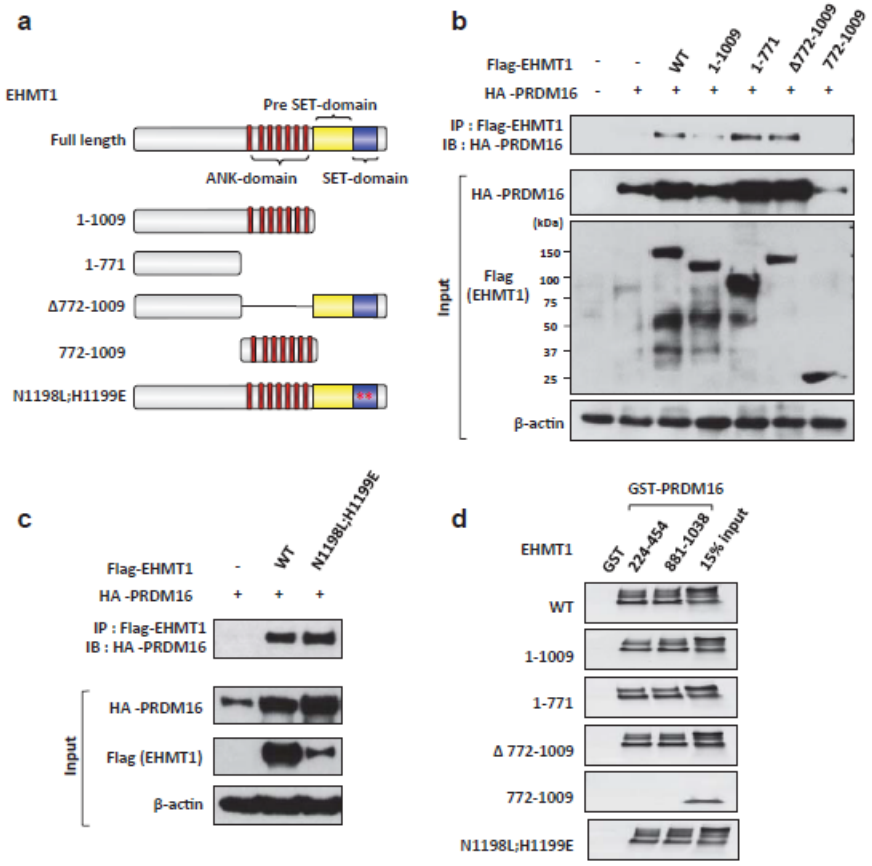

Supplementary Figure 13. Mapping of EHMT1 domains that are required for interaction with PRDM16.
a, Schematic illustration of EHMT1 protein structure. Deletion mutants and a point mutant of EHMT1 are shown. Two mutations in the N1198L;H1199E mutant are indicated by stars. b-c, HA-tagged full length PRDM16 was transiently expressed together with wild-type or the mutant forms of EHMT1 (as indicated) in COS7 cells. EHMT1 was immunoprecipitated using flag M2 antibody, separated by SDS-PAGE, and PRDM16 protein was detected by Western blotting. The inputs are shown in bottom panels. d, In vitro binding assay of 35S-labeled EHMT1 mutants (as indicated) and purified GST-PRDM16 fusion proteins. GST-fusion proteins were separated by SDS-PAGE. EHMT1 proteins were detected by autoradiography.

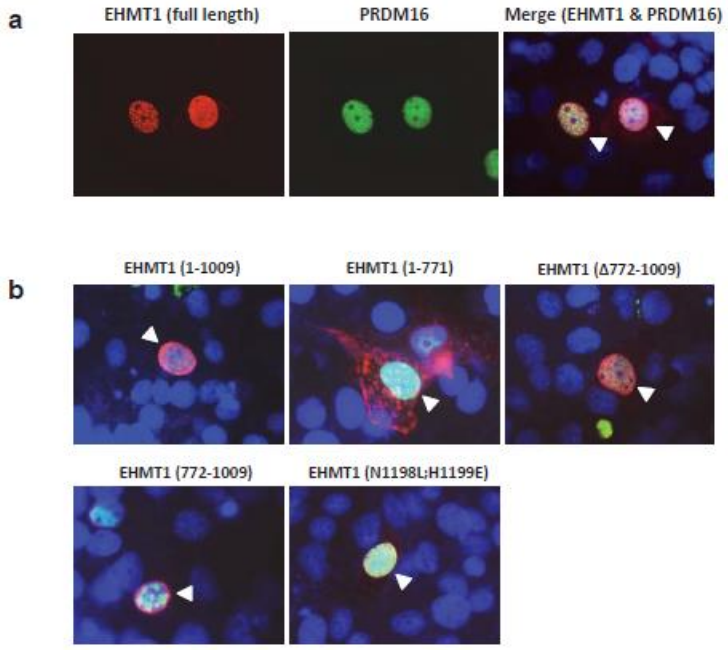

Supplementary Figure 14. Mapping of EHMT1 domains that are required for co-localization with PRDM16.
a, Nuclear localization of full length EHMT1 (red, left) and PRDM16 (green, middle). Flag-tagged EHMT1 and GFP-PRDM16 were transiently expressed in COS7 cells. Flag-EHMT1 was immunostained using M2 flag antibody. Nuclei were stained with DAPI (4′,6-diamidino-2-phenylindole). Merged image (right) shows co-localization of EHMT1 and PRDM16 in nucleus, as indicated by arrow heads. b, Flag-tagged deletion mutants and point mutant of EHMT1were transiently expressed together with GFP-PRDM16 in COS7 cells. Co-localization of EHMT1 and PRDM16 were shown by arrow heads. Note that the 1-771 region of EHMT1 was ubiquitously expressed.

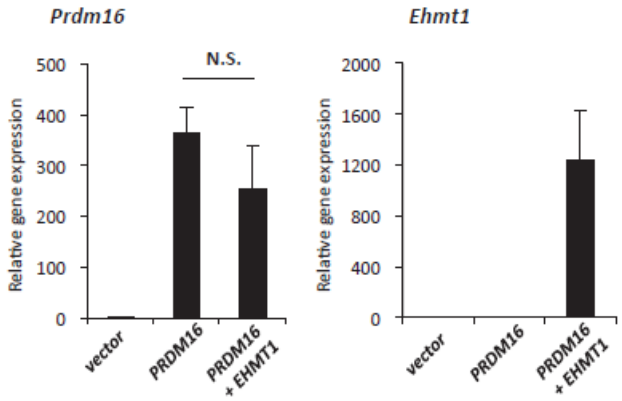

Supplementary Figure 15. Ectopic expression of EHMT1 does not affect mRNA expression of PRDM16 in the protein stability assay.
EHMT1 was transiently expressed together with PRDM16 or vector in COS7 cells. Forty-eight hours after transfection, total RNA was extracted from the cells and treated with DNase I. Subsequently, mRNA expression of ectopically expressed flag-tagged PRDM16 was measured by qRT-PCR. n=3; Data are presented as mean and s.e.m.

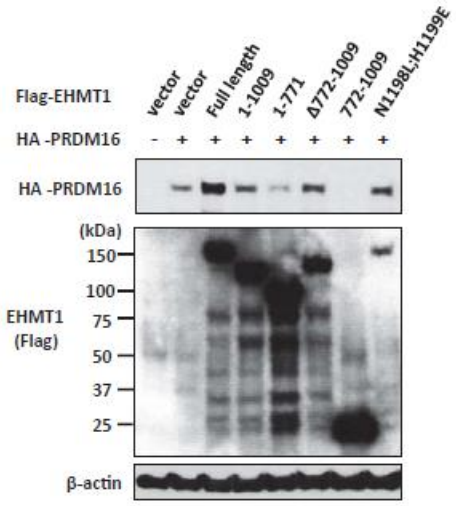

Supplementary Figure 16. EHMT1 induces protein accumulation of PRDM16 through direct interaction.
HA-tagged PRDM16 was transiently expressed together with wild-type or the mutant forms of EHMT1 (as indicated) or vector. Total cell lysates were isolated 48 hours after transfection, and subjected to SDS-PAGE. PRDM16 and EHMT1 were detected by Western blotting using HA or flag antibody. β-actin protein was shown as a loading control.

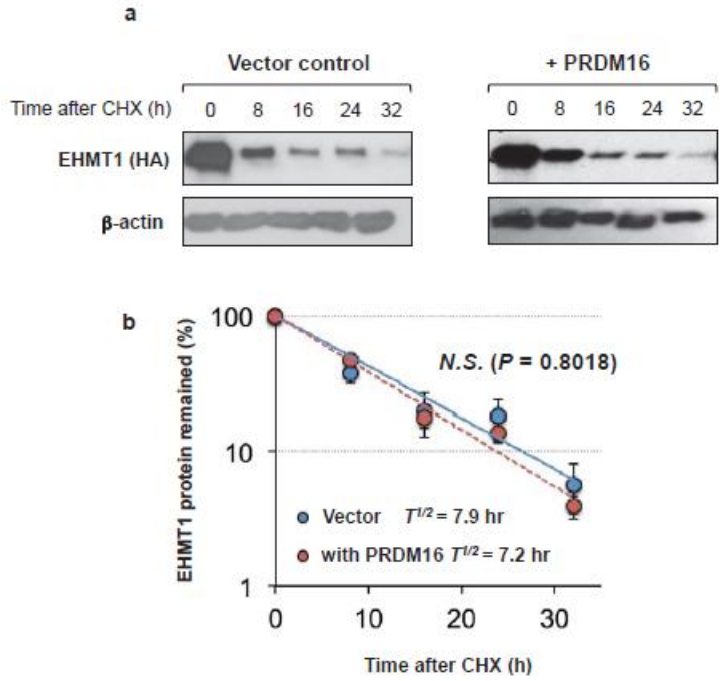

Supplementary Figure 17. EHMT1 protein stability is not affected by PRDM16 expression.
a, EHMT1 protein stability was assessed by cycloheximide (CHX) chase experiments in the presence or absence of PRDM16. COS7 cells were transiently expressed with full length EHMT1 together with PRDM16 or vector control. Cells were treated with CHX for indicated hours and harvested. EHMT1 protein levels were analyzed by Western blotting. β-actin protein was shown as a loading control. b, Regression analysis of EHMT1 protein stability in a. Significance between curves was determined by two-way repeated measures ANOVA. Pvalue of main effect (vector or PRDM16) was not significant. n=3 per group. Data are presented as mean and s.e.m.

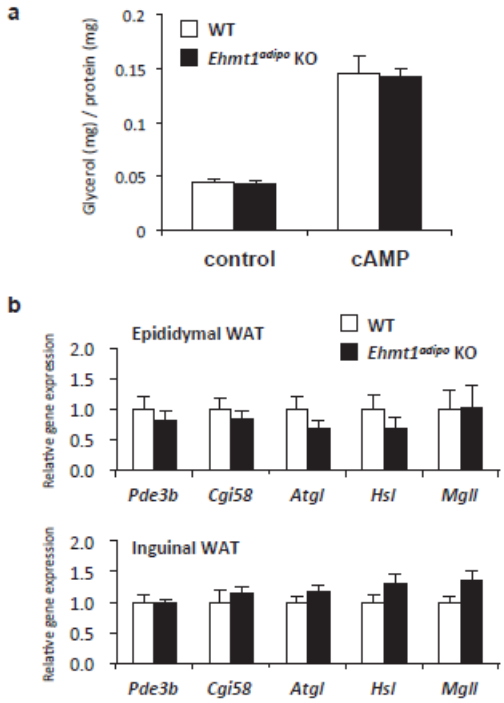

Supplementary Figure 18. Lipolysis capacity in WAT from Ehmt1^{adipo} KO mice was indistinguishable from wild-type mice.

a, Glycerol release was measured in primary adipocytes isolated from the epididymal WAT of wild-type and Ehmt1adipo KO mice. The adipocytes were treated with or without cAMP (isoproterenol, 1 μM) for 1.5 hours. n=3. b, mRNA levels of genes involved in fat lipolysis (as indicated) were measured in the epididymal WAT (upper panel) and in the inguinal WAT (lower panel) by qRT-PCR. n=3-5 per group; data are presented as mean and s.e.m. Note that no statistical difference was found between wild-type and Ehmt1^{adipo} KO mice.

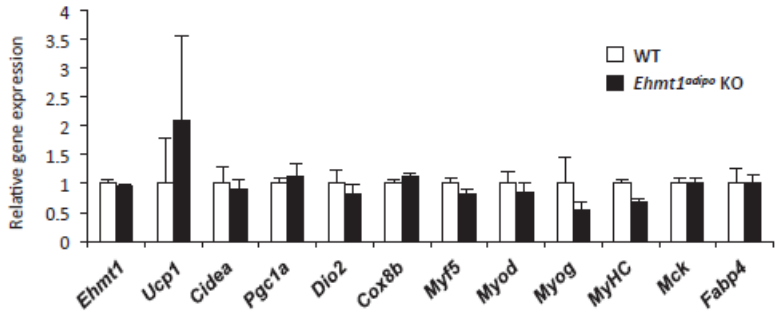

Supplementary Figure 19. Expression of BAT- and skeletal muscle-selective genes were not altered in the skeletal muscle of Ehmt1^{adipo} KO mice in response to cold exposure.
Total RNA was extracted from the skeletal muscle of wild-type and Ehmt1^{adipo} KO mice after cold exposure (4^{o}C) for 5 hours. mRNA levels of genes (as indicated) were measured by qRT-PCR. n=6 per group; data are presented as mean and s.e.m.

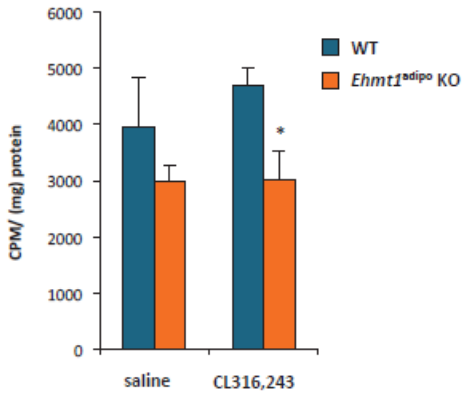

Supplementary Figure 20. Fatty acid uptake was reduced in the BAT of Ehmt1^{adipo} KO mice.
Wild-type and Ehmt1^{adipo} KO mice were injected intraperitoneally with saline or CL316,243 at a dose of 0.5 mg/kg. Six hours after the injection, BAT were isolated and incubated in DMEM containing 14C-Oleic acid for 15min. 14C radioactivity in the BAT was measured by liquid scintillation counter and normalized to the total protein content. n=4; data are presented as mean and s.e.m.; * P< 0.05.

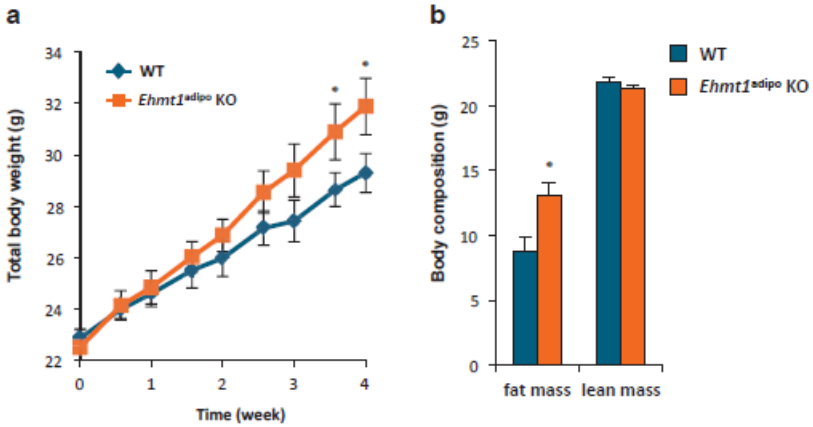

Supplementary Figure 21. Total body weight and body composition of wild-type and Ehmt1^{adipo} KO mice under a high-fat diet.

a, Male mice at 6-week-old were kept in individual cages under a high-fat diet at thermoneutrality. Total body weight of each mouse was monitored for 4 weeks. n=16. Genotype and time interaction effect was statistically significant. (P = 0.0113) b, Body composition (fat and lean mass) in wild-type and Ehmt1^{adipo} KO mice after 4 weeks of high fat diet, as assessed by Magnetic resonance imaging system (EchoMRI-3in1, Echo Medical Systems). Data are presented as mean and s.e.m.; * P< 0.05.

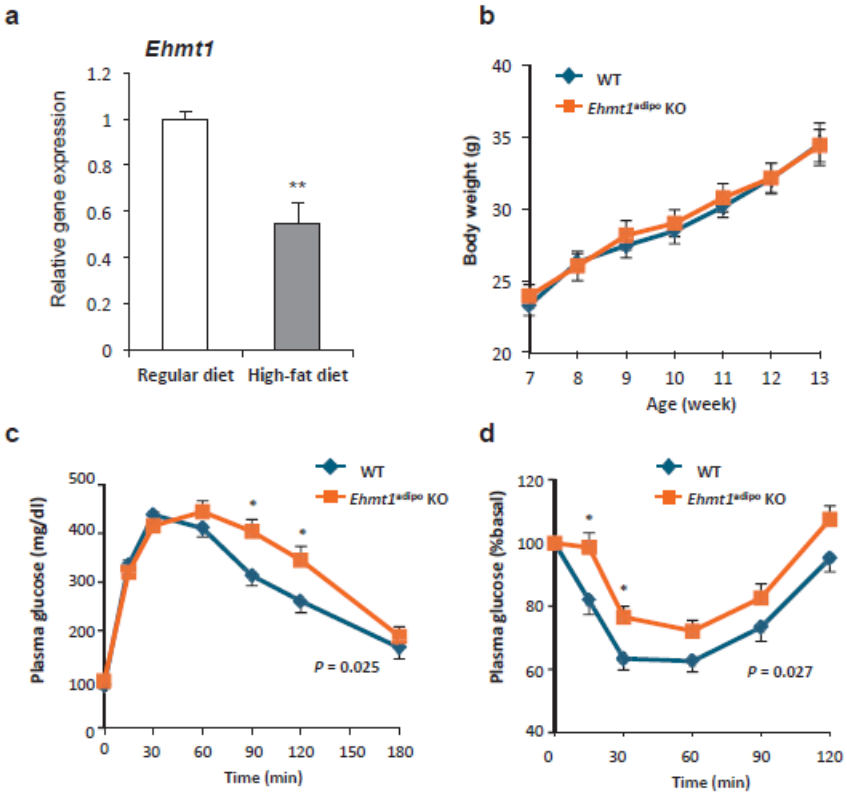

Supplementary Figure 22. Metabolic phenotypes of Ehmt1^{adipo} KO mice under a high-fat diet at ambient temperature. a, mRNA expression of Ehmt1 was measured by qRT-PCR in the interscapular BAT from wild-type mice under a regular diet or high-fat diet for 14 weeks. n=4. b, Body weight increase of wild-type (WT) and Ehmt1^{adipo} KO mice under a high-fat diet at ambient temperature. c, Glucose tolerance test in 9-week high-fat diet-fed wild-type (WT) and Ehmt1^{adipo} KO mice. Serum glucose levels were measured after an overnight fast (time 0) and at the indicated times after an intraperitoneal injection of glucose. The genotype and time interaction was significant (P<0.05). h, Insulin tolerance test in 10-week high-fat diet-fed wild-type (WT) and Ehmt1^{adipo} KO mice. Serum glucose levels were after an overnight fast (time 0) and at the indicated times after an intraperitoneal injection of insulin (0.75U/kg). n=8-12 per genotype. Data are presented as mean and s.e.m.; * P< 0.05, ** P <0.01.

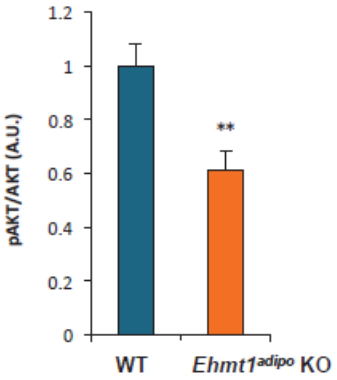

Supplementary Figure 23. Impaired insulin signaling in the liver of Ehmt1^{adipo} KO mice under a high-fat diet. Insulin (5U) was injected into the inferior venae cavae of wild-type and Ehmt1^{adipo} mice. Two minutes after the injection, liver tissues were lysed. Phosphorylated (S473) and total Akt proteins were detected by Western blotting. The bands were quantified by Image J software. n=5 per genotype. Data are presented as mean and s.e.m.; ** P <0.01.

Table S1. Metabolic parameters of WT and Ehmt1^{adipo} KO mice at thermoneutrality.

Food intake (n=6)	WT	*Ehmt1*^{adipo}KO	*P* value
Food intake (day, g/12h)	0.9±0.1	1.0±0.1	*P* = 0.47
Food intake (night, g/12h)	1.8±0.1	1.7±0.1	*P* = 0.66

Serum (n=8)	WT	*Ehmt1*^{adipo}KO	*P* value
Insulin [mg/dl]	1.21±0.13	1.84±0.22 *	*P* < 0.05
Triglycerides [mg/dl]	78±3	72±6	*P* = 0.39
Free fatty acid [mmol/l]	0.61±0.03	0.61±0.06	*P* = 0.91

Weight (n=16)	WT	*Ehmt1*^{adipo}KO	*P* value
Body weight (g)	29.3±0.8	31.9±1.1 *	*P* < 0.05
Liver (g)	1.11±0.03	1.16±0.04	*P* = 0.39
Heart (g)	0.121±0.002	0.128±0.007	*P* = 0.47

Table S2. Primer sequences

Gene	Usage	Forward Primer	Reverse Primer
Acts	qPCR	CCCAAAGCTAACCGGGAGAAG	CCAGAATCCAACACGATGCC
Adipoq	qPCR	GCACTGGCAAGTTCTACTGCAA	GTAGGTGAAGAGAACGGCCTTGT
Atgl	qPCR	CCAACGCCACTCACATCTAC	CCTCAATAATGTTGGCACCTG
Cd137	qPCR	CGTGCAGAACTCCTGTGATAAC	GTCCACCTATGCTGGAGAAGG
Cgi58	qPCR	TGGTGTCCCACATCTACATCA	CAGCGTCCATATTCTGTTTCCA
Cidea	qPCR	ATCACAACTGGCCTGGTTACG	TACTACCCGGTGTCCATTTCT
Cited1	qPCR	AACCTTGGAGTGAAGGATCGC	GTAGGAGAGCCTATTGGAGATGT
Cox3a	qPCR	GCAGGATTCTTCTGAGCGTTCT	GTCAGCAGCCTCCTAGATCATGT
Cox5b	qPCR	GCTGCATCTGTGAAGAGGACAAC	CAGCTTGTAATGGGTTCCACAGT
Cox7a	qPCR	CAGCGTCATGGTCAGTCTGT	AGAAAACCGTGTGGCAGAGA
Cox8b	qPCR	GAACCATGAAGCCAACGACT	GCGAAGTTCACAGTGGTTCC
Cryab	qPCR	GTTCTTCGGAGAGCACCTGTT	GAGAGTCCGGTGTCAATCCAG
Dio2	qPCR	CAGTGTGGTGCACGTCTCCAATC	TGAACCAAAGTTGACCACCAG
Ehmt1	qPCR	GGCACCTTTGTCTGCGAATAC	AGAACCGAGCGTCAATGCAG
Elovl3	qPCR	TCCGCGTTCTCATGTAGGTCT	GGACCTGATGCAACCCTATGA
Fabp4	qPCR	ACACCGAGATTTCCTTCAAACTG	CCATCTAGGGTTATGATGCTCTTCA
Flnc	qPCR	GAAGGCCAACATCCGAGACAA	AGGGCGAGTAAGGGATCTCAT
Hsl	qPCR	CACACCTACTACACAAATCC	GGCATAGTAGGCCATAGCA
Mck	qPCR	GCAAGCACCCCAAGTTTGA	ACCTGTGCCGCGCTTCT
Mgll	qPCR	ACTCTGACCCACTCGTCTGC	CAGCAGGAATGGCAGTGTC
Mhc	qPCR	TCCAAACCGTCTCTGCACTGTT	AGCGTACAAAGTGTGGGTGTGT
Myf5	qPCR	CAGCCCCACCTCCAACTG	GGGACCAGACAGGGCTGTTA
Myl6b	qPCR	AAGCCTGCTGCCAAGTCTAC	ATCACCACTTTGGAGAGATCAAC
Mylpf	qPCR	TTCAAGGAGGCGTTCACTGTA	TAGCGTCGAGTTCCTCATTCT
Myod	qPCR	CGCCACTCCGGGACATAG	GAAGTCGTCTGCTGTCTCAAAGG
Myogenin	qPCR	CCTTAAAGCAGAGAGCATCC	GGAATTCGAGGCATATTATGA
Pde3b	qPCR	TCCTGAACATCTTGCCACTG	AGTACCGCGGAGGAAAAAGT
Pdli3	qPCR	TGGGGGCATAGACTTCAATCA	CTCCGTACCAAAGCCATCAATAG
Pgc1α	qPCR	AGCCGTGACCACTGACAACGAG	GCTGCATGGTTCTGAGTGCTAAG
PparY2	qPCR	GCATGGTGCCTTCGCTGA	TGGCATCTCTGAGTCAACCATG
Prdm16	qPCR	GGCGAGGAAGCTAGCCAAA	GGTCTCCTCCTCGGCACTCT
Ryr1	qPCR	CAGTTTTTGCGGACGGATGAT	CACCGGCCTCCACAGTATTG
Tbp	qPCR	ACCCTTCACCAATGACTCCTATG	TGACTGCAGCAAATCGCTTGG
Tnni1	qPCR	ATGCCGGAAGTTGAGAGGAAA	TCCGAGAGGTAACGCACCTT
Tpm2	qPCR	GTGGCTGAGAGTAAATGTGGG	TTGGTGGAATACTTGTCCGCT
Ucp1	qPCR	CACCTTCCCGCTGGACACT	CCCTAGGACACCTTTATACCTAATGG
Acts	ChIP qPCR	CCTGGACACACGATTGCTGAC	TTTCCATCCCTACCTGGAGC
Gapdh	ChIP qPCR	AAGCCAAACTAGCAGCTAGG	GGGCTAGTCTATCATTGCAG
Mylpf	ChIP qPCR	TCTTCCAGAACTGTGGGCTTCC	GGATGCAAGTCTCGTTAGGACC
Myogenin	ChIP qPCR	GAATCACATGTAATCCACTGGA	ACACCAACTGCTGGGTGCCA
Ryr1	ChIP qPCR	ACCTGTTGTCCCAAGTCCCATC	CCTTGGCTTCAGCCTTCTGC
Tnni1	ChIP qPCR	AGGGTCTCTGTTTGCTGACTG	AGGCTTCAGGAGGTAGACAG

REFERENCES

1. Nedergaard, J., T. Bengtsson, and B. Cannon, Unexpected evidence for active brown adipose tissue in adult humans. Am J Physiol Endocrinol Metab, 2007. 293(2): p. E444-52.
2. Saito, M., et al., High incidence of metabolically active brown adipose tissue in healthy adult humans: effects of cold exposure and adiposity. Diabetes, 2009. 58(7): p. 1526-31.
3. van Marken Lichtenbelt, W.D., et al., Cold-activated brown adipose tissue in healthy men. N Engl J Med, 2009. 360(15): p. 1500-8.
4. Virtanen, K.A., et al., Functional brown adipose tissue in healthy adults. N Engl J Med, 2009. 360(15): p. 1518-25.
5. Atit, R., et al., Beta-catenin activation is necessary and sufficient to specify the dorsal dermal fate in the mouse. Dev Biol, 2006. 296(1): p. 164-76.
6. Seale, P., et al., PRDM16 controls a brown fat/skeletal muscle switch. Nature, 2008. 454(7207): p. 961-7.
7. Timmons, J.A., et al., Myogenic gene expression signature establishes that brown and white adipocytes originate from distinct cell lineages. Proc Natl Acad Sci U S A, 2007. 104(11): p. 4401-6.
8. Kajimura, S., et al., Initiation of myoblast to brown fat switch by a PRDM16-C/EBP-beta transcriptional complex. Nature, 2009. 460(7259): p. 1154-8.
9. Kajimura, S., P. Seale, and B.M. Spiegelman, Transcriptional control of brown fat development. Cell Metab, 2010. 11(4): p. 257-62.
10. Shing, D.C., et al., Overexpression of sPRDM16 coupled with loss of p53 induces myeloid leukemias in mice. J Clin Invest, 2007. 117(12): p. 3696-707.
11. Pinheiro, I., et al., Prdm3 and Prdm16 are H3K9me1 methyltransferases required for mammalian heterochromatin integrity. Cell, 2012. 150(5): p. 948-60.
12. Tachibana, M., et al., Histone methyltransferases G9a and GLP form heteromeric complexes and are both crucial for methylation of euchromatin at H3-K9. Genes Dev, 2005. 19(7): p. 815-26.
13. Kleefstra, T., et al., Disruption of the gene Euchromatin Histone Methyl Transferase1 (Eu-HMTase1) is associated with the 9q34 subtelomeric deletion syndrome. J Med Genet, 2005. 42(4): p. 299-306.
14. Cormier-Daire, V., et al., Cryptic terminal deletion of chromosome 9q34: a novel cause of syndromic obesity in childhood? J Med Genet, 2003. 40(4): p. 300-3.
15. Willemsen, M.H., et al., Update on Kleefstra Syndrome. Mol Syndromol, 2012. 2(3-5): p. 202-212.

16. Kajimura, S., et al., Regulation of the brown and white fat gene programs through a PRDM16/CtBP transcriptional complex. Genes Dev, 2008. 22(10): p. 1397-409.
17. Seale, P., et al., PRDM16 controls a brown fat/skeletal muscle switch. Nature, 2008. 454: 961-967.
18. Schaefer, A., et al., Control of cognition and adaptive behavior by the GLP/G9a epigenetic suppressor complex. Neuron, 2009. 64(5): p. 678-91.
19. Tachibana, M., et al., G9a/GLP complexes independently mediate H3K9 and DNA methylation to silence transcription. EMBO J, 2008. 27(20): p. 2681-90.
20. Eguchi, J., et al., Transcriptional control of adipose lipid handling by IRF4. Cell Metab, 2011. 13(3): p. 249-59.
21. Almind, K., et al., Ectopic brown adipose tissue in muscle provides a mechanism for differences in risk of metabolic syndrome in mice. Proc Natl Acad Sci U S A, 2007. 104(7): p. 2366-71.
22. Cannon, B. and J. Nedergaard, Nonshivering thermogenesis and its adequate measurement in metabolic studies. J Exp Biol, 2011. 214(Pt 2): p. 242-53.
23. Ouellet, V., et al., Outdoor temperature, age, sex, body mass index, and diabetic status determine the prevalence, mass, and glucose-uptake activity of 18F-FDG-detected BAT in humans. J Clin Endocrinol Metab, 2011. 96(1): p. 192-9.
24. Wu, Q., et al., Fatty acid transport protein 1 is required for nonshivering thermogenesis in brown adipose tissue. Diabetes, 2006. 55(12): p. 3229-37.
25. Feldmann, H.M., et al., UCP1 ablation induces obesity and abolishes diet-induced thermogenesis in mice exempt from thermal stress by living at thermoneutrality. Cell Metab, 2009. 9(2): p. 203-9.
26. Yoneshiro, T., et al., Impact of UCP1 and beta3AR gene polymorphisms on age-related changes in brown adipose tissue and adiposity in humans. Int J Obes (Lond), 2013. 37(7): p. 993-8.
27. Huh, M.S., et al., Rb is required for progression through myogenic differentiation but not maintenance of terminal differentiation. J Cell Biol, 2004. 166(6): p. 865-76.
28. Mao, X., et al., APPL1 binds to adiponectin receptors and mediates adiponectin signalling and function. Nat Cell Biol, 2006. 8(5): p. 516-23.
29. Aune, U.L., L. Ruiz, and S. Kajimura, Isolation and differentiation of stromal vascular cells to beige/brite cells. J Vis Exp, 2013(73).
30. Takahashi, A., et al., DNA damage signaling triggers degradation of histone methyltransferases through APC/C(Cdh1) in senescent cells. Mol Cell, 2012. 45(1): p. 123-31.
31. Kurn, N., et al., Novel isothermal, linear nucleic acid amplification systems for highly multiplexed applications. Clin Chem, 2005. 51(10): p. 1973-81.

32. Trapnell, C., et al., Differential analysis of gene regulation at transcript resolution with RNA-seq. Nat Biotechnol, 2013. 31(1): p. 46-53.
33. Huang da, W., B.T. Sherman, and R.A. Lempicki, Systematic and integrative analysis of large gene lists using DAVID bioinformatics resources. Nat Protoc, 2009. 4(1): p. 44-57.
34. Kersey, P.J., et al., The International Protein Index: an integrated database for proteomics experiments. Proteomics, 2004. 4(7): p. 1985-8.
35. Elias, J.E. and S.P. Gygi, Target-decoy search strategy for increased confidence in large-scale protein identifications by mass spectrometry. Nat Methods, 2007. 4(3): p. 207-14.
36. Seale, P., et al., Transcriptional control of brown fat determination by PRDM16. Cell Metab, 2007. 6(1): p. 38-54.
37. Ohno, H., et al., PPARgamma agonists induce a white-to-brown fat conversion through stabilization of PRDM16 protein. Cell Metab, 2012. 15(3): p. 395-404.

CHAPTER. II

A synergistic anti-obesity effect by a combination of capsinoids and cold temperature through promoting beige adipocyte biogenesis

Chapter. II

A synergistic anti-obesity effect by a combination of capsinoids and cold temperature through promoting beige adipocyte biogenesis

INTRODUCTION

Obesity develops from a chronic imbalance in energy homeostasis between energy intake and energy expenditure. Currently all the available anti-obesity medications act by limiting energy intake through suppression of appetite or inhibiting intestinal lipid absorption; however, chronic use of such medications is often associated with adverse effects, such as depression and steatorrhoea (1). Over the past few years, a growing body of evidence from studies on rodent models and adult humans indicate that activating thermogenesis in brown adipose tissue (BAT) is a plausible alternative approach to modulate whole body energy balance (2).

Brown adipocytes dissipate chemical energy and produce heat through the BAT-specific mitochondrial protein uncoupling protein 1 (UCP1). UCP1's thermogenic capacity to uncouple cellular respiration from ATP synthesis is highly regulated by the activation of β-adrenoreceptors (β-AR) via the sympathetic nerve system (SNS). At a molecular level, catecholamines released from sympathetic nerve terminals binds to β-ARs in response to cold exposure, leading to the production of free fatty acid (FAA) by lipolysis. The produced FFA is a critical switch for UCP1's proton uncoupling activity (3). Indeed, extensive efforts have been made in order to pharmacologically activate BAT thermogenesis using synthetic β-AR agonists. Recently, it has been demonstrated that a

selective β3-AR agonist, Mirabegron, powerfully activates BAT metabolic activity, as assessed by ^{18}F-fluoro-2-deoxy-d-glucose positron emission tomography computed tomography (^{18}F-FDG-PET/CT) scans, which leads to increased resting metabolic rate in healthy adult humans who possess detectable BAT depots (4). On the other hand, efficacy of the β3-AR agonists was marginal or absent in obese population (5, 6). Furthermore, impaired expression and functional activity of β3-AR are reported in obese animals and in humans. As an example, a variant allele of the human β3-AR gene (64Trp/Arg) is associated with reduced β3-AR signaling (7, 8) and with increased BMI and adiposity (9, 10). Hence, it is important to understand the regulatory circuits that enhance the β-AR signaling pathway within adipose tissues such that clinically significant efficacy can be achieved even in obese subjects.

Rodents and humans possess two distinct forms of UCP1-positive thermogenic adipocytes: classical brown adipocytes and beige adipocytes (also referred to as brite adipocytes). While classical brown adipocytes and beige adipocytes share many functional characteristics (*i.e.*, thermogenesis), they are distinct cell types at developmental, anatomical, and molecular levels. Classical brown adipocytes are prenatally derived from a subset of dermomyotom, whereas beige/brite adipocytes postnatally emerge within white adipose tissue (WAT) in response to a certain environmental cues, such as chronic cold exposure, exercise, and long-term treatment with Peroxisome Proliferator-Activated Receptor-γ (PPARγ) agonists (11-13). The environmental cue-induced beige adipocyte biogenesis in WAT is often referred to as the WAT browning. Of note, it has been shown that molecular signatures of adult human BAT resemble mouse beige adipocytes (12, 14-17). Our recent study found that clonally-derived adult human brown adipocytes possess beige-like characteristics based on the

unbiased RNA-sequencing analyses (17). Furthermore, chronic cold exposure up to 6 weeks was able to recruit new active BAT depots in adult humans who did not possess appreciable levels of BAT depots before cold exposure (18-20). Importantly, an emergence of the newly recruited BAT was associated with an increase in cold-stimulated energy expenditure or with improved post-prandial insulin sensitivity. These studies suggest that adult human BAT is largely composed of the recruitable form of thermogenic adipocytes, that is, beige adipocytes. Hence, understanding molecular circuits that preferentially promote beige adipocyte biogenesis may provide a new opportunity of anti-obesity therapies for obese or old subjects who do not possess active BAT depots.

Capsinoids are capsaicin analogs found in a non-pungent type of chili pepper, 'CH-19 Sweet' (21, 22). While capsinoids differ from capsaicin in its chemical structure only at an ester-bond in the center linkage, it possesses substantially less pungency than capsaicin at least by 1000-fold. Curiously, dietary supplementation of capsinoids leads to an increase in energy expenditure and reduced body weight gain in animal models as well as in adult humans (23, 24). As an example, a recent study by Yoneshiro et al. showed that prolonged dietary supplementation of capsinoids for 6 weeks increased cold-induced thermogenesis in adult humans (20). Given the relevance of beige adipocytes in adult humans, it is hypothesized that chronic capsinoids treatment promotes beige adipocyte biogenesis. However, the underlying mechanisms remain poorly understood.

Here we report that dietary supplementation of capsinoids under mild cold environment (17˚C) powerfully and preferentially promotes beige adipocyte biogenesis in rodent models. This WAT browning effect by capsinoids was well associated with an increase in whole body energy expenditure. Gain- and loss-of-function studies showed that beige adipocyte biogenesis by capsinoids is mediated, in large part, through an

activation of the β2-adrenoceptor signaling pathway. Notably, we found that an activation of β2-adrenoceptor signaling pathway enhanced the protein half-life of PRDM16, a dominant transcriptional regulator of brown and beige adipocyte development. These results illuminate a molecular circuit that preferentially promotes beige adipocyte development *in vivo*. This study also suggests a plausible approach to increase whole body energy expenditure by dietary components.

Research Design and Methods

Animals

Male C57BL/6J mice were purchased from Charles River at 7 weeks of age. Triple knockout mice of the β1, β2, and β3-adrenoceptor (β-less mice) were a kind gift from Dr. B. B. Lowell at Harvard Medical School. Mice were kept at 17 ± 1°C (17°C) or 25 ± 1°C (25°C) in a controlled-light environment (12-hr cycle). The temperature was precisely controlled by an animal environmental control system (LP-30CCFL-8CTAR, NK system).

After one-week acclimation at 17°C or 25°C under a regular diet, the mice were randomly assigned into two groups. One group (n=6) was allowed *ad libitum* access to a high-fat diet (HFD) and the other group (n=6) received a HFD supplemented with 0.3% (w/w) capsinoids, which contain capsiate (62.7%), dihydrocapsiate (32.2%), and nordihydrocapsiate (5.5%) (Yoyu-Lab), for 8 weeks. Nutritional contents of the HFD containing capsinoids are provided in Table S1. The experiments in β-less mice were performed for 4 weeks.

For the pharmacological experiments using β-adrenoceptor antagonists, male 9-week-old C57BL/6 mice were kept at 17°C and fed a HFD or HFD supplemented with 0.3% capsinoids. Mice were injected subcutaneously with a β2-adrenoceptor antagonist

(ICI 118,551; TOCRIS) at a dose of 2 mg/kg/day or a β3-adrenoceptor antagonist (SR59230A; Sigma-Aldrich) at a dose of 1 mg/kg/day for 4 weeks. For the experiments using β-adrenoceptor agonists, 8-week-old male C57BL/6J mice were injected intraperitoneally (i.p.) with a β2-adrenoceptor agonist (formoterol; Santa Cruz) at a dose of 1 mg/kg or a β3-adrenoceptor agonist (CL316243; Sigma-Aldrich) at a dose of 1 mg/kg for 1 week. The dose of each compound was based on the previous studies using the β3 adrenoceptor agonist for the induction of beige adipocyte development in mice (15). All animal protocols were approved by the Animal Committee of Ajinomoto Co., Inc. or by the Institutional Animal Care and Use Committee at UCSF.

Metabolic parameters

Whole-body energy expenditure of mice was assessed using a metabolic chamber (ARCO2000-RAT/ANI System; Arco) as described previously (23). Mice were injected i.p. with vehicle (saline) or CL316243 at a dose of 0.01 mg/kg during the measurements. The respiratory quotient (VCO_2/VO_2) was calculated based on the study by Weir et al. (25). Spontaneous activity of the mice was simultaneously measured with an activity sensor (NS-AS01; Neuroscience). All measurements were performed at 4.5-min intervals.

For glucose tolerance test (GTT), mice were injected i.p. with glucose (1 g/kg) after a 6-hr fast. Insulin tolerance test (ITT) was performed by injecting insulin (0.75 U/kg) after an overnight fast. Blood glucose levels were measured using blood glucose test strips (Arkary) after 15-, 30-, 60-, and 120 min of injection. Fasting plasma glucose levels were determined using Fuji-drychem (Fujifilm). Plasma insulin levels were measured using a commercially available enzyme-linked immunosorbent assay (ELISA; Morinaga). Plasma triglyceride (TG) levels were measured using the TG-test Wako kit

(Wako). Total liver lipids were extracted with a chloroform:methanol mixture (2:1 v/v) as described by Folch et al. (26). The liver TG concentration in the lipid extracts was measured using the TG-test Wako kit (Wako).

Cell culture

Stromal vascular (SV) fraction was isolated as described by Ohno et al. (27). Adipocyte differentiation was induced in advanced DMEM/F12 medium (D-glucose, 25 mM) containing 10% fetal bovine serum (FBS), 0.5 mM isobutylmethylxanthine, 125 nM indomethacin, 5 μM dexamethasone, 850 nM insulin, and 1 nM T3. Two days later the cells were placed in maintenance medium containing 10% FBS, 850 nM insulin, and 1 nM T3.

For PRDM16 knockdown experiments in cultured adipocytes, we infected inguinal WAT-derived SV cells with adenoviral vectors expressing short-hairpin RNA targeting PRDM16 or a scramble control (27). The cells were allowed to differentiate for 7 days into mature adipocytes in the absence or presence of 1 μM of the β2-adrenoceptor agonist formoterol.

Gene expression analysis

Total RNA was isolated using Ribozol (AMRESCO) according to the manufactures protocol. Reverse transcription reactions were performed using an iScript cDNA synthesis kit (Bio-Rad). The primer sequences used in the amplification are shown in Table S2. qRT–PCR was performed with iTaq Fast SYBR green Supermix (Bio-Rad) using an ABI ViiA7 PCR machine (Life Technologies). Relative mRNA expression was determined by the ΔΔ-Ct method using TATA-binding protein (TBP) as an internal

control.

Western blotting

Total tissue lysates from BAT and WAT were prepared in RIPA buffer containing 25 mM Tris-HCl (pH 7.6), 1% NP-40, 0.5% sodium deoxycholate, 0.1% SDS, and 150 mM NaCl supplemented with 1% protease inhibitor (Nacalai tesque). The protein content was determined by Bradford method (Bio-Rad). Proteins were separated by using 7.5% or 10% SDS-polyacrylamide gels and transferred to nitrocellulose membranes (Bio-Rad). The membranes were subsequently probed with antibodies for UCP1 (ab10983; Abcam, 1:2000 dilution) or Prdm16 (ab106410; Abcam, 1:2000 dilution). A β-actin antibody (ab8228; Abcam, 1:5000 dilution) was used as a loading control. Proteins were detected using horseradish peroxidase-conjugated IgG secondary antibody (goat anti-rabbit IgG-HRP, 4010-05; Southern Biotech, 1:10000 dilution) and Chemi-Lumi One Super (Nacalai tesque).

Immunohistochemistry

Tissues were fixed overnight at 4°C in 4% paraformaldehyde, washed three times in phosphate-buffered saline (PBS), infiltrated with 12.5 - 30% sucrose followed by OCT compound, and frozen in liquid nitrogen. Using a Leica CM3050S cryostat (Leica Microsystems), 8 - 12 μm-thick sections were cut, fixed, permeabilized in 10 mM citric acid (pH 6.0) for 20 min at 121°C, and incubated for 20 min with 2% BSA in PBS. They were incubated for 1 hr with an antibody for UCP1 (ab10983; Abcam, 1:2000 dilution) followed by incubating with secondary HRP-conjugated antibodies (goat anti-rabbit IgG-HRP, 4010-05, Southern Biotech, 1:200 dilution) and detected with the AEC Chromogen

Kit (Sigma).

Protein stability assay

Inguinal WAT-derived SV cells were differentiated into mature adipocytes in the presence or absence of 1 μM formoterol. Subsequently, the differentiated adipocytes were incubated in medium containing cycloheximide (20 μg/ml) for 1-, 8-, 16-, and 24 hrs. Cell lysates were subjected to Western blotting to quantify the endogenous PRDM16 protein levels. β-actin was used as a loading control. Image J software was used for quantifying the signal intensity.

Oxygen consumption assays

Mice were anesthetized and transcardially perfused with Krebs-Ringer bicarbonate buffer (KRBH) containing 120 mM NaCl, 4 mM KH_2PO_4, 1 mM $MgSO_4$, 0.75 mM $CaCl_2$, 10 mM $NaHCO_3$, and 30 mM HEPES (pH 7.4). Adipose depots were carefully dissected and minced in KRBH supplemented with 0.45 mg/mL D-glucose, 10 mg/mL fatty acid-free BSA, and 1 mg/mL collagenase II (Sigma). After 1-hr incubation at 37°C adipose tissues were filtered through 200-μm nylon mesh and centrifuged at 200 x g for 1 min at ambient temperature. Oxygen consumption rate (OCR) of the isolated adipocytes (4 - 6 x 10^5 cells from inguinal WAT) was measured using a Clark-type oxygen electrode at 37°C in buffer containing KRBH supplemented with 0.486 mg/mL D-glucose and 40 mg/mL fatty acid-free BSA in a total volume of 2 ml. Saline or norepinephrine (100 nM) was added to assess thermogenic response to cAMP stimuli. OCR was measured every 0.5 sec up to 10 min.

Statistical analysis

Statistical analysis was performed by JMP version 10.0 (SAS Institute Inc.). Repeated-measures ANOVA were applied to compare the time courses. Statistical significance was determined with the unpaired two-tailed Student *t*-test for single- and two-way ANOVA followed by Bonferroni post-tests for multiple variables. Values are shown as the mean ± SEM unless otherwise stated. P values less than 0.05 were considered significant.

RESULTS

A synergistic anti-obesity effect by capsinoids and mild cold exposure.

We first examined if the effect of capsinoids on whole body energy metabolism is influenced by temperature. To this end, C57BL/6J male mice were fed a high fat-diet (HFD) containing capsinoids at a concentration of 0.3% or vehicle under ambient temperature (RT: 25°C) and mild cold conditions (17°C) for 8 weeks. Consistent with the previous studies (23), mice gained modestly but significantly less body weight under a capsinoids-supplemented diet compared to mice under a control-diet, when the mice were kept at ambient temperature. Strikingly, the anti-obesity effect by capsinoids was significantly enhanced under mild cold at 17°C (**Fig. 1A**). This anti-obesity effect by the combination of capsinoids and mild cold exposure was synergistic because capsinoids supplementation under 17°C led to a 31% suppression of diet-induced body weight gain compared to control mice, whereas capsinoids or mild cold exposure alone reduced body weight gain by 14% and 12%, respectively. The synergy is statistically significant based on the analysis by interaction plot (P=0.03). This synergistic anti-obesity effect was independent of changes in energy intake and behavior because no major difference was

observed in food intake and locomotor activity between vehicle and capsinoids treated groups both at ambient and cold temperature (**Fig. S1A and B**). Importantly, we found that the anti-obesity effect by capsinoids was completely blunted under thermoneutral conditions at 30°C (**Fig. 1B**). These data indicate that dietary supplementation of capsinoids promotes cold-induced thermogenesis *in vivo.*

We next measured changes in whole body O_2 consumption rate of mice treated with vehicle and capsinoids in response to the β3-adrenoceptor (AR) agonist CL316243 in order to mimic cold-induced activation of the β3-AR signaling. As shown in **Fig. 1C**, CL316243 significantly increased whole body O_2 consumption rate, representing BAT-mediated thermogenesis (28). The β3-AR agonist-induced whole-body O_2 consumption rate was increased in mice treated with capsinoids compared to vehicle-treated mice under 17°C (**Fig. 1C and S2**).

To further examine metabolic consequences of capsinoid supplementation and mild cold exposure, we assessed systemic glucose homeostasis and lipid metabolism of the mice by examining fasting glucose levels, insulin levels, and hepatic lipid contents. Consistent with the changes in body weight, we found that fasting plasma concentrations of glucose and insulin were significantly lower in mice treated with capsinoids under 17°C than those in vehicle-treated mice and in mice kept under ambient temperature (**Fig. 1D**). In addition, glucose tolerance and insulin sensitivity, as assessed by GTT and ITT, respectively, were significantly improved in mice treated with capsinoids under 17°C (**Fig. S3A and B**). We also found that hepatic steatosis was improved by the combination of capsinoids and mild cold because total lipids and triglyceride (TG) contents in the liver was significantly reduced in mice treated with capsinoids under 17°C (**Fig. 1E)**.

Capsinoids and mild cold exposure synergistically promote beige adipocyte biogenesis in inguinal WAT.

Based on the above observation that capsinoids supplementation under mild cold temperature at 17°C synergistically increased energy expenditure, we hypothesized that this increase was through an activation of the thermogenic program in the interscapular BAT depots and/or through recruitment of new beige adipocytes in the subcutaneous WAT depots. To this end, we first measured mRNA expression of the BAT-selective genes and beige adipocyte-selective genes in the inguinal WAT and in the interscapular BAT depots by qPCR. Expression of the BAT-selective genes, such as *Ucp1*, *Pgc1α*, and *Cidea*, and beige adipocyte-selective genes, such as *Cd137* and *Tmem26*, was significantly higher in the inguinal WAT of mice treated capsinoids under 17°C, compared to that in vehicle-treated mice and in mice under ambient temperature (**Fig. 2A and S4A left panel**). No significant change was observed in the expression of a general adipogenic marker, *Adiponectin (Adipoq)* **(Fig.S5)**. We did not observe statistically significant changes in mRNA expression of the thermogenic genes and beige adipocyte-selective markers in the interscapular BAT depots by capsinoids treatment, although the UCP1 mRNA levels were about 100 fold higher in the BAT than in inguinal WAT (**Fig. 2A, S4A right panel, and Fig.S4B**).

Consistent with the increase in *Ucp1* mRNA expression, we also observed a striking increase in UCP1 protein expression in the inguinal WAT of mice treated with capsinoids under 17°C (**Fig. 2B, left panel**). In contrast, we did not observe major changes in UCP1 protein expression in the interscapular BAT by capsinoids and mild cold exposure (**Fig. 2B, right panel**), although UCP1 expression in BAT was 50-fold higher than in inguinal WAT when normalized to β-actin (**Fig. 2B and S6**). This significant

increase in UCP1 expression in the inguinal WAT was tightly associated with an increase in the number of UCP1-positive beige adipocytes containing multilocular lipid droplets (**Fig. 2C, left panels**). We did not observe major changes in UCP1 density in the interscapular BAT depots, while adipocyte size appeared smaller in the BAT from mice treated with capsinoids (**Fig. 2C, right panels**).

To examine thermogenic function of the newly recruited beige adipocytes, we measured cellular respiration of adipocytes isolated from the inguinal WAT of mice treated with capsinoids under 17°C or ambient temperature. As shown in Fig. 2D, adipocytes from mice treated with capsinoids under 17°C exhibited significantly higher cellular respiration in response to norepinephrine (NE) stimulation, while no major change was seen in adipocytes from vehicle-treated mice and from mice under ambient temperature. Together, these results suggest that a combination of capsinoids supplementation and mild cold exposure synergistically and preferentially promote beige adipocyte biogenesis *in vivo*.

Although capsinoids are hydrolytically unstable under aqueous conditions and quickly degraded in the gastrointestinal tract (29), we tested the possibility that capsinoids in the circulation may directly promote beige adipocyte biogenesis using the plasma from mice fed with capsinoids. The plasma samples were isolated from the mice that exhibited higher levels of UCP1 and other beige-selective gene expression by capsinoids treatment. As shown in **Fig. S7**, the plasma from mice fed with capsinoids did not affect the expression of thermogenic genes in inguinal WAT-derived primary adipocytes.

The β-adrenoceptor pathway is required for the capsinoids-induced anti-obesity effect and beige adipocyte biogenesis.

We have previously shown that capsinoids activate the sympathetic nervous system through the gastrointestinal TRPV1 channel (30). Since β-adrenoceptors (β-ARs) play a dominant role in the control of brown and beige adipocyte biogenesis, we hypothesized that capsinoids act through the β-adrenergic signaling pathway to promote beige adipocyte development. To test this hypothesis, we treated β-less mice (31) that lack all three forms of β-ARs (*i.e.,* β1, β2, and β3-ARs) with capsinoids under 17°C. As β-less mice were bred in mixed genetic background (FVB/C57BL6/DBA/2/129SvJ) (31), we used the corresponding age-matched wild-type (WT) mice (6 week old) in mixed genetic background as a control group. Hereafter, we performed all the metabolic studies under 17°C. Consistent with the results in C57BL/6J strain, capsinoids treatment for 4 weeks significantly (although modestly) suppressed high fat diet-induced body weight gain in WT mice (**Fig. 3A, left panel**). In contrast, the suppression in body weight gain by capsinoids treatment was completely abolished in β-less mice (**Fig. 3A, right panel**). Expression of BAT-selective genes, such as *Ucp1, Pgc1α,* and *Dio2* was significantly higher in the inguinal WAT of wild-type mice treated with capsinoids under 17°C, whereas this induction was largely impaired in β-less mice (**Fig. 3B, top panel**). Consistent with the previous study (31), basal level of *Ucp1* expression was significantly lower in the interscapular BAT of beta-less mice compared to that of wild-type mice. However, capsinoids treatment did not alter the BAT-selective gene expression in the interscapular BAT of wild-type and β-less mice (**Fig. 3B, bottom panel**). Similarly, capsinoids treatment increased UCP1 protein expression in the inguinal WAT of WT mice but not in that of β-less mice (**Fig. 3C**). These results suggest that the β-adrenergic pathway is required for the capsinoids-induced beige adipocyte biogenesis.

β2-adrenoceptor mediates the capsinoids-induced beige adipocyte biogenesis.

Since three types of β-ARs (β1, β2, and β3-AR) are expressed in WAT, we next asked which form of the β-ARs mediates the biological effect of capsinoids on the browning of WAT *in vivo*. Of note, we found that expression of β2-AR was significantly higher in the inguinal WAT of mice treated with capsinoids, while no significant difference was observed in the expression of β1-AR and β3-AR (**Fig. 4A**). Hence, we hypothesized that capsinoids promote beige adipocyte biogenesis through the β2-AR pathway. To this end, we examined the requirement of β2-AR signaling on the WAT browning by using a specific β2-AR antagonist (ICI 118,551). As shown in **Fig. 4B, left panel**, mice co-treated with capsinoids and the β2-AR antagonist ICI 118,551 at a dose of 2 mg/kg/day near completely abolished the anti-obesity effect of capsinoids in mice even under 17°C. Expression of the BAT-selective genes, such as *Ucp1*, *Cidea,* and *Dio2*, in the inguinal WAT was significantly increased by the capsinoids treatment under 17°C; however, such induction was completely blunted when the β2-AR antagonist was co-administered (**Fig. 4C).** Consistent with the changes in gene expression levels, co-treatment with the β2-AR antagonist blocked the increase in UCP1 protein expression by capsinoids **(Fig. 4D**). Intriguingly, we found that the β3-AR antagonist (SR59230A) did not block the increase in UCP1 protein and mRNA expression by capsinoids, indicating that a selective requirement of β2-AR for the capsinoids-induced beige adipocyte biogenesis (**Fig. 4B, right panel and 4D**).

We next tested if activation of the β2-AR pathway is sufficient to promote beige adipocyte biogenesis *in vivo*. Mice were treated with the β2-AR agonist (formoterol) or the β3-AR agonist (CL316243) at a dose of 1 mg/kg for 1 week. Formoterol is known to selectively bind and activate β2-AR as compared to β3-AR by 645.7 fold (32). As shown

in **Fig. 4E**, the β2-AR agonist significantly increased mRNA expression of the BAT-selective genes, such as *Ucp1, Cidea* and *Cox8b*, in the inguinal WAT, without affecting mRNA expression of β-ARs. Additionally, other β2-AR agonists (selevtivity to β2-AR compared to β3-AR; Procaterol: 1318.36 fold and Salmeterol: 851.1 fold) also recruited browning (**Fig. S8**). Formoterol also powerfully increased UCP1 protein expression (**Fig. 4F)** as well as the number of multilocular beige adipocytes in inguinal WAT (**Fig. 4G**). These data support our hypothesis that the β2-adrenoceptor pathway largely mediates the effects of capsinoids in promoting beige adipocyte biogenesis *in vivo*.

Capsinoids stimulate a stabilization of the PRDM16 protein thorough the β2-AR pathway.

PRDM16 functions as a dominant transcriptional regulator of brown and beige adipocyte development (33-37). We have previously shown that protein stabilization of PRDM16 is a crucial event for PPARγ agonist-induced beige adipocyte development (27). Notably, we found that capsinoids robustly increased PRDM16 protein expression in the inguinal WAT of mice under ambient temperature and 17°C without affecting its mRNA levels **(Fig. 5A).** Furthermore, the increase in PRDM16 protein expression by capsinoids was completely abolished in β-less mice (**Fig. 5B**) as well as in mice injected with the β2-AR antagonist (ICI 118,551) (**Fig. S9**). These results indicate that capsinoids stimulate PRDM16 protein accumulation through the β2-AR pathway.

To test if an activation of the β2-AR pathway is sufficient to increase PRDM16 protein expression, we injected WT mice with the specific β2-AR agonist formoterol at 1 mg/kg for 1 week. As shown in **Fig. 5C**, treatment with the β2-AR agonist led to a robust increase in PRDM16 protein expression in the inguinal WAT. This increase in PRDM16

protein expression was tightly correlated with increases in BAT-selective gene expression and the number of UCP1-positive beige adipocytes, as shown in **Fig. 4E-G**. Furthermore, we found that the β2-AR agonist increased PRDM16 protein expression in a cell-autonomous manner, as formoterol treatment in cultured inguinal WAT-derived primary adipocytes increased PRDM16 protein expression without affecting its mRNA expression (**Fig. 5D).** Consistent with the animal experiments, the β2-AR agonist-induced PRDM16 protein expression was highly correlated with an increase in BAT-selective gene expression *in vitro* (**Fig. S10**). The β3-AR agonist did not increase PRDM16 protein expression **(Fig. 5D)**, indicating that that β3-AR activation may induce browning of WAT through a distinct mechanism from β2-AR agonist.

Next we tested if the accumulation of PRDM16 protein by β2-AR stimulation was due to changes in the rate of protein degradation. To this end, we measured the protein half-life of endogenous PRDM16 by cycloheximide chase experiments in inguinal WAT-derived primary adipocytes. As shown in **Fig. 5E**, the β2-AR agonist formoterol powerfully extended the protein half-life of PRDM16 from 5.6 hr to 23.9 hr. Lastly, we tested the requirement of PRDM16 for the β2-AR agonist-induced browning effect. To this end, inguinal WAT-derived primary preadipocytes were infected with adenoviral vectors expressing short-hairpin RNA targeting PRDM16 (sh-PRDM16) or a scramble control (sh-scr) in the presence or absence of formoterol at a dose of 1 μM throughout adipocyte differentiation. As shown in **Fig. 5F and 5G**, the β2-AR agonist formoterol did not increase UCP1 expression when adipocytes were depleted with PRDM16. All together, these data indicate that capsinoids act through the β2-AR pathway to stimulate PRDM16 protein stabilization, leading to a powerful activation of the beige adipocyte gene program in inguinal WAT.

DISCUSSION

Capsinoids, including capsiate, dihydrocapsiate, and nordihydrocapsiate, are unique capsaicin analogs that are found abundantly in a non-pungent type of chili pepper, 'CH-19 Sweet' (21, 22). The three forms of capsinoids can directly bind to TRPV1 at a similar binding affinity to capsaicin; however, the capsinoids' potency to increase intercellular Ca^{2+} levels was approximately 10 times lower than capsaicin (38). In addition, chemical structure of capsinoids is distinct from capsaicin at an ester bond, making capsinoids hydrolytically unstable in an aqueous environment, such that capsinoids are quickly degraded in the gastrointestinal tract and not detectable in circulation (29). Hence, capsinoids promote the browning of WAT largely through the CNS-mediated signaling, rather than the direct action via circulation (see **Fig. S5**). How does capsinoids synergistically promote BAT-mediated thermogenesis together with mild cold exposure *in vivo*? As illustrated in Fig. 6, previous studies have shown that capsinoids act on TRPV1 in the gut, leading to an activation of vagal afferent nerves that project into the ventromedial hypothalamus (VMH) (30). Capsinoids also activate several brain regions, including VMH, in a TRPV1-dependent fashion (39). Of note, the VMH is known to control BAT-mediated thermogenesis by stimulating sympathetic efferent (40, 41) and also promote beige adipocyte biogenesis in WAT (42), likely through rRPa neurons (43). In addition, we found that capsinoids increased β2-AR expression in the inguinal WAT. On the other side, cold exposure acts on distinct neuronal circuits from capsinoids to activate thermogenesis. In response to cold exposure, thermal sensory receptors transmit signals to second-order thermal sensory neurons in the dorsal horn (DH). These neurons activate the signal to the preoptic area (POA) where GABAnergic

neurons control the outputs to the neurons at the dorsomedial nucleus of the hypothalamus (DMH) and subsequently in the rostral raphe pallidus nucleus (rRPa) (44). Hence, it is conceivable that capsinoids and mild cold exposure stimulate the respective neuronal circuits independently such that a combination of the two independent stimuli promotes an additive thermogenic response more potently than single stimulation alone.

Within the inguinal WAT of mice treated with capsinoids, we found that PRDM16 protein level was robustly increased without affecting its mRNA expression. PRDM16 functions as a dominant transcriptional regulator of brown and beige adipocyte development (33-37). Requirement of PRDM16 for beige adipocyte development has been demonstrated by the recent studies in which adipose-specific depletion of PRDM16 significantly impairs beige adipocyte biogenesis in response to cold exposure or to chronic treatment with PPARγ agonists (27, 33). We have shown that PPARγ agonists, such as rosiglitazone, promote beige adipocyte differentiation by powerfully extending the protein half-life of PRDM16 through inhibiting E3 ligase-mediated ubiquitination (27). In addition, rosiglitazone deacetylates PPARγ on Lys268 and Lys293 by Sirt1, leading to an enhanced complex formation between PRDM16 and PPARγ (45). In this study, we found that capsinoids treatment induces the protein stabilization of PRDM16 via the β2-AR signaling. It has been known that an activation of β2-AR leads to phosphorylation of protein kinase A (PKA), p38 mitogen-activated protein kinase (p38MAPK), extracellular signal-regulated kinase (ERK), and AMP-activated protein kinase (AMPK) (46-48). It is possible that PRDM16 protein is phosphorylated in response to an activation of β2-AR signaling, leading to an increase in the PRDM16 protein stability. Future studies are warranted to better understand the molecular mechanisms by which β2-AR signal extends the half-life of PRDM16 protein.

Previous studies have shown that obese propensity in response to a high-fat diet is highly strain dependent (49). In addition, browning capacity in the subcutaneous WAT depot is highly variable among mouse strains (50-52). While we found that anti-obesity and browning effects by mild cold exposure and capsinoids was more potent in C57BL/6J background than in mixed background, the anti-obesity and browning effects were consistently observed in both strains. On the other hand, previous studies showed that capsinoids' effects on hepatic steatosis were observed even under ambient temperature. For instance, treatment of capsinoids alone was sufficient to reduce hepatic lipid and TG contents by 44% and 29%, respectively. The present study also found that capsinoids treatment increased the expression of genes involved in hepatic fatty acid oxidation, such as *Hsl*, *Atgl*, and *Aco*, under ambient temperature (**Fig. S11**). This increase in hepatic fatty acid oxidation may contribute to the improvement in lipid metabolism in the liver (*e.g.*, reduced hepatic lipid and TG contents) by capsinoids treatment. Relative contribution of liver versus adipose tissue to the improvement of systemic glucose homeostasis remains to be determined.

Biological significance of beige fat in whole body metabolism has been a topic of discussion because total expression level of UCP1 protein in beige fat is substantially lower than that found in interscapular BAT depots even though beige adipocytes are functionally thermogenic (**Fig.S6**) (53). In this study, we found that an increased beige fat mass by capsinoids and mild cold exposure was tightly associated with an increase in whole body energy expenditure. Importantly, the increase in energy expenditure leads to a robust reduction in body weight gain under a high-fat diet, indicating that beige fat significantly contributes to the regulation of whole body energy expenditure. This is consistent with several genetic mouse models in which selective modulation of beige fat

mass is sufficient to alter whole body metabolism. For example, transgenic expression of PRDM16 driven by the *Fabp4* gene promoter preferentially stimulates the formation of beige adipocytes in the subcutaneous WAT depots without major changes in the interscapular BAT depots. The *Fabp4*-PRDM16 transgenic mice exhibit increased whole body energy expenditure and reduced body weight gain under a high-fat diet (54). Conversely, adipose-selective genetic deletion of *Prdm16* or its co-factor EHMT1 by using *Adiponectin*-Cre mice selectively attenuates beige adipocyte development and reduces whole body energy expenditure (33, 55). It is also important to note that beige fat plays a major role in systemic glucose and lipid homeostasis. Because brown and beige adipocytes possess high oxidative phosphorylation capacity, they function as a "metabolic sink" for glucose and fatty acids. Indeed, we found that liver TG level was strikingly lower in mice treated with capsinoids under mild cold in parallel with an increased beige fat mass. Conversely, developmental defect in brown/beige adipocytes is sufficient to cause hepatic steatosis and insulin resistance in mice (33, 55). Hence, the therapeutic benefit of increased beige fat mass is not limited to anti-obesity effects *per se*, but also can include improvements in hepatic steatosis and insulin resistance.

In summary, the current study found a previously unappreciated molecular circuit that preferentially promotes beige adipocyte biogenesis *in vivo*. Given the relevance of this cell type in adult humans, this study also illuminates a plausible approach to increase whole body energy expenditure and to improve lipid and glucose homeostasis by combining dietary components and environmental cues. It has been reported that chronic supplementation of capsinoids at a dose of 9 mg per day for 6 weeks was able to increase cold-stimulated whole-body energy expenditure even in adult humans who lacked detectable active BAT depots before the treatment (20). Since 1 g dry weight of CH-19

sweet contains approximately 5 mg of capsinoids (56), we speculate that supplementary intake would be a realistic approach to achieve the levels of capsinoids that can activate BAT thermogenesis. Future studies aim to establish practical approaches to activate BAT thermogenesis by capsinoids supplementation and mild cold with no deleterious effects.

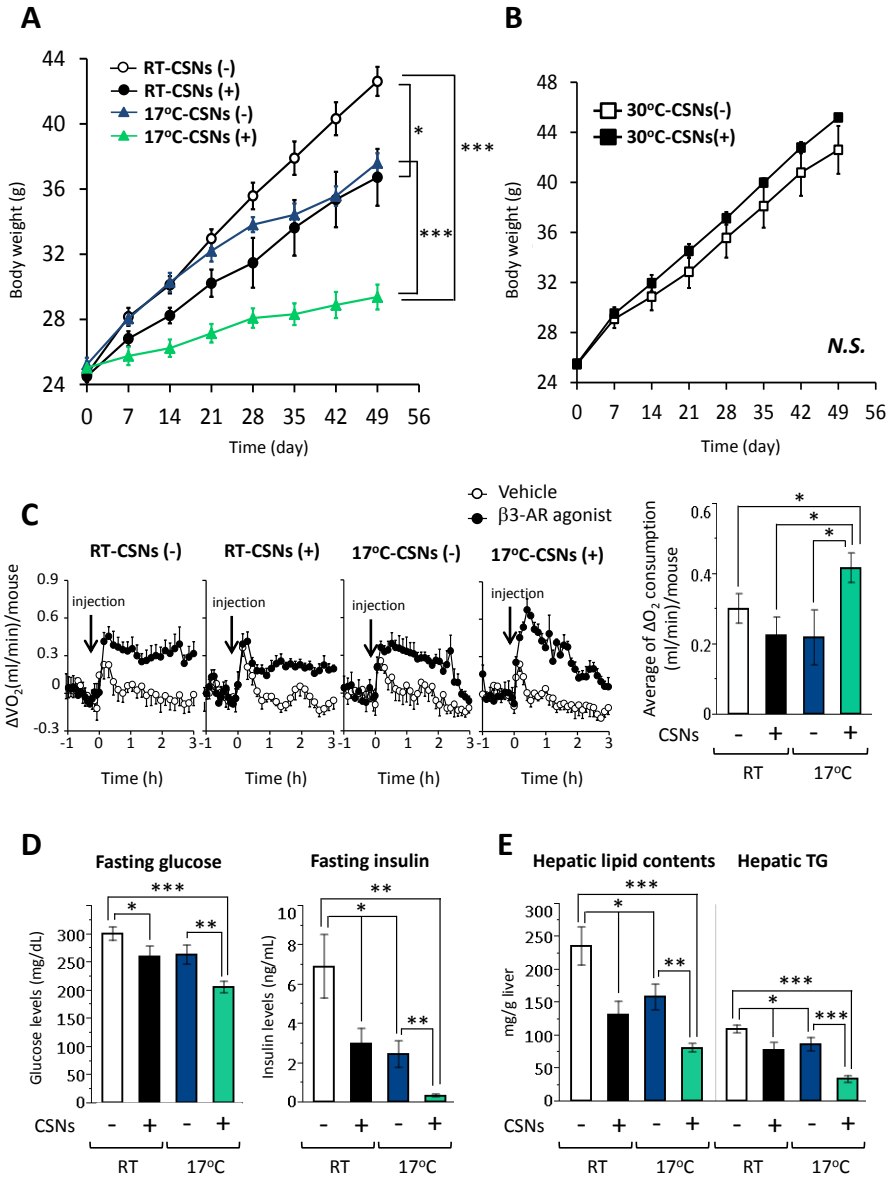

Figure 1

Capsinoids and mild cold exposure synergistically suppressed body weight gain and increased whole-body energy expenditure under a high-fat diet.

(A) Changes in body weight (BW) of C57BL/6J male mice (n=6). Mice were fed a high-fat diet supplemented with 0.3% capsinoids (CSNs+) or vehicle (CSNs-) for 8 weeks under ambient temperature (RT) or 17°C. Data are expressed as the mean ± SEM. *p < 0.05, ***p < 0.001. (B) Changes in BW of C57BL/6J mice kept under thermoneutral conditions (30°C) (n=6). C57BL/6J male mice were fed a high-fat diet supplemented with 0.3% (CSNs+) or vehicle (CSNs-) for 8 weeks. N.S., not significant. (C) Whole-body O_2 consumption rate (ml/min) per mouse was measured in C57BL/6J male mice fed a high-fat diet supplemented with 0.3% capsinoids (CSNs+) or vehicle (CSNs-) at ambient temperature (RT) or at 17°C (n=6). To stimulate BAT-thermogenesis, mice were injected with vehicle (saline) or the β3-AR agonist (CL316243) at a dose of 0.01 mg/kg BW. O_2 consumption rate was monitored for 3 hours after the injection. Right; quantification of changes in VO_2 in response to CL316243. These changes were calculated by subtracting the VO_2 of vehicle-treated mice from the VO_2 of β3-AR agonist-treated mice. *p < 0.05. (D) Fasting blood glucose levels (left) and fasting insulin levels (right) in mice in (A). Mice were fasted for 3 hours prior to blood collection. *p < 0.05, **p < 0.01, ***p < 0.001. (E) Total lipid contents (left) and TG contents (right) were measured in the liver of mice in (A). *p < 0.05, **p < 0.01, ***p < 0.001.

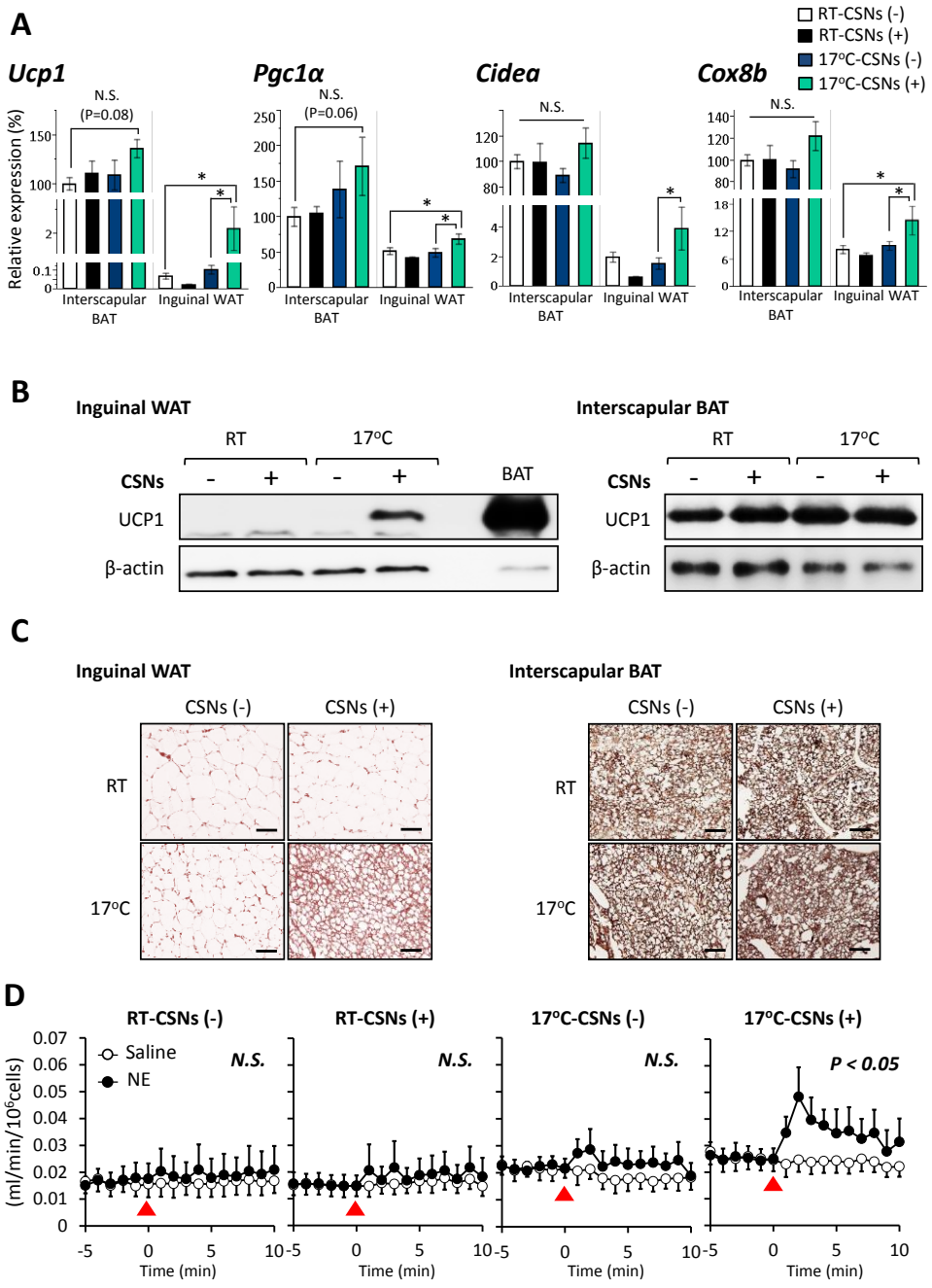

Figure 2

Capsinoids and mild cold exposure synergistically promote beige adipocyte biogenesis in inguinal WAT.

(A) Relative mRNA expression levels of *Ucp1*, *Pgc1α*, *Cidea*, and *Cox8b* were measured by qRT-PCR in the inguinal WAT and in the interscapular BAT of mice kept under RT or 17°C (n=6). Mice were fed a high-fat diet supplemented with 0.3% capsinoids (CSNs+) or vehicle (CSNs-) for 8 weeks. Data are expressed as the mean ± SEM. *p < 0.05. N.S., not significant. (B) UCP1 protein levels were analyzed by Western blotting in the inguinal WAT (left) and the interscapular BAT (right) from mice in (A). β-actin was used as a loading control. (C) Immunohistochemistry of UCP1 in the inguinal WAT (left) and the interscapular BAT (right) from mice in (A). Scale bar, 100 μm. (D) Cellular respiration was measured in isolated adipocytes from the inguinal WAT of mice in (A). To stimulate thermogenesis, the cells were treated with saline or norepinephrine (NE) at a dose of 1 μM at 0 time point (indicated by red arrowheads).

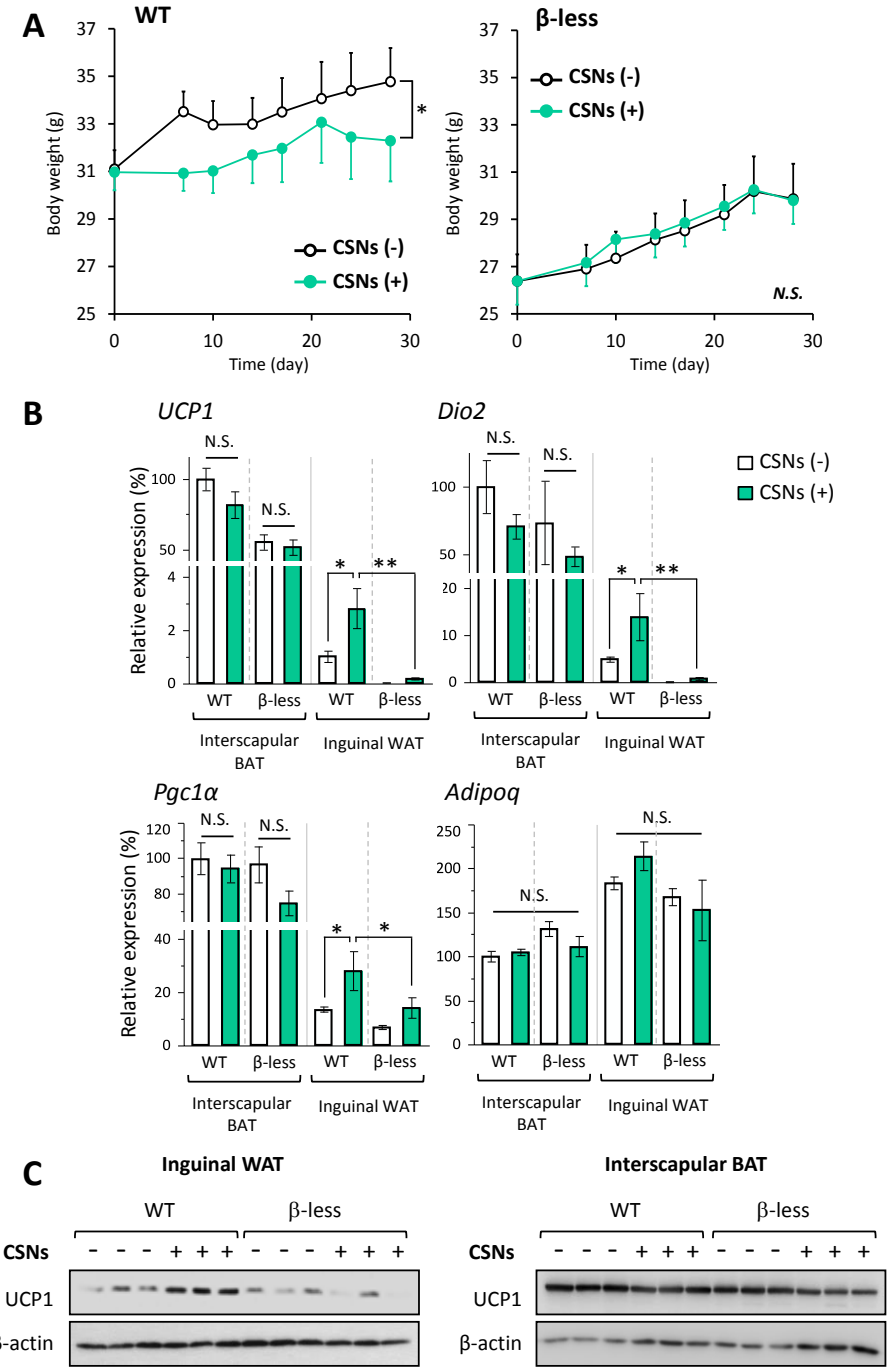

Figure 3

The β-adrenoceptor pathway is required for the capsinoids-induced anti-obesity effect and beige adipocyte biogenesis.

(A) Changes in BW of wild-type (WT, left) and β-less mice (right) that were fed a high-fat diet supplemented with 0.3% capsinoids (CSNs+) or vehicle (CSNs-) for 4 weeks (n=6-8). Mice were kept under 17°C throughout the experiments. Data are expressed as the mean ± SEM. *p < 0.05. N.S., not significant. (B) Relative mRNA expression levels of *Ucp1*, *Pgc1α*, *Dio2*, and *Adipoq* were measured by qRT-PCR in the inguinal WAT and the interscapular BAT from mice shown in (A). *p < 0.05. N.S., not significant. (C) UCP1 protein expression was analyzed by Western blotting in the inguinal WAT (left) and the interscapular BAT (right) from mice shown in (A). β-actin was used as a loading control.

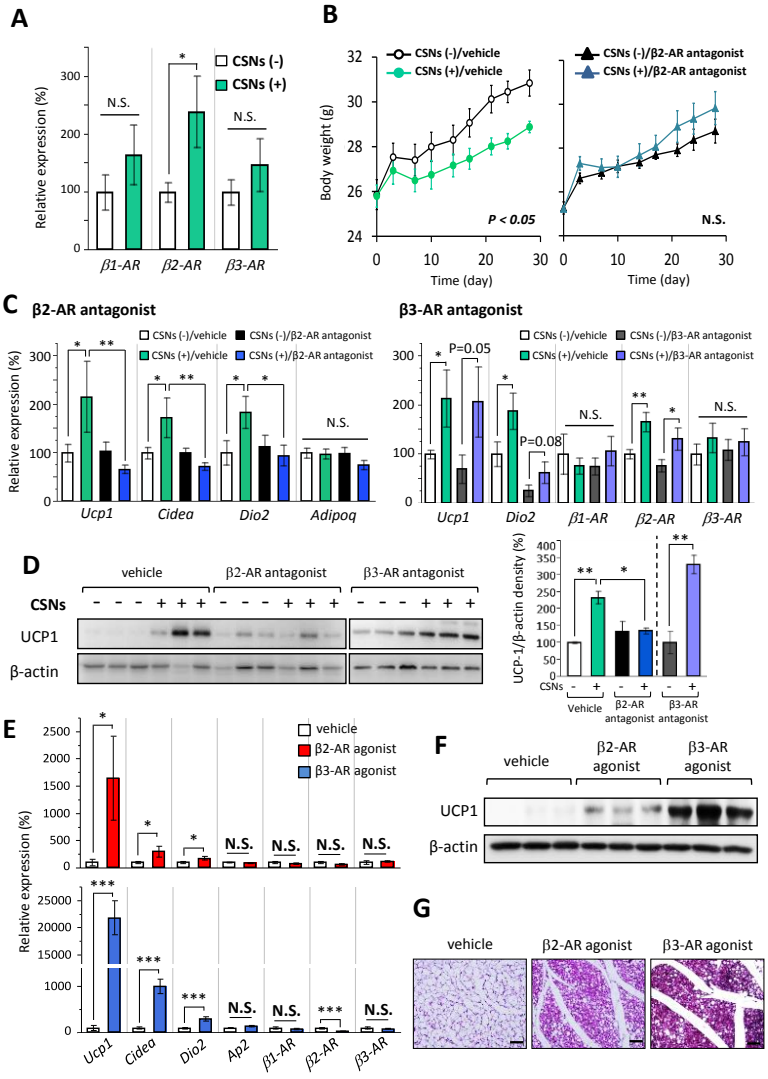

Figure 4

β2-adrenoceptor mediates the capsinoids-induced beige adipocyte biogenesis.

(A) Relative mRNA expression levels of *β1-AR, β2-AR, and β3-AR* were measured by qRT-PCR in the inguinal WAT of mice fed a high-fat diet supplemented with 0.3% capsinoids (CSNs+) or vehicle (CSNs-) for 8 weeks (n=6). Mice were kept under 17°C throughout the experiments. Data are expressed as the mean ± SEM. *p < 0.05. N.S., not significant. (B) Changes in BW of WT mice fed a high-fat diet supplemented with 0.3% capsinoids (CSNs+) or vehicle (CSNs-) for 4 weeks (n=6). The mice under 17°C were daily injected with vehicle (saline) or the β2-AR antagonist (ICI 118,551) at a dose of 2 mg/kg/day. N.S., not significant. (C) Relative mRNA expression levels of *Ucp1*, *Cidea*, *Dio2*, *Adipoq*, *β1-AR*, *β2-AR*, and *β3-AR* were measured by qRT-PCR in the inguinal WAT of mice in (B) and mice injected with vehicle (saline) or a β3-AR antagonist (SR59230A) at a dose of 1 mg/kg/day. *p < 0.05, **p < 0.01. (D) UCP1 protein expression was analyzed by Western blotting in the inguinal WAT of mice shown in (B) and mice injected with the β3-AR antagonist (SR59230A) at a dose of 1 mg/kg/day. β-actin was used as a loading control. Right; quantification of the UCP1/β-actin. Density of UCP1/β-actin was calculated by ImageJ. Data are expressed as the mean ± SEM. *p < 0.05, **p < 0.01. (E) Relative mRNA expression levels of of *Ucp1*, *Cidea*, *Cox8b*, *aP2*, *β1-AR*, *β2-AR*, and *β3-AR* were measured by qRT-PCR in the inguinal WAT of mice injected with vehicle (saline) or the β2-AR agonist (formoterol) at a dose of 1 mg/kg/day or β3-AR agonist (CL316234) at a dose of 1 mg/kg/day under ambient temperature for 1 week (n=6). *p < 0.05, ***p < 0.001. N.S., not significant. (F) UCP1 protein expression was analyzed by Western blotting in the inguinal WAT of mice shown in (E). β-actin was used as a loading control. (G) Hematoxylin and Eosin (H&E) staining of the inguinal WAT of mice shown in (E). Scale bar, 100 μm. Note that β2-AR agonist (formoterol) treatment lead to a striking increase in the number of multilocular adipocytes in the inguinal WAT.

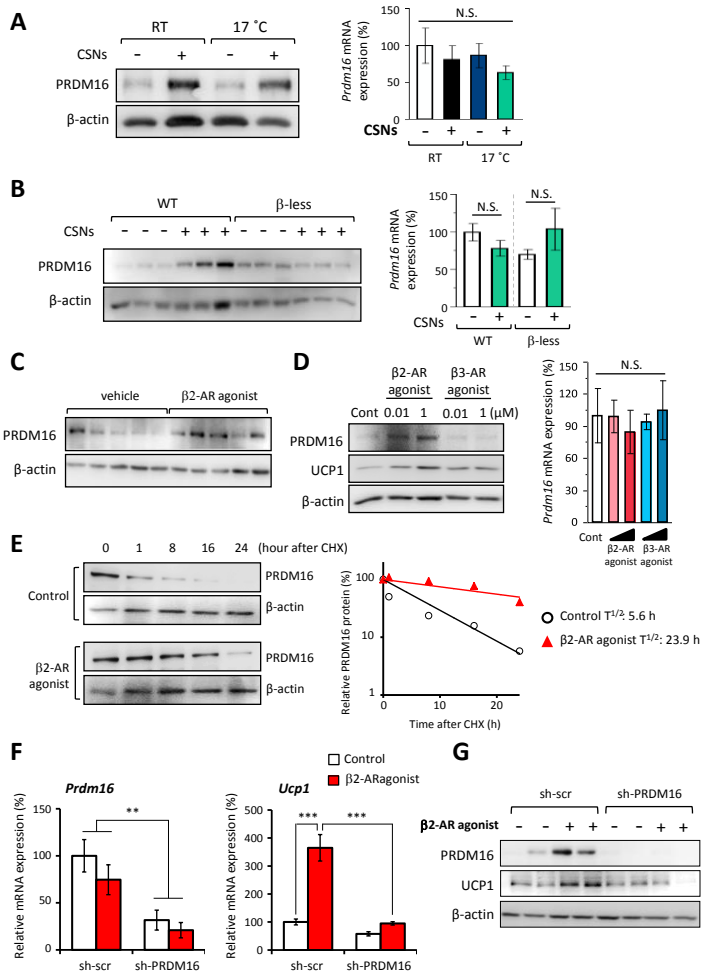

Figure 5

Capsinoids stimulates a stabilization of the PRDM16 protein thorough the β2-AR pathway.

(A)Endogenous PRDM16 protein (left) and relative mRNA expression of *Prdm16* (right) in the inguinal WAT of mice kept under ambient temperature (RT) or 17°C (n=6). Mice were fed a high-fat diet supplemented with 0.3% capsinoids (CSNs+) or vehicle (CSNs-) for 8 weeks. β-actin was used as a loading control for Western blotting. The Prdm16 *mRNA* expression data are expressed as the mean ± SEM. N.S., not significant. (B) Endogenous PRDM16 protein (left) and relative mRNA expression of *Prdm16* (right) in the inguinal WAT of wild-type (WT) mice and β-less mice under 17°C (n=6). Mice were fed a high-fat diet supplemented with 0.3% capsinoids (CSNs+) or vehicle (CSNs-) for 4 weeks. β-actin was used as a loading control for Western blotting. (C) PRDM16 protein expression was analyzed by Western blotting in the inguinal WAT of mice injected with vehicle (saline) or the β2-AR agonist (formoterol) at a dose of 1 mg/kg/day for 1 week (n=5). β-actin was used as a loading control. (D) Protein expression of PRDM16 and UCP1 was analyzed by Western blotting in primary inguinal WAT-derived adipocytes. The cells were cultured in the absence or presence of the β2-AR agonist (formoterol) or β3-AR agonist (CL316243) at doses of 0.01 and 1 μM throughout adipocyte differentiation (n=3). β-actin was used as a loading control. Relative *Prdm16* mRNA expression in these cells is shown in right panel. N.S., not significant. (E) Cycloheximide chase experiment in primary inguinal WAT-derived adipocytes. Endogenous PRDM16 protein expression was analyzed by Western blotting. Differentiated adipocytes were treated with vehicle or β2-AR agonist (formoterol) at a dose of 1 μM in the presence of cycloheximide for 1, 8, 16, and 24 hours. β-actin was used as a loading control. Regression analysis of PRDM16 protein stability was shown in the right graph. (F) Relative mRNA expression of *Prdm16* and *Ucp1* was measured by qRT-PCR in primary inguinal-WAT derived adipocytes infected with control scramble shRNA or shRNA targeting PRDM16 (n=3). The adipocytes were treated with vehicle (control) and the β2-AR agonist (formoterol) at a dose of 1 μM throughout adipocyte differentiation. **p < 0.01, ***p < 0.001. (G) PRDM16 and UCP1 protein expression was analyzed by Western blotting in the primary inguinal-WAT derived adipocytes shown in (F). β-actin was used as a loading control.

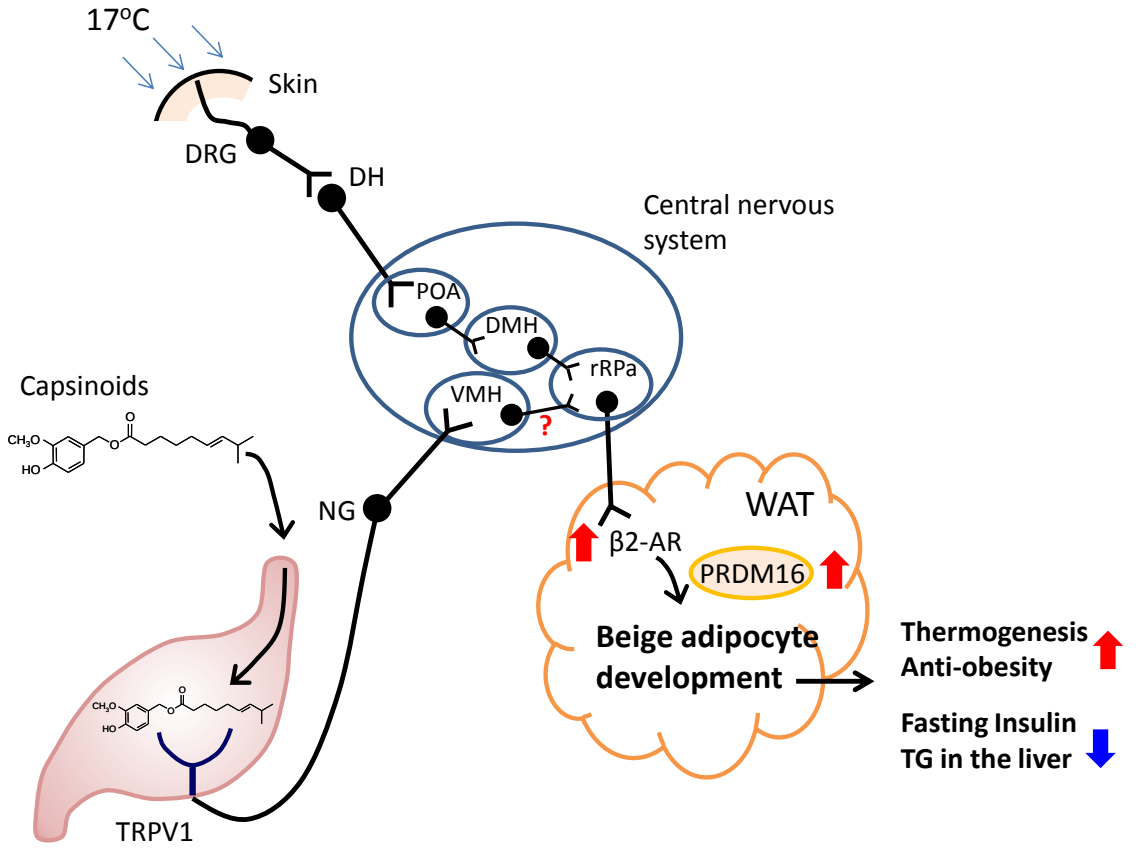

Figure 6

Proposed mechanisms by which capsinoids and mild cold temperature promote beige adipocyte biogenesis and energy expenditure.

Capsinoids bind to transient receptor potential vanilloid type 1 (TRPV1) in gut. The signal is transmitted to CNS *via* vagal nerves that project into the ventromedial hypothalamus (VMH). The signal is subsequently transmitted to subcutaneous WAT depots through the β2-adrenoceptor (AR) in inguinal WAT. Capsinoids increased the expression of β2-adrenoceptor. On the other side, cold is sensed by skin and transmitted to the somatosensory nerves through second-order thermal sensory neurons in the dorsal horn (DH). These neurons activate the signal to the preoptic area (POA) where GABAnergic neurons control the outputs to the neurons at the dorsomedial nucleus of the hypothalamus (DMH) and subsequently in the rostral raphe pallidus nucleus (rRPa). These stimuli synergistically promote beige adipocyte biogenesis through stabilizing PRDM16 protein in inguinal WAT, leading to an increase in whole body energy expenditure and a decrease in fasting insulin levels and hepatic triglyceride (TG) contents.

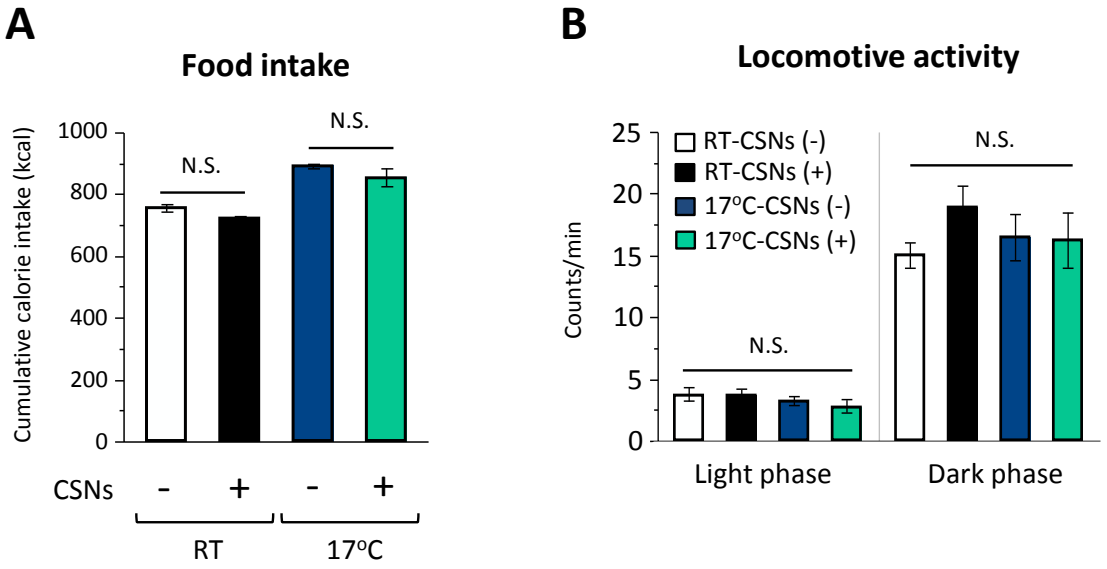

Figure S1.

Capsinoids treatment did not affect food intake and locomotor activity.

(A) Total cumulative food intake during 8 weeks cohort of C57BL/6J mice (n=6). Mice were fed a high-fat diet supplemented with 0.3% capsinoids (CSNs+) or vehicle (CSNs-) for 8 weeks under ambient temperature (RT) or 17°C. Data are expressed as the mean ± SEM. N.S., not significant.

(B) Locomotive activity was measured in mice in (A) during the light phase and dark phase. Data are expressed as the mean ± SEM. N.S., not significant.

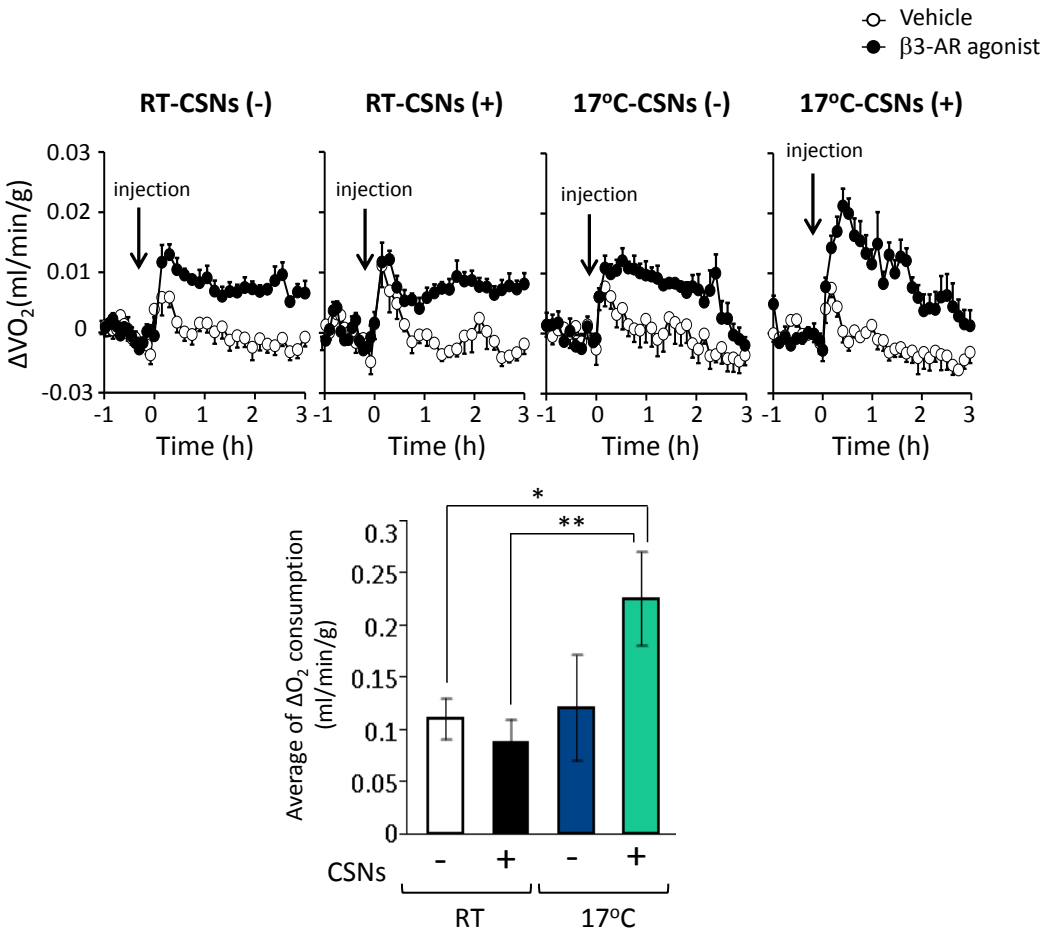

Figure S2

Capsinoids treatment under 17°C increased whole-body energy expenditure in response to to β3-adrenergic activation.

Whole body O_2 consumption rate (ml/min/g) was measured in C57BL/6J male mice fed a high-fat diet supplemented with 0.3% capsinoids (CSNs+) or vehicle (CSNs-) under ambient temperature (RT) or 17°C (n=6). To stimulate BAT-thermogenesis, mice were injected with vehicle (saline) or the β3-AR agonist (CL316243) at a dose of 0.01 mg/kg BW. O_2 consumption rate was monitored for 3 hours after the injection. Bottom; quantification of changes in VO_2 in response to CL316243. These changes were calculated by subtracting the VO_2 of vehicle-treated mice from the VO_2 of β3-AR agonist-treated mice. *$p < 0.05$, **$p < 0.01$.

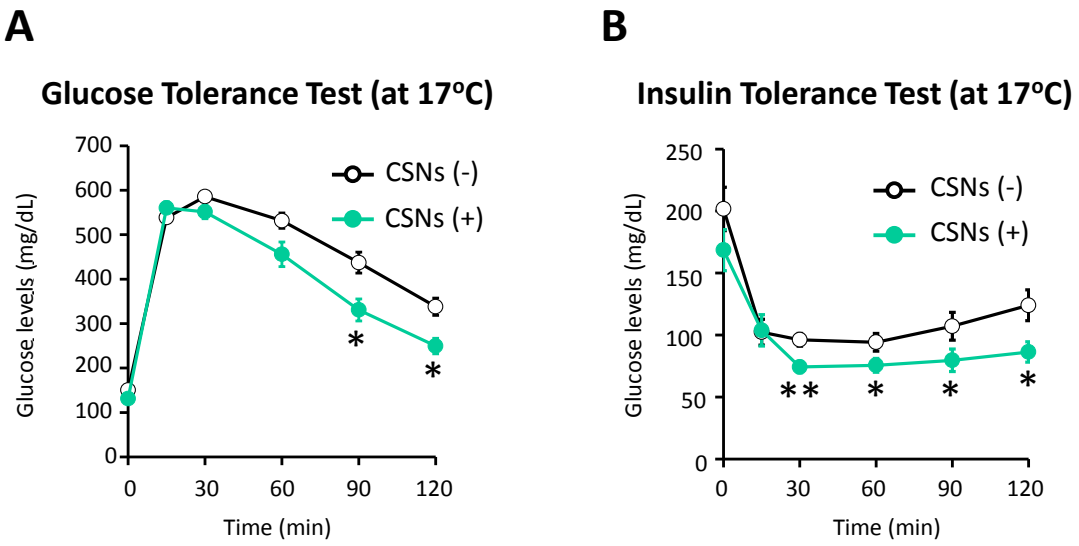

Figure S3.

Capsinoids treatment under 17°C improved systemic glucose homeostasis.

(A) Glucose tolerance test (GTT) was performed in mice fed a high-fat diet supplemented with 0.3% capsinoids (CSNs+) or vehicle (CSNs-) for 6 weeks under 17 ˚C (n=6). Blood glucose level was measured over the course of 120 min after injecting glucose at a dose of 2 g/kg BW. Data are expressed as the mean ± SEM. *p < 0.05 relative to vehicle treated (CSNs-) group.

(B) Insulin tolerance test (ITT) was performed in mice fed a high-fat diet supplemented with 0.3% capsinoids (CSNs+) or vehicle (CSNs-) for 7 weeks under 17 ˚C (n=6). Blood glucose level was measured over the course of 120 min after injecting insulin at a dose of 0.75 U/kg BW. Data are expressed as the mean ± SEM. *p < 0.05, **p < 0.01.

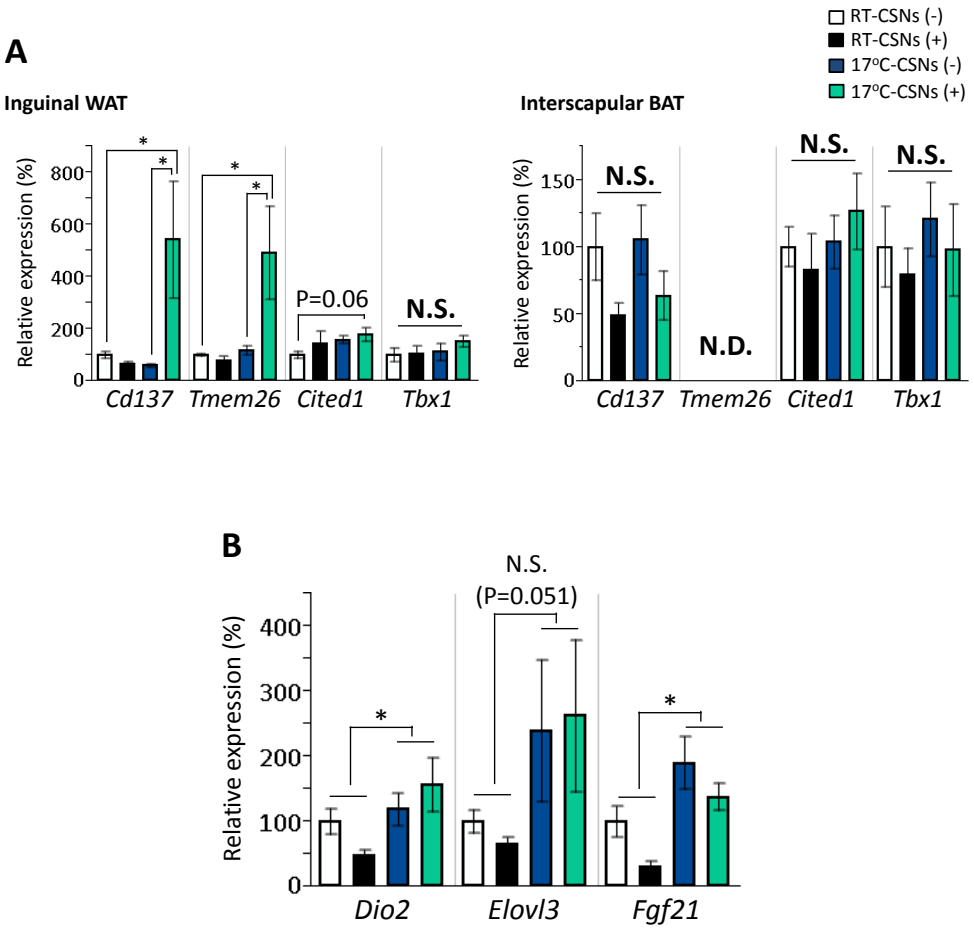

Figure S4

Capsinoids and mild cold exposure synergistically increased the expression of beige adipocyte-selective genes in inguinal WAT.

(A) Relative mRNA expression levels of *Cd137*, *Tmem26*, *Cited1*, and *Tbx1* were measured by qRT-PCR in the inguinal WAT (left) and in the interscapular BAT (right) of mice kept under RT or 17°C (n=6). Mice were fed a high-fat diet supplemented with 0.3% capsinoids (CSNs+) or vehicle (CSNs-) for 8 weeks. Data are expressed as the mean ± SEM. *p < 0.05. N.S., not significant.

(B) Relative mRNA expression levels of *Dio2*, *Elovl3*, and *Fgf21* were measured by qRT-PCR in the interscapular BAT of mice in (A). Data are expressed as the mean ± SEM. *p < 0.05. N.S., not significant.

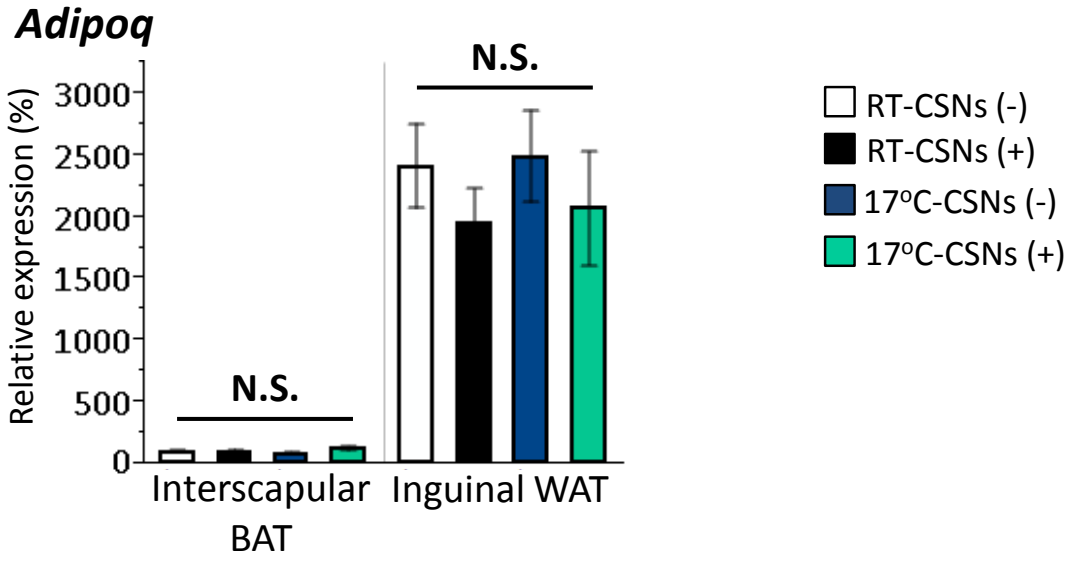

Figure S5

Expression levels of thermogenic genes in inguinal WAT and interscaplar BAT.

Relative mRNA expression levels of *Adipoq* were measured by qRT-PCR in the inguinal WAT and in the interscapular BAT of mice kept under RT or 17°C (n=6). Mice were fed a high-fat diet supplemented with 0.3% capsinoids (CSNs+) or vehicle (CSNs-) for 8 weeks. Data are expressed as the mean ± SEM. N.S., not significant.

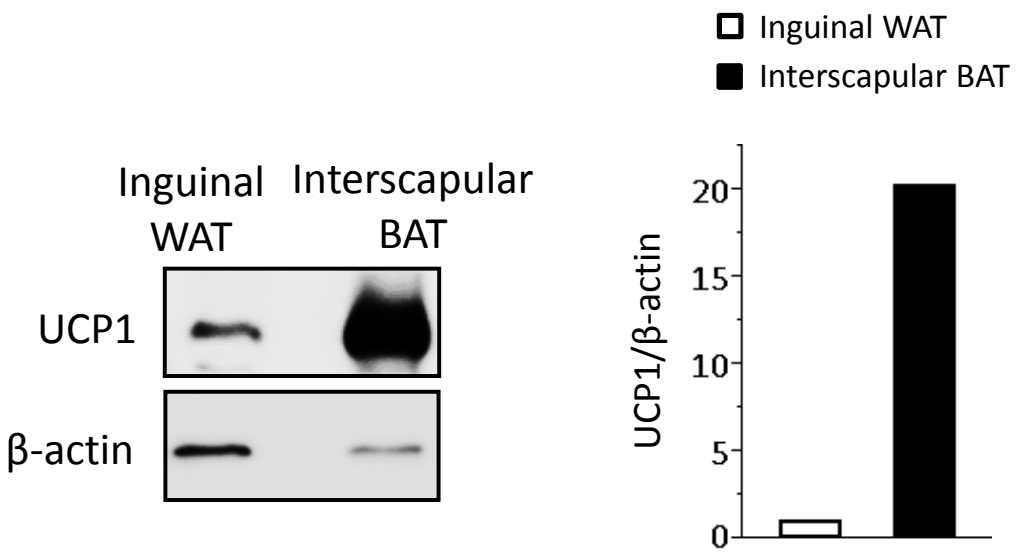

Figure S6

UCP1 protein expression in inguinal WAT and interscaplar BAT.

UCP1 protein levels were analyzed by Western blotting in the inguinal WAT and the interscapular BAT from mice kept under RT or 17°C (n=6)**.** β-actin was used as a loading control. Right; quantification of density of UCP-1/β-actin.

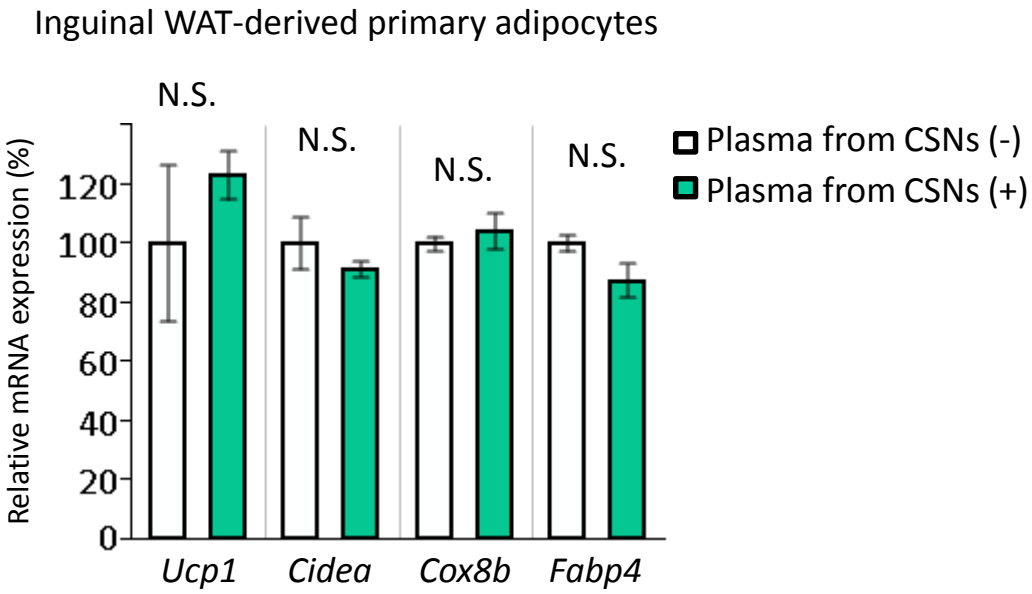

Figure S7

Capsinoids-induced circulation factors do not contribute to the development of beige adipocytes.

Relative mRNA expression levels of *Ucp1*, *Cidea*, *Cox8b*, and *Pgc1α* were measured by qRT-PCR in the differentiated primary inguinal adipocytes from C57BL/6J mice (n=3). The adipocytes were treated with 2% plasma from mice fed HFD with or without 0.3% CSNs at 17°C for 8 weeks. Data are expressed as the means ± SEM.

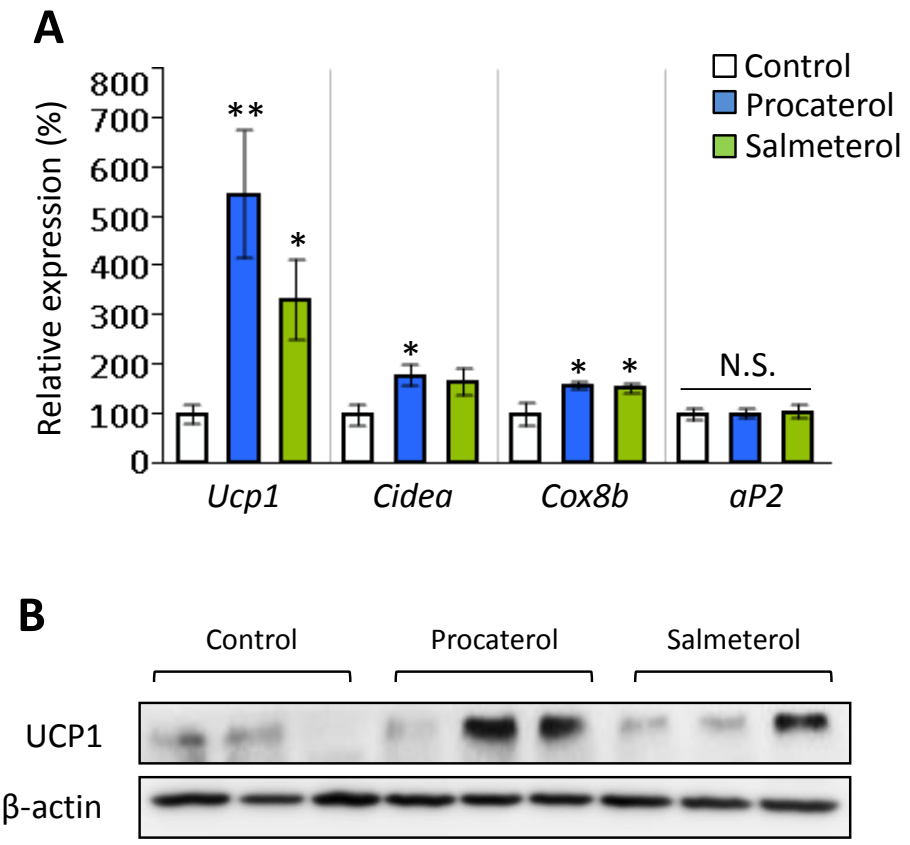

Figure S8

β2-AR agonists recruited beige adipocyte biogenesis.

(A) Relative mRNA expression levels of of *Ucp1*, *Cidea*, *Cox8b*, and *aP2* were measured by qRT-PCR in the inguinal WAT of mice injected with vehicle (saline) or the β2-AR agonists (procaterol or salmeterol) at a dose of 1 mg/kg/day under ambient temperature for 1 week (n=6). *p < 0.05, **p < 0.001. N.S., not significant.

(B) UCP1 protein expression was analyzed by Western blotting in the inguinal WAT of mice shown in (A). β-actin was used as a loading control.

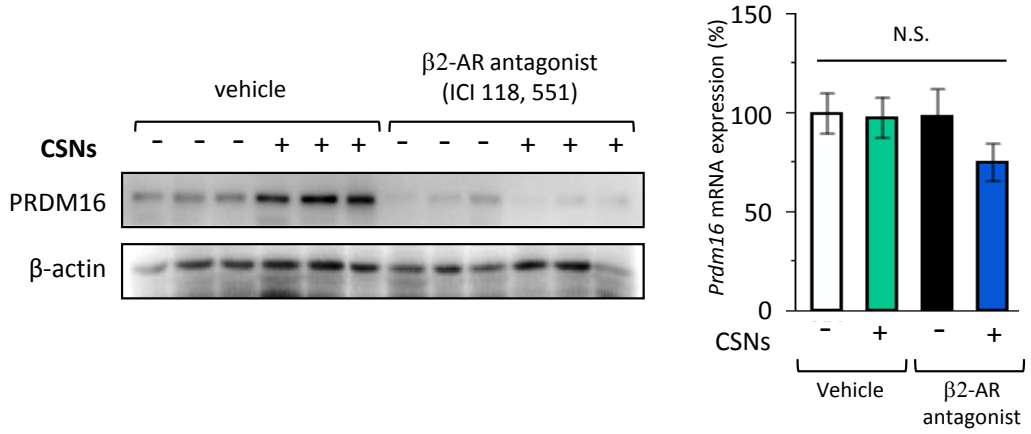

Figure S9

β2-AR antagonist blocked the capsinoids-induced PRDM16 protein accumulation without affecting its mRNA expression.

Mice were fed a high-fat diet supplemented with 0.3% capsinoids (CSNs+) or vehicle (CSNs-) for 4 weeks under 17 ˚C (n=6). The mice were daily injected with vehicle (saline) or the β2-AR antagonist (ICI 118,551) at a dose of 2 mg/kg/day. Endogenous PRDM16 protein expression in the inguinal WAT of these mice was analyzed by Western blotting (left). β-actin was used as a loading control. Relative *Prdm16* mRNA expression was measured by qRT-PCR (right). Data are expressed as the mean ± SEM. N.S., not significant.

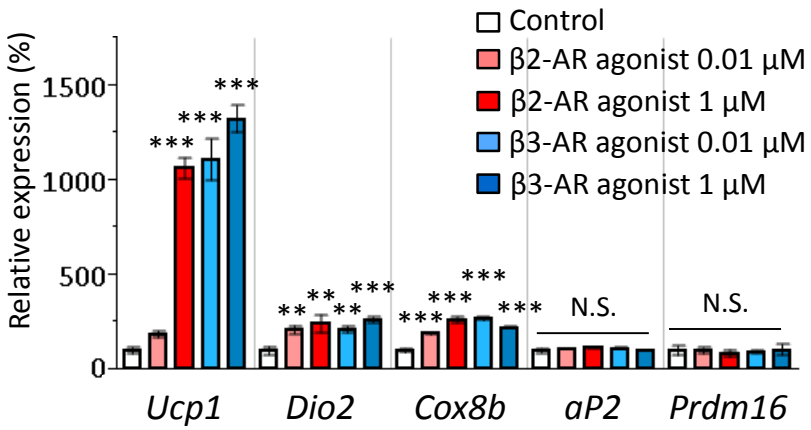

Figure S10

A β3-AR agonist did not induce PRDM16 accumulation in cultured inguinal WAT-derived primary adipocytes. Inguinal WAT-derived primary preadipocytes were differentiated in the presence or absence of the β2-AR agonist (formoterol) or the β3-AR agonist (CL316243) at doses of 0.01 and 1 μM. The relative mRNA expression levels of *Ucp1*, *Dio2*, *Cox8b*, and *aP2* were measured by qRT-PCR. Data are expressed as the mean ± SEM. *p < 0.05, **p < 0.01, ***p < 0.001 relative to the vehicle-treated (control) group.

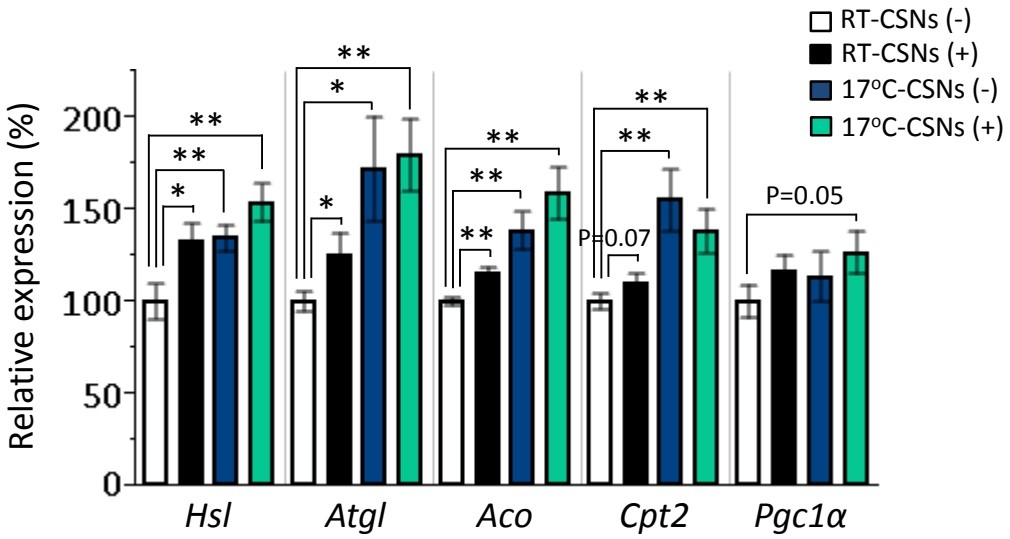

Figure S11

Capsinoids increased the expression of fatty acid oxidative genes in the liver

Relative mRNA expression levels of *Hsl*, *Atgl*, *Aco*, *Cpt2*, and *Pgc1α* were measured by qRT-PCR in the inguinal WAT (left) and in the interscapular BAT (right) of mice kept under RT or 17°C (n=6). Mice were fed a high-fat diet supplemented with 0.3% capsinoids (CSNs+) or vehicle (CSNs-) for 8 weeks. Data are expressed as the mean ± SEM. *p < 0.05, **p < 0.01.

REFERENCES

1. Cheung BM, Cheung TT,Samaranayake NR: Safety of antiobesity drugs. Therapeutic advances in drug safety 4(4):171-181, 2013
2. Kajimura S,Saito M: A new era in brown adipose tissue biology: molecular control of brown fat development and energy homeostasis. Annual review of physiology 76:225-249, 2014
3. Fedorenko A, Lishko PV,Kirichok Y: Mechanism of fatty-acid-dependent UCP1 uncoupling in brown fat mitochondria. Cell 151(2):400-413, 2012
4. Cypess AM, Weiner LS, Roberts-Toler C, Elia EF, Kessler SH, Kahn PA, English J, Chatman K, Trauger SA, Doria A,Kolodny GM: Activation of Human Brown Adipose Tissue by a beta3-Adrenergic Receptor Agonist. Cell Metab 21(1):33-38, 2015
5. Carey AL, Formosa MF, Van Every B, Bertovic D, Eikelis N, Lambert GW, Kalff V, Duffy SJ, Cherk MH,Kingwell BA: Ephedrine activates brown adipose tissue in lean but not obese humans. Diabetologia 56(1):147-155, 2013
6. Redman LM, de Jonge L, Fang X, Gamlin B, Recker D, Greenway FL, Smith SR,Ravussin E: Lack of an effect of a novel beta3-adrenoceptor agonist, TAK-677, on energy metabolism in obese individuals: a double-blind, placebo-controlled randomized study. J Clin Endocrinol Metab 92(2):527-531, 2007
7. Kimura K, Sasaki N, Asano A, Mizukami J, Kayahashi S, Kawada T, Fushiki T, Morimatsu M, Yoshida T,Saito M: Mutated human beta3-adrenergic receptor (Trp64Arg) lowers the response to beta3-adrenergic agonists in transfected 3T3-L1 preadipocytes. Hormone and metabolic research = Hormon- und Stoffwechselforschung = Hormones et metabolisme 32(3):91-96, 2000
8. Pietri-Rouxel F, St John Manning B, Gros J,Strosberg AD: The biochemical effect of the naturally occurring Trp64-->Arg mutation on human beta3-adrenoceptor activity. European journal of biochemistry / FEBS 247(3):1174-1179, 1997
9. Mitchell BD, Blangero J, Comuzzie AG, Almasy LA, Shuldiner AR, Silver K, Stern MP, MacCluer JW,Hixson JE: A paired sibling analysis of the beta-3 adrenergic receptor and obesity in Mexican Americans. J Clin Invest 101(3):584-587, 1998
10. Sipilainen R, Uusitupa M, Heikkinen S, Rissanen A,Laakso M: Polymorphism of the beta3-adrenergic receptor gene affects basal metabolic rate in obese Finns. Diabetes 46(1):77-80, 1997
11. Harms M,Seale P: Brown and beige fat: development, function and therapeutic potential. Nat Med 19(10):1252-1263, 2013
12. Lidell ME, Betz MJ, Dahlqvist Leinhard O, Heglind M, Elander L, Slawik M, Mussack T, Nilsson D, Romu T, Nuutila P, Virtanen KA, Beuschlein F, Persson A, Borga M,Enerback S: Evidence for two types of brown adipose tissue in humans. Nat Med 19(5):631-634, 2013

13. McDonald ME, Li C, Bian H, Smith BD, Layne MD,Farmer SR: Myocardin-related transcription factor a regulates conversion of progenitors to beige adipocytes. Cell 160(1-2):105-118, 2015
14. Lee P, Werner CD, Kebebew E,Celi FS: Functional thermogenic beige adipogenesis is inducible in human neck fat. Int J Obes (Lond) 38(2):170-176, 2014
15. Sharp LZ, Shinoda K, Ohno H, Scheel DW, Tomoda E, Ruiz L, Hu H, Wang L, Pavlova Z, Gilsanz V,Kajimura S: Human BAT possesses molecular signatures that resemble beige/brite cells. PloS one 7(11):e49452, 2012
16. Wu J, Bostrom P, Sparks LM, Ye L, Choi JH, Giang AH, Khandekar M, Virtanen KA, Nuutila P, Schaart G, Huang K, Tu H, van Marken Lichtenbelt WD, Hoeks J, Enerback S, Schrauwen P,Spiegelman BM: Beige adipocytes are a distinct type of thermogenic fat cell in mouse and human. Cell 150(2):366-376, 2012
17. Shinoda K, Luijten I, Hasegawa Y, Si S, Xue R, Cypess A, Nedergaard J, Tseng Y-H, Hong H, Chondronikola M,Shingo K: Genetic and functional characterization of clonally-derived adult human brown adipocytes. Nature Medicine, 2015
18. Lee P, Linderman JD, Smith S, Brychta RJ, Wang J, Idelson C, Perron RM, Werner CD, Phan GQ, Kammula US, Kebebew E, Pacak K, Chen KY,Celi FS: Irisin and FGF21 are cold-induced endocrine activators of brown fat function in humans. Cell Metab 19(2):302-309, 2014
19. van der Lans AA, Hoeks J, Brans B, Vijgen GH, Visser MG, Vosselman MJ, Hansen J, Jorgensen JA, Wu J, Mottaghy FM, Schrauwen P,van Marken Lichtenbelt WD: Cold acclimation recruits human brown fat and increases nonshivering thermogenesis. J Clin Invest 123(8):3395-3403, 2013
20. Yoneshiro T, Aita S, Matsushita M, Kayahara T, Kameya T, Kawai Y, Iwanaga T,Saito M: Recruited brown adipose tissue as an antiobesity agent in humans. The Journal of clinical investigation 123(8):3404-3408, 2013
21. Kobata K, Sutoh K, Todo T, Yazawa S, Iwai K,Watanabe T: Nordihydrocapsiate, a new capsinoid from the fruits of a nonpungent pepper, capsicum annuum. J Nat Prod 62(2):335-336, 1999
22. Kobata K TT, Yazawa S, Iwai K, Watanabe T: Novel Capsaicinoid-like Substances, Capsiate and Dihydrocapsiate, from the Fruits of a Nonpungent Cultivar, CH-19 Sweet, of Pepper (Capsicum annuum L.). . J. Agric. Food Chem. 46:1695-1697., 1998
23. Ohnuki K, Haramizu S, Oki K, Watanabe T, Yazawa S,Fushiki T: Administration of capsiate, a non-pungent capsaicin analog, promotes energy metabolism and suppresses body fat accumulation in mice. Biosci Biotechnol Biochem 65(12):2735-2740, 2001

24. Snitker S, Fujishima Y, Shen H, Ott S, Pi-Sunyer X, Furuhata Y, Sato H,Takahashi M: Effects of novel capsinoid treatment on fatness and energy metabolism in humans: possible pharmacogenetic implications. Am J Clin Nutr 89(1):45-50, 2009
25. Weir JB: New methods for calculating metabolic rate with special reference to protein metabolism. J Physiol 109(1-2):1-9, 1949
26. Folch J, Lees M,Sloane Stanley GH: A simple method for the isolation and purification of total lipides from animal tissues. J Biol Chem 226(1):497-509, 1957
27. Ohno H, Shinoda K, Spiegelman BM,Kajimura S: PPARgamma agonists Induce a White-to-Brown Fat Conversion through Stabilization of PRDM16 Protein. Cell metabolism 15(3):395-404, 2012
28. Cannon B,Nedergaard J: Brown adipose tissue: function and physiological significance. Physiological reviews 84(1):277-359, 2004
29. Shirai Y, Ueno S, Nakayama A, Ikeuchi K, Ubukata K, Mihara R,Bernard BK: Studies of the toxicological potential of capsinoids, XII: pharmacokinetic study of capsinoid-containing CH-19 Sweet extract in rats. International journal of toxicology 29(2 Suppl):15S-21S, 2010
30. Ono K, Tsukamoto-Yasui M, Hara-Kimura Y, Inoue N, Nogusa Y, Okabe Y, Nagashima K,Kato F: Intragastric administration of capsiate, a transient receptor potential channel agonist, triggers thermogenic sympathetic responses. J Appl Physiol 110(3):789-798, 2011
31. Bachman ES, Dhillon H, Zhang CY, Cinti S, Bianco AC, Kobilka BK,Lowell BB: betaAR signaling required for diet-induced thermogenesis and obesity resistance. Science (New York, N.Y.) 297(5582):843-845, 2002
32. Baker JG: The selectivity of beta-adrenoceptor agonists at human beta1-, beta2- and beta3-adrenoceptors. British journal of pharmacology 160(5):1048-1061, 2010
33. Cohen P, Levy JD, Zhang Y, Frontini A, Kolodin DP, Svensson KJ, Lo JC, Zeng X, Ye L, Khandekar MJ, Wu J, Gunawardana SC, Banks AS, Camporez JP, Jurczak MJ, Kajimura S, Piston DW, Mathis D, Cinti S, Shulman GI, Seale P,Spiegelman BM: Ablation of PRDM16 and beige adipose causes metabolic dysfunction and a subcutaneous to visceral fat switch. Cell 156(1-2):304-316, 2014
34. Kajimura S, Seale P, Kubota K, Lunsford E, Frangioni JV, Gygi SP,Spiegelman BM: Initiation of myoblast to brown fat switch by a PRDM16-C/EBP-beta transcriptional complex. Nature 460(7259):1154-1158, 2009
35. Kajimura S, Seale P, Tomaru T, Erdjument-Bromage H, Cooper MP, Ruas JL, Chin S, Tempst P, Lazar MA,Spiegelman BM: Regulation of the brown and white fat gene programs through a PRDM16/CtBP transcriptional complex. Genes & development 22(10):1397-1409, 2008

36. Seale P, Bjork B, Yang W, Kajimura S, Chin S, Kuang S, Scime A, Devarakonda S, Conroe HM, Erdjument-Bromage H, Tempst P, Rudnicki MA, Beier DR,Spiegelman BM: PRDM16 controls a brown fat/skeletal muscle switch. Nature 454(7207):961-967, 2008
37. Seale P, Kajimura S, Yang W, Chin S, Rohas LM, Uldry M, Tavernier G, Langin D,Spiegelman BM: Transcriptional control of brown fat determination by PRDM16. Cell metabolism 6(1):38-54, 2007
38. Sasahara I, Furuhata Y, Iwasaki Y, Inoue N, Sato H, Watanabe T,Takahashi M: Assessment of the biological similarity of three capsaicin analogs (Capsinoids) found in non-pungent chili pepper (CH-19 Sweet) fruits. Biosci Biotechnol Biochem 74(2):274-278, 2010
39. Tsurugizawa T, Nogusa Y, Ando Y,Uneyama H: Different TRPV1-mediated brain responses to intragastric infusion of capsaicin and capsiate. The European journal of neuroscience 38(11):3628-3635, 2013
40. Perkins MN, Rothwell NJ, Stock MJ,Stone TW: Activation of brown adipose tissue thermogenesis by the ventromedial hypothalamus. Nature 289(5796):401-402, 1981
41. Saito M, Minokoshi Y,Shimazu T: Ventromedial hypothalamic stimulation accelerates norepinephrine turnover in brown adipose tissue of rats. Life sciences 41(2):193-197, 1987
42. Beiroa D, Imbernon M, Gallego R, Senra A, Herranz D, Villarroya F, Serrano M, Ferno J, Salvador J, Escalada J, Dieguez C, Lopez M, Fruhbeck G,Nogueiras R: GLP-1 agonism stimulates brown adipose tissue thermogenesis and browning through hypothalamic AMPK. Diabetes 63(10):3346-3358, 2014
43. Martinez de Morentin PB, Gonzalez-Garcia I, Martins L, Lage R, Fernandez-Mallo D, Martinez-Sanchez N, Ruiz-Pino F, Liu J, Morgan DA, Pinilla L, Gallego R, Saha AK, Kalsbeek A, Fliers E, Bisschop PH, Dieguez C, Nogueiras R, Rahmouni K, Tena-Sempere M,Lopez M: Estradiol regulates brown adipose tissue thermogenesis via hypothalamic AMPK. Cell Metab 20(1):41-53, 2014
44. Morrison SF, Madden CJ,Tupone D: Central neural regulation of brown adipose tissue thermogenesis and energy expenditure. Cell Metab 19(5):741-756, 2014
45. Qiang L, Wang L, Kon N, Zhao W, Lee S, Zhang Y, Rosenbaum M, Zhao Y, Gu W, Farmer SR,Accili D: Brown remodeling of white adipose tissue by SirT1-dependent deacetylation of Ppargamma. Cell 150(3):620-632, 2012
46. Collins S, Cao W,Robidoux J: Learning new tricks from old dogs: beta-adrenergic receptors teach new lessons on firing up adipose tissue metabolism. Molecular endocrinology 18(9):2123-2131, 2004
47. Gauthier MS, Miyoshi H, Souza SC, Cacicedo JM, Saha AK, Greenberg AS,Ruderman NB: AMP-activated protein kinase is activated as a consequence of lipolysis in the adipocyte: potential mechanism and physiological relevance. J Biol Chem 283(24):16514-16524, 2008

48. Omar B, Zmuda-Trzebiatowska E, Manganiello V, Goransson O,Degerman E: Regulation of AMP-activated protein kinase by cAMP in adipocytes: roles for phosphodiesterases, protein kinase B, protein kinase A, Epac and lipolysis. Cellular signalling 21(5):760-766, 2009
49. Montgomery MK, Hallahan NL, Brown SH, Liu M, Mitchell TW, Cooney GJ,Turner N: Mouse strain-dependent variation in obesity and glucose homeostasis in response to high-fat feeding. Diabetologia 56(5):1129-1139, 2013
50. Guerra C, Koza RA, Yamashita H, Walsh K,Kozak LP: Emergence of brown adipocytes in white fat in mice is under genetic control. Effects on body weight and adiposity. J Clin Invest 102(2):412-420, 1998
51. Xue B, Rim JS, Hogan JC, Coulter AA, Koza RA,Kozak LP: Genetic variability affects the development of brown adipocytes in white fat but not in interscapular brown fat. Journal of lipid research 48(1):41-51, 2007
52. Li Y, Bolze F, Fromme T,Klingenspor M: Intrinsic differences in BRITE adipogenesis of primary adipocytes from two different mouse strains. Biochim Biophys Acta 1841(9):1345-1352, 2014
53. Shabalina IG, Petrovic N, de Jong JM, Kalinovich AV, Cannon B,Nedergaard J: UCP1 in brite/beige adipose tissue mitochondria is functionally thermogenic. Cell reports 5(5):1196-1203, 2013
54. Seale P, Conroe HM, Estall J, Kajimura S, Frontini A, Ishibashi J, Cohen P, Cinti S,Spiegelman BM: Prdm16 determines the thermogenic program of subcutaneous white adipose tissue in mice. The Journal of clinical investigation 121(1):96-105, 2011
55. Ohno H, Shinoda K, Ohyama K, Sharp LZ,Kajimura S: EHMT1 controls brown adipose cell fate and thermogenesis through the PRDM16 complex. Nature 504(7478):163-167, 2013
56. Tanaka Y: Research on capsiconinoid contents, nonpungent capsaicinoid analogues, in Capsicum cultivars. Scientific reports of Okayama Univ. Agriculture department 103:37-43, 2014

CHAPTER. III

A combination of exercise and capsinoids supplementation additively suppressed diet-induced obesity by increasing energy expenditure in mice

Chapter. III

A combination of exercise and capsinoids supplementation additively suppressed diet-induced obesity by increasing energy expenditure in mice

INTRODUCTION

Obesity is rapidly becoming a major global health problem (4) and is a major risk factor for several common diseases, including type 2 diabetes, cardiovascular diseases and cancer (32). Obesity develops when the energy intake chronically exceeds the total energy expenditure (51). Conventional anti-obesity strategies have focused on repressing energy intake by suppressing appetite or inhibiting intestinal fat absorption; however, increasing energy expenditure by activating the metabolic function of skeletal muscle or brown fat could serve as an alternative and effective anti-obesity intervention, thereby avoiding the potential adverse effects associated with conventional anti-obesity therapies, such as depression, oily bowel movements and steatorrhea.

Exercise is one of the most efficient ways to prevent obesity and type 2 diabetes through an increase in energy expenditure (25, 27, 52). However, people in the developed world are becoming less physically active as a result of changes in their lifestyles and the nature of their work. Moreover, constraints such as time, limited access and injuries frequently become barriers to exercise (48). For example, a recent epidemiological study estimated that in a 1-year period, 39% of women adopted some type of physical activity,

but the attrition rate exceeded 30% within only months (46).

Capsaicin is the pungent component in chili pepper and is known to have an anti-obesity effect (18, 20). Capsinoids (CSNs) are capsaicin analogs found in a non-pungent type of chili pepper, 'CH-19 Sweet' (23, 24). CSNs differ from capsaicin in chemical structure only at the center linkage of an ester bond, resulting in reduced (<0.1%) pungency while maintaining the metabolic effect, which facilitates daily intake. Several studies have shown that CSNs increase energy expenditure and suppress body fat accumulation in mice (31). A single administration of capsiate, a capsinoid, increased oxygen consumption, and its chronic administration for 2 weeks diminished fat accumulation in mice (31, 39). Moreover, chronic treatment with CSNs via their inclusion in a high-fat diet for 12 weeks dramatically suppressed body weight gain and fat accumulation (16). Importantly, in adult humans, a 4-week treatment with CSNs increased oxygen consumption, and a 12-week treatment decreased the abdominal fat mass in subjects with body mass indices (BMIs) of 25-35 (15, 50). Mechanistically, oral CSNs supplements have been reported to activate transient receptor potential vanilloid subtype 1 (TRPV1) in the gut (14, 47), resulting in increased sympathetic efferent activity and thermogenesis (41). Interestingly, the activation of TRPV1 signaling has been reported to positively regulate exercise endurance and energy expenditure in mice (30).

We propose that the combination of dietary supplements with exercise may be effective and realistic in terms of obesity control. Although there have been many investigations into the beneficial effects of exercise or dietary supplements individually, little is known about their combined effects. Thus, we investigated the effects of a daily intake of CSNs in combination with exercise on the development of obesity in C57BL/6J mice.

MATERIAL&METHODS

Animals and diets

C57BL/6J male mice were purchased from Charles River (Kanagawa, Japan) at 7 weeks of age and were housed in a controlled-lighting environment (lights on from 1600 to 0400 h) at 25 ± 1°C. They were fed CRF-1 (Charles River JAPAN, Kanagawa, Japan) for 2 weeks to stabilize their metabolic condition. The mice were divided into two groups: one group was given free access to a running wheel (Ex group; wheel diameter, 14 cm: Melquest, Toyama, Japan) connected to a counter, and the other group could not access the wheel. After habituation to wheel running for 1 week, the mice were divided into two groups by body weight, food intake and wheel running counts. The mice were allowed *ad libitum* access to water and either the high-fat diet (HFD) or HFD supplemented with 0.3% (w/w) capsinoids (CSNs; Yoyu-Lab, Gunma, Japan), depending on the group. The compositions of the diets are listed in Table 1. Thus, we prepared four groups: 1) sedentary-HFD (Control: Ex[-]/CSNs[-]), 2) sedentary-CSNs (CSN: Ex[-]/CSNs[+]), 3) voluntary running-HFD (Exercise: Ex[+]/CSNs[-]) and 4) voluntary running-CSNs (Exercise+CSN: Ex[+]/CSNs[+]). The mice were maintained on these diets for 8 weeks. Body weight, food intake and running distance were monitored twice a week. All animal protocols were approved by the Animal Committee of Ajinomoto Co., Inc.

Sampling Procedures

At the end of the experiment, the mice were anesthetized with isoflurane, and blood samples were collected by aortic puncture after 3 h of fasting. The blood samples were

centrifuged at 3,000 rpm for 20 min at 4°C and stored at -20°C until analyzed. The organs (liver, mesenteric white adipose tissue [WAT], perirenal WAT, epididymal WAT, subcutaneous WAT, brown adipose tissue [BAT], gastrocnemius muscle and soleus muscle) were excised and weighed. The organs were then immediately frozen in liquid nitrogen and stored at -80°C.

Blood analysis

The plasma levels of glucose and glutamic pyruvic transaminase (GPT) were determined using a Fuji-drychem (Fujifilm, Tokyo, Japan). The plasma insulin levels and leptin levels were determined by an enzyme-linked immunosorbent assay (ELISA) (Morinaga, Kanagawa, Japan). The plasma levels of triglyceride (TG) and cholesterol were determined using a TG-test Wako kit (Wako, Osaka, Japan) and a Cholesterol-E test Wako kit (Wako), respectively.

Liver lipid analysis

Lipids in liver and gastrocnemious muscle were extracted using the Folch partition method (10) with slight modifications as follows: a portion of these tissue was homogenized in 2.5 ml of methanol, and 5 ml of chloroform was added. The mixture was horizontally shaken for 10 min and extracted at 4°C overnight. The extracted samples were filtered using a Kiriyama-rohto (Kiriyama, Tokyo, Japan), and the volume was increased to 8 ml with aliquots of methanol:chloroform (2:1, v/v). Then, 1.6 ml of saline was added. The mixture was horizontally shaken for 10 min and centrifuged at 2,000 rpm for 5 min at 4°C. The supernatant was removed, and the lower chloroform phase was

filled to 6 ml with chloroform. Next, 2.5 ml of the lipid fraction in this phase was dried and weighed. The dried lipids were dissolved in 1 ml of 10% Triton / isopropanol, and the TG and non-esterified fatty acids (NEFA) levels were determined using a TG-test Wako kit (Wako) and a NEFA-C test Wako kit (Wako, Osaka, Japan), respectively.

Quantitative Real-Time RT-PCR

Total RNA was isolated from the gastrocnemius muscle and subcutaneous WAT using Ribozol (AMRESCO, OH, USA). The cDNAs were synthesized from 1 μg of the RNA using an iScrip cDNA Synthesis Kit (Bio-rad, CA, USA). After cDNA synthesis, quantitative real-time PCR was performed in 10 μl of iTaq Fast SYBR Green Supermix (Bio-rad, CA, USA) using a fluorometric thermal cycler (ViiA 7 System; Life Technologies, CA, USA). The reaction mixtures were incubated for an initial denaturation at 95°C for 10 s, followed by 45 cycles of 95°C for 5 s and 60°C for 20 s. The sequences of the sense and antisense primers used in the amplification are shown in Table 2. Glyceraldehyde-3-phosphate dehydrogenase (GAPDH) or TATA box binding protein (TBP) was used as an internal control.

Histology

Subcutaneous WAT was fixed in 4% paraformaldehyde for 24 h at 4°C. The samples were then dehydrated, embedded in paraffin, sliced into 7-μm-thick sections with a Leica RM2255 (Leica Microsystems; Vienna, Austria), deparaffinized and rehydrated. The sections were then stained with hematoxylin and eosin (H&E).

Respiratory gas analysis and measurement activity

Utilizing a respiratory gas analysis system consisting of an acrylic metabolic chamber, gas analyzers and a switching system (ARCO2000-RAT/ANI System; Arco, Chiba, Japan), the O_2 and CO_2 concentrations of sampled gas from each metabolic chamber were measured as described previously (39). Briefly, room air was constantly pumped through the chamber, and expired air was dried in a thin cotton column and then introduced into the gas analyzer. The respiratory quotient (RQ, VCO_2/VO_2) was calculated according to Weir (56). Fat oxidation was calculated based on the VO_2 and carbon dioxide production. The spontaneous activities of the mice were simultaneously measured using an activity sensor (NS-AS01; Neuroscience, Tokyo, Japan). All measurements were performed in 4.5-min intervals.

cAMP levels and PKA activity in BAT

cAMP levels and PKA activity were determined using cAMP Direct Immunoassay Kit (Abcam, Cambridge, UK) and PKA Kinase Activity Assay Kit (Abcam), respectively.

Fatty acid oxidation in muscle

The muscle fatty acid oxidation rate was determined in the fresh muscle homogenate using a modification of the method of Kim et al. (19). The oxidation rate of palmitate was measured by collecting and counting the $^{14}CO_2$ produced during incubation. Twenty microliters of muscle homogenate was incubated with 380 μl of reaction mixture (pH 8.0) for 1 h. The final concentrations of the reaction mixture were as follows in millimoles per liter: sucrose, 100; Tris-HCl, 10; potassium phosphate, 5; potassium chloride, 80;

magnesium chloride, 1; L-carnitine, 2; malate, 0.1; ATP, 2; coenzyme A (CoA), 0.05; dithiothreitol, 1; EDTA, 0.2; nicotinamide, 5; trichostatin A, 0.001; and bovine serum albumin, 0.3%. The substrates used were [1-^{14}C]palmitate (0.4 μCi) with 2 mM BSA. After 60 min of incubation at 37°C, 200 μl of 1 M perchloric acid was injected to stop the reaction. The CO_2 produced during the incubation was trapped by Whatman filter paper with 15 μl of hyamine hydroxide. Then, the filter paper was transferred to a glass scintillation vial that contained 4 ml of Emulsifier-Safe. The average counts per minutes (cpm) was measured over 3 min.

Statistical analysis

The statistical analysis was performed using JMP version 9.0 (SAS Institute Inc., NC, USA). The main and interaction effects of the CSNs and Ex on the metabolic parameters were determined by two-way analysis of variance (ANOVA). Repeated measures ANOVA with *t* tests were used to compare the time courses. The other statistical comparison was assessed using a two-tailed Student's *t* test. The results are given as the means ± SEM unless otherwise stated. A P value less than 0.05 was considered significant throughout the study.

RESULTS

Effects of exercise and CSNs supplementation on body weight gain and adiposity

The metabolic effects of exercise and CSNs were evaluated in an 8-week cohort of diet-induced obese mice. The mice given CSNs gained significantly less weight in either the normal or exercised group under an HFD (**Fig. 1A**). The combination of exercise and CSNs dramatically (17%) suppressed the weight gain at 56 days compared with that in the control (Ex[-]/CSNs[-]) group. The body weight gains were significantly different between the Ex(-) and Ex(+) groups and between the CSNs(-) and CSNs(+) groups (**Fig. 1B**). The main effects of the CSNs and exercise on the final body weight gain were significant as judged by two-way ANOVA, whereas their interaction was not significant (P = 0.915). The reduction of body mass was accounted for by a decrease in fat as reflected in the weights of various white fat depots, including the epididymal, mesenteric and perirenal WAT (**Fig. 1C**). However, the heart weight was not significantly affected by either the exercise or the CSNs treatment. Consistent with these results, the combination of exercise and CSNs significantly improved the metabolic profiles. The blood glucose, insulin, leptin and cholesterol levels were significantly decreased by the combination of exercise and CSNs (**Table 3**).

Effects of exercise and CSNs supplementation on energy expenditure

The critical parameter contributing to body weight control is the energy balance between caloric intake and energy expenditure (29). The food intake was not affected by the CSNs in either the Ex(-) or Ex(+) groups (**Fig. 2A**). We then measured the energy

expenditure, which comprises physical activity and thermogenesis. The physical activity (locomotive activity and running distance) of the mice during the treatment was not affected by the CSNs supplementation (**Fig. 2B, C**). However, the whole-body oxygen consumption and fat oxidation were significantly increased by the combination of exercise and CSNs compared with the control group (**Fig. 2D, E**).

CSNs supplementation with exercise improved the high-fat diet-induced liver steatosis

Next, we examined the metabolic consequences of the anti-obesity effects of exercise and CSNs. It is well known that a high-fat diet induces liver steatosis; thus, lipids should accumulate in the liver. Therefore, we measured the lipid content in the liver, as assessed by the levels of total lipids, TG and NEFA. The total lipids tended to be decreased by the exercise or the CSNs treatment, but not significantly. However, the combination of exercise and CSNs significantly reduced the total lipid content in the liver (**Fig. 3A**). Similar effects were observed for TG and NEFA levels (**Fig. 3B, C**). Importantly, the combination of exercise and CSNs significantly reduced the total lipid, TG and NEFA contents in the liver by 64%, 46% and 78%, respectively (**Fig. 3A-C**). The plasma levels of GPT, a sensitive parameter in diagnosing fatty liver in humans (21), were significantly reduced in the mice that exercised (**Fig. 3D**).

CSNs supplementation with exercise diminished the cell size in subcutaneous WAT

The morphological and biochemical changes in WAT in response to exercise and CSNs were examined. Metabolic improvements are strongly associated with a reduction in

adipose cell size. The histological examination (H&E staining) of the subcutaneous WAT revealed that the adipocyte size significantly decreased in the WAT from the mice treated with exercise and CSNs (**Fig. 4A**). To quantitatively assess the difference, we calculated the average cell size in a 1-mm field of view of the H&E-stained tissue, and the exercise and CSNs indeed significantly diminished the cell size (**Fig. 4B**). Because we observed a significant increase in the energy expenditure that was associated with exercise and CSNs supplementation (**Fig. 2C**), we hypothesized that non-shivering thermogenesis through brown adipocytes may be altered. Thus, we measured the mRNA expression levels of thermogenic genes (uncoupling protein-1 (*Ucp1*) and peroxisome proliferator-activated receptor gamma, coactivator 1α (*Pgc-1α*)) in the WAT. As previously reported (5, 58), exercise significantly increased the *Ucp-1* and *Pgc-1α* expression levels (main effect *P*-value = 0.02), although the effects of CSNs did not reach significant levels, with p-values of 0.64 (*Ucp-1)* and 0.87 (*Pgc-1α*) (**Fig. 4C**). However, the expression levels of lipoprotein lipase (*Lpl*), a key enzyme of lipolysis, and adiponectin (*AdipQ*), a differentiation marker, were not changed among the groups (**Fig. 4C**).

CSNs supplementation combined with exercise increased lipolysis in the BAT

It is well known that the sympathetic nervous system (SNS) is activated during exercise (54). Also, it is reported that CSNs increase BAT sympathetic nervous activity (41). Then we hypothesized CSNs treatment with exercise additively activated the SNS. To address this hypothesis we determined cAMP levels in the BAT. Exercise significantly increased cAMP levels, and the combination of exercise and CSNs tended to further increase cAMP levels (Ex; 54%, Ex+CSNs; 87%) in the BAT (**Fig. 5A**). Next we

determined PKA activity in the BAT, because increase of intercellular cAMP activates PKA. As same as cAMP levels, combination of exercise and CSNs showed the highest PKA activity (**Fig.5B**).

CSNs supplementation combined with exercise increased fatty acid oxidation in the gastrocnemius muscle

It is known that a high-fat diet induces lipid accumulation not only in the liver but also in the muscle. Exercise significantly decreased TG levels, and the combination of exercise and CSNs tended to further decrease TG levels (Ex; 37%, Ex+CSNs; 42%) in the gastrocnemius muscle (**Fig. 6A**). Skeletal muscle is one of the most active organs in dissipating energy and plays a central role in systemic energy homeostasis. Exercise is well known to increase the expression levels of genes that are involved in fatty acid oxidation, such as acyl-CoA oxidase (*Aco*) and cytochrome c oxidase-1 (*Cox-1*), through the transcriptional pathway of *Pgc-1α* (28, 45, 59). Hence, we hypothesized that exercise and CSNs would additively activate the expression of fat oxidative genes in the muscle, which could contribute to the increase in energy expenditure. As shown in Fig. 5B, the combination of exercise and CSNs significantly increased the mRNA levels of *Lpl*, *Cox-1*, *Aco* and medium-chain acyl dehydrogenase (*Mcad*) compared with the expression levels in the control group. Additionally, CSNs significantly increased the mRNA levels of *Cox-1* under the exercise conditions. By contrast, the myosin heavy chain-1/β (*Mhc-1/β*) mRNA expression was not changed (**Fig. 6B**), indicating that muscle fiber type changes did not occur in this setting. Furthermore, we directly determined the fatty acid oxidation rate in muscle using ^{14}C-palmitate. The oxidation rate tended to be increased by the

exercise or the CSNs treatment, but not significantly. However, the combination of exercise and CSNs significantly increased the oxidation rate in the gastrocnemius muscle (**Fig. 6C**).

DISCUSSION

Exercise is important in treating obesity because of its capacity to increase energy expenditure (13, 17). Despite the well-documented health benefits of exercise, constraints such as time, limited access and injuries frequently become barriers to exercise (48). Hence, we propose that the combination of anti-obesity food components with exercise might be effective in weight control by compensating for or adding to the individual effects. Although there have been many investigations into the beneficial effects of exercise or food components individually, little is known about their combined effects on obesity development. This study demonstrated that the combination of exercise and CSNs additively reduced adiposity (**Fig. 1C**). Furthermore, CSNs supplementation with exercise improved peripheral markers, such as the blood glucose, insulin and leptin levels, providing additional supporting evidence for the additive effect (**Table 3**). Although several groups, including ours, have reported the independent effects of CSNs on obesity (16, 31, 39), this report is the first to show that CSNs have an anti-obesity effect even under an exercise condition. The combination of exercise and tea catechin was also reported to be more effective than the individual component effects in suppressing obesity (33). Catechins, such as EGCG (epigallocatechin gallate), have anti-obesity effects in mice and humans (22, 34, 35, 57). These observations support our claims that the combination of exercise and anti-obesity food components is more effective at suppressing obesity and that CSNs are a promising candidate for combining with exercise.

The anti-obesity mechanisms of CSNs include increased energy expenditure (15, 39, 40). While also considering the established effect of exercise on energy expenditure, we

expected an additive increase in the energy expenditure from the CSNs. The results revealed that the combination of exercise and CSNs increased the whole-body fat oxidation, whereas the food intake and exercise amounts were unchanged (**Fig. 2**). Thus, the combination of exercise and CSNs might conceivably suppress obesity via an increase in basal energy expenditure through a significant increase in the fat oxidation that involves an increase in fatty acid oxidative genes in the muscle (**Fig. 6B, C**). Exercise is well known to up-regulate *Pgc-1α* gene expression, and some genes are transcriptionally regulated by *Pgc-1α* (28, 45, 59). For example, swimming exercise results in a 2-fold increase of the *Pgc-1α* mRNA and protein in the skeletal muscle of rats (2), and exercise training induces a marked increase in the *Pgc-1α* mRNA content in humans (44). Additionally, chronic administration of CSNs has been shown to increase the expression levels of *Pgc-1α* and its target genes in the gastrocnemius muscle (16). However, in the aforementioned study, the degree of difference in the increase of the *Pgc-1α* expression by only exercise or CSNs was smaller than in previous reports ($P = 0.15$ and $P = 0.07$) (data not shown). These results might be due to differences in the experimental conditions, such as the follow-up length or the type of exercise (forced or voluntary). These results suggested that the increase of fat oxidation in the muscle that is induced by the combination of exercise and CSNs performed an important role in increasing the energy expenditure of the whole body.

Both single and chronic CSNs supplementation protocols have been reported to increase energy expenditure (11, 15, 31, 39, 40, 50). This CSNs-dependent increase in energy expenditure might be due to the activation of the sympathetic nervous system (SNS). CSNs increase BAT sympathetic nervous activity and the release of

norepinephrine (41). Because the SNS is activated and the release of catecholamines is increased during exercise (55), the release of catecholamines might be synergistically regulated by the combination of exercise with CSNs. The catecholamines released from sympathetic nerve terminals promote lipid mobilization and thermogenesis *via* β3-adrenoreceptors (12. 36). Actually, the cAMP levels in the BAT were additively increased by the exercise and CSNs combination (**Fig.5A**). This result indicates that exercise and CSNs additively activated β3-adrenoreceptors. Increase of the cAMP levels by combination of exercise and CSNs activated PKA (**Fig. 5B**). Activation of PKA phosphorylates hormone sensitive lipase (HSL) and induces lipolysis (1, 8). Because fatty acid is a UCP-1 substrate (9), combination of exercise and CSNs could induce energy expenditure and thermogenesis via driving UCP-1 activity.

UCP-1 is a thermogenous protein that produces heat by uncoupling electron transport from ATP production (6) when adaptive non-shivering thermogenesis occurs (36); UCP-1 has recently attracted attention as a target to suppress obesity. CSNs and exercise have been reported to increase the UCP-1 levels in interscapular BAT (31, 37, 38). Furthermore, exercise has been reported to induce browning in the subcutaneous WAT (5). However, in this research, we did not observe an increase in *Ucp-1* in the interscapular BAT in response to the exercise and the CSNs treatment (data not shown). Moreover, we did not note any differences in the mRNA levels in the subcutaneous WAT among the groups. These results suggest that the suppression of obesity by the combination of exercise and CSNs did not involve an increase of the expression in *Ucp-1* in either the interscapular BAT or the subcutaneous WAT.

Recently, CSNs have been reported to activate the transient receptor potential cation

channel, subfamily A, member 1 (TRPA1) channel and the TRPV1 channel (49). TRPA1 is sensitive to cold stimuli below 17°C (43) and to various reagents, such as allyl isothiocyanate, cinnamaldehyde and farnesyl thiosalicylic acid (3). However, the specific function of this protein has not yet been determined. To elucidate the role of the activation of TRPA1 by CSNs in the anti-obesity effect, further study is required.

The excessive accumulation of TG in the liver in response to a high-fat diet has been reported to induce disorders such as fatty liver and to lead to liver cirrhosis and even hepatocellular cancer (54). The combination of exercise and CSNs decreased the total lipid, TG and NEFA contents in the liver (**Fig. 3A-C**). The plasma cholesterol and GPT levels were also significantly reduced by the combination of exercise and CSNs (**Table 3, Fig. 3D**). Many papers have reported that exercise suppresses liver lipid accumulation (26), possibly via mechanisms involving increased fat oxidation and decreased lipogenesis in the liver (7, 42). Furthermore, capsiate was reported to reduce the hepatic TG levels in rats fed a high-fat diet (53), and CSNs were shown to reduce the hepatic TG levels in mice fed a high-fat diet (16). These data suggested that the combination of exercise and CSNs might suppress lipid accumulation by increasing fat oxidation in the liver. Hence, we measured the expression levels of genes that are involved in fatty acid oxidation in the liver. However, they were not changed in this cohort (data not shown). Therefore, the suppressed lipid accumulation is thought to be a secondary effect of increasing the energy expenditure in muscle.

Some papers have reported that CSNs increased energy expenditure and suppressed obesity in humans. Yoneshiro *et al*. reported that CSNs acutely increased energy expenditure through the activation of BAT in humans (60) and that chronic CSNs

treatment increased the cold-induced thermogenesis in humans (61). Additionally, CSNs or CH-19 sweet pepper fruits containing CSNs decreased visceral adiposity in subjects with BMIs of 25-35 kg/m^2 (19, 50). CSNs have already been filed as a "new dietary ingredient (NDI)" by the FDA. Combining exercise with CSNs in the human diet could be a powerful and plausible tool for fighting obesity.

Table 1. Compositions of the experimental diets (%)

	HFD	HFD + CSNs (0.3%)
Casein	20	20
Sucrose	10	10
Corn starch	22.48	22.48
α-corn starch	7.47	7.47
L-cysteine	0.3	0.3
Cellulose	5	5
Lard	30	30
Mineral mix	3.5	3.5
Vitamin mix	1	1
Choline bitartrate	0.25	0.25
Capsinoids	-	0.3

Table 2. Primers used for real-time PCR analysis

Gene	Sense	Antisense	Entrez Gene ID
Gapdh	CTGAGGACCAGGTTGCTCC	ACCACCCTGTGCTGTAGCC	14433
Tbp	ACCCTTCACCAATGACTCCTATG	TGACTGCAGCAAATCGCTTGG	21374
Aco	CATTGGCATGTGAGAACAG	AGCAAATCTGATGGCTTTGA	11430
Cox-1	CACTAATAATCGGAGCCCCA	TTCATCCTGTTCCTGTCCT	17708
Lpl	CCAGCAACATTATCCAGTGCTAG	CAGTTGATGAATCTGTCCT	16956
Mcad	GCTCGTGAGCACATTGAAAA	CATTGTCCAAAAGCCAAACC	11364
Pgc-1α	CACTACAGACACCGCACACA	AGGCTTCATAGCTGTCGTACC	19017
Ucp-1	CACCTTCCCCCTGGACACT	CCCTAGGACACCTTTATACCT	22227
Cidea	ATCACAACTGGCCTGGTTACG	TACTACCCGGTGTCCATTTCT	12683
Cox8B	GAACCATGAAGCCAACGACT	GCGAAGTTCACAGTGGTTCC	12869

Table 3. Effects of CSNs supplementation with exercise on blood parameters
The levels of blood glucose, insulin, leptin, cholesterol and TG were measured in C57BL/6J mice fed an HFD (Control), HFD supplemented with CSNs (CSN), HFD in addition to voluntary exercise (Exercise) and HFD supplemented with CSNs in addition to voluntary exercise (Exercise+CSN) for 56 days. The values represent the means ± S.E. (n=7-8). P values were calculated by one-way ANOVA. † and ‡, significant differences of $P < 0.05$ and $P < 0.01$, respectively, compared with the control group.

	Control	CSN	Exercise	Exercise + CSN	P-Value
Blood glucose (mg/mL)	31.45 ± 2.27	25.28 ± 0.90†	21.84 ± 0.80‡	23.00 ± 1.14‡	0.0003
Insulin (ng/mL)	6.00 ± 1.08	3.89 ± 0.56	3.63 ± 0.53†	3.12 ± 0.63‡	0.0481
Leptin (ng/mL)	22.81 ± 1.45	21.47 ± 2.75	16.93 ± 3.61	12.03 ± 1.98‡	0.0262
Cholesterol (mg/mL)	18.79 ± 0.98	15.13 ± 1.15†	16.11 ± 0.40†	15.15 ± 0.44‡	0.0120
TG (mg/mL)	5.36 ± 0.63	5.51 ± 0.34	5.04 ± 0.47	4.70 ± 0.21	0.5755

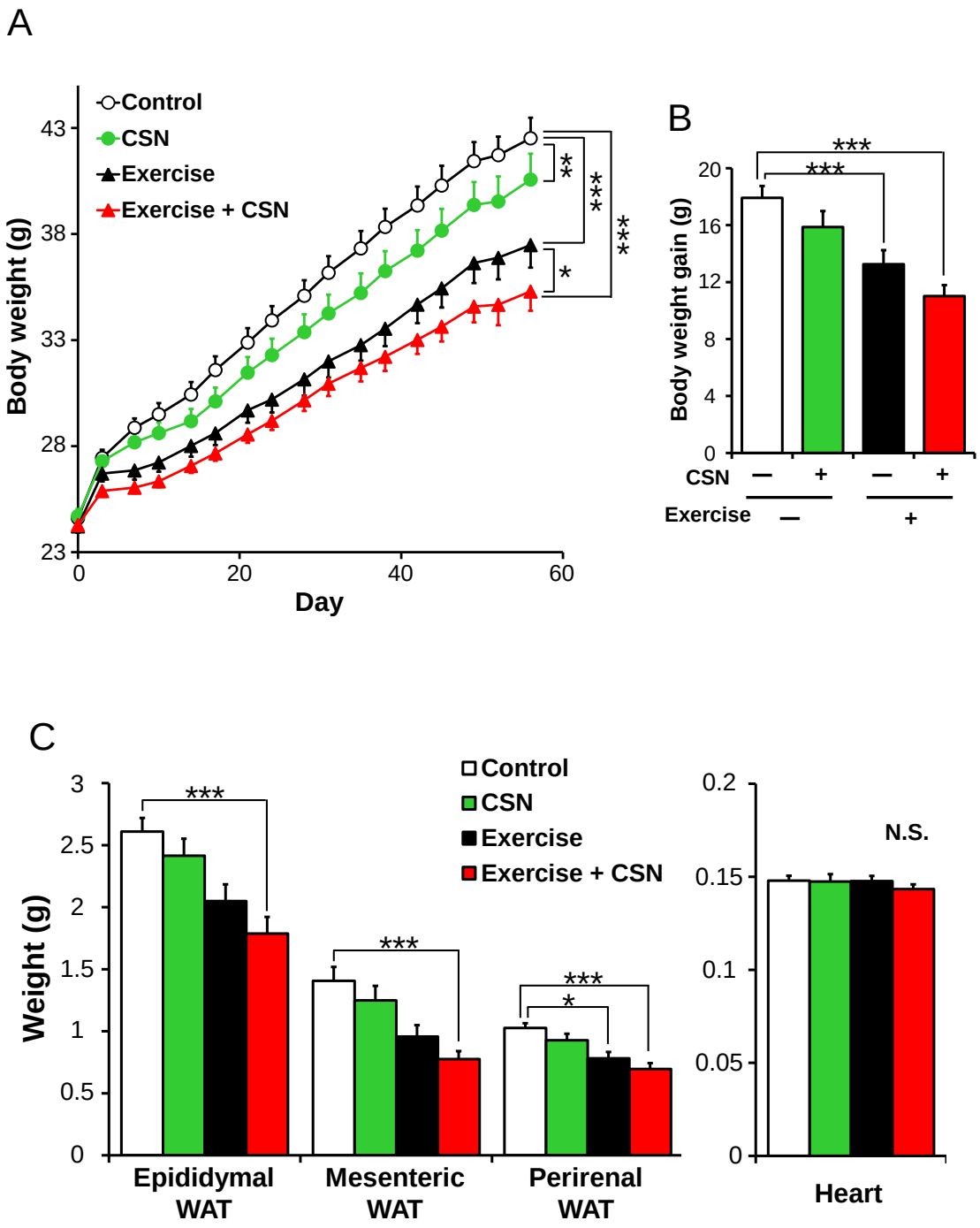

Fig. 1. CSNs supplementation with exercise additively suppressed the body weight gain and adiposity in diet-induced obesity.

A, body weight development; B, body weight gain; and D, tissue weight of C57BL/6J mice fed an HFD (Control), HFD supplemented with CSNs (CSN), HFD in addition to voluntary exercise (Exercise), and HFD supplemented with CSNs in addition to voluntary exercise (Exercise + CSN) for 56 days. The values represent the means ± S.E. (n=7-8). *, $p < 0.05$, **, $p < 0.01$, *** $p < 0.001$.

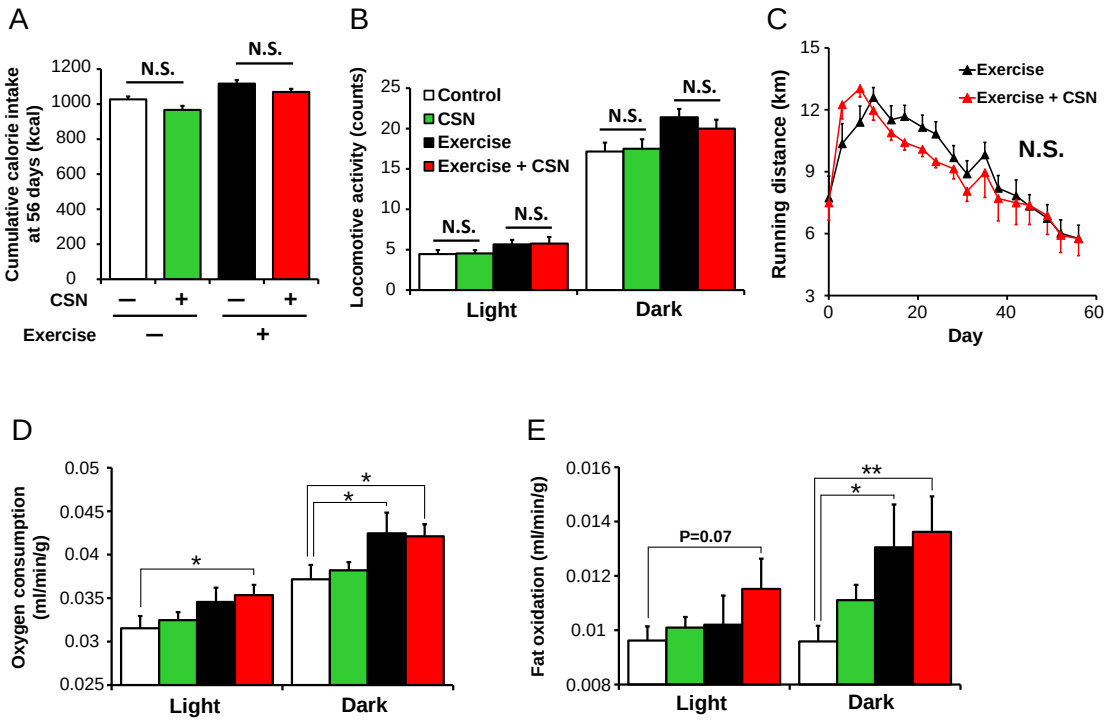

Fig. 2. CSNs supplementation with exercise additively increased energy expenditure.
A, food intake; B, locomotive activity; C, running distance; D, oxygen consumption; and E, fat oxidation of C57BL/6J mice fed an HFD (Control), HFD supplemented with CSNs (CSN), HFD in addition to voluntary exercise (Exercise), and HFD supplemented with CSNs in addition to voluntary exercise (Exercise + CSN) for 56 days. The values represent the means ± S.E. (n=7-8). *, $p < 0.05$, **, $p < 0.01$, *** $p < 0.001$.

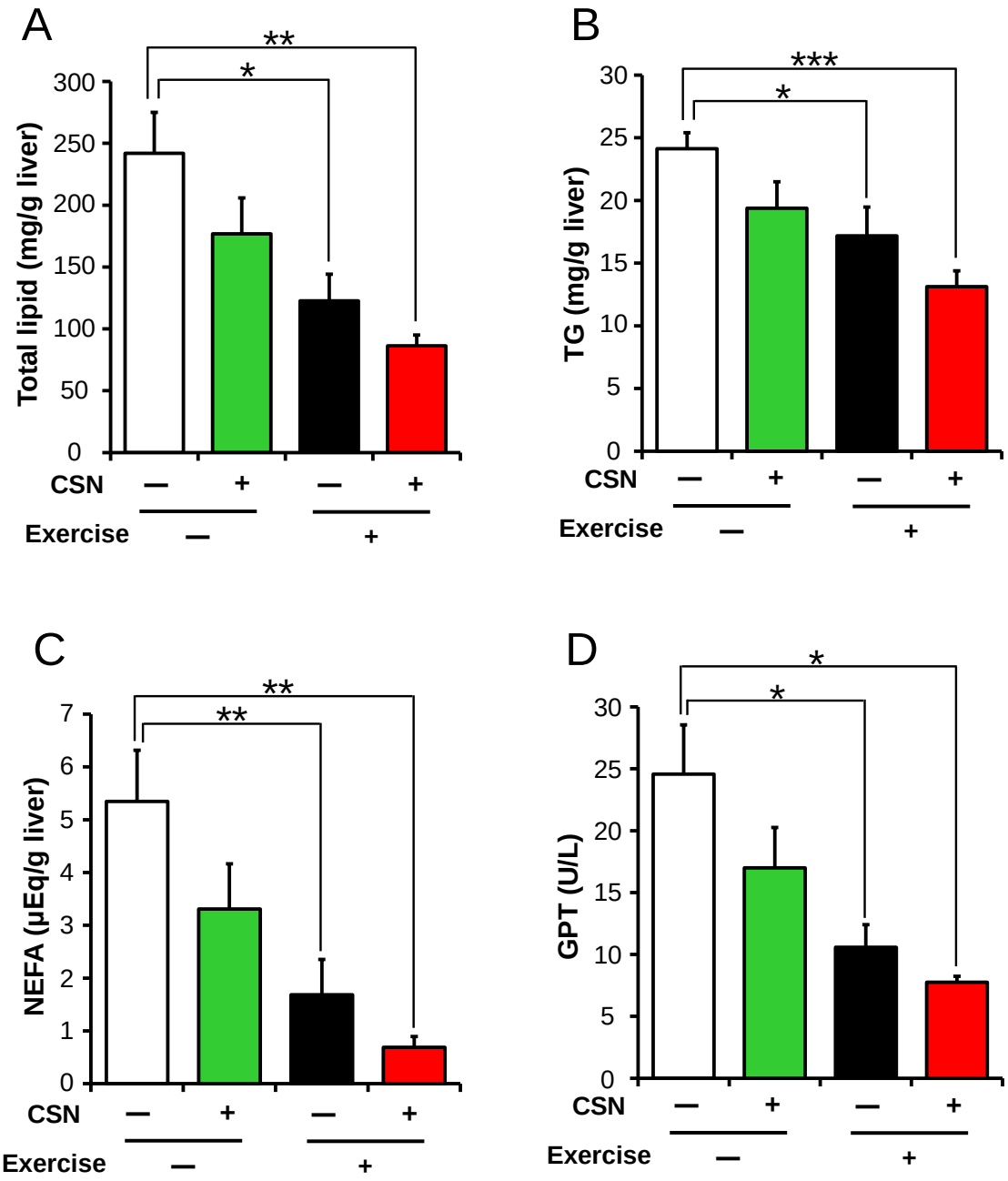

Fig. 3. CSNs supplementation with exercise improved HFD-induced liver steatosis.
A, HE liver staining. B-D, Liver levels of: B, total lipids; C, TG; and D, NEFA. F, GPT levels in the plasma of C57BL/6J mice. Mice were fed an HFD (Control), HFD supplemented with CSNs (CSN), HFD in addition to voluntary exercise (Exercise), and HFD supplemented with CSNs in addition to voluntary exercise (Exercise + CSN) for 56 days. The values represent the means ± S.E. (n=7-8). *, $p < 0.05$, **, $p < 0.01$, *** $p < 0.001$.

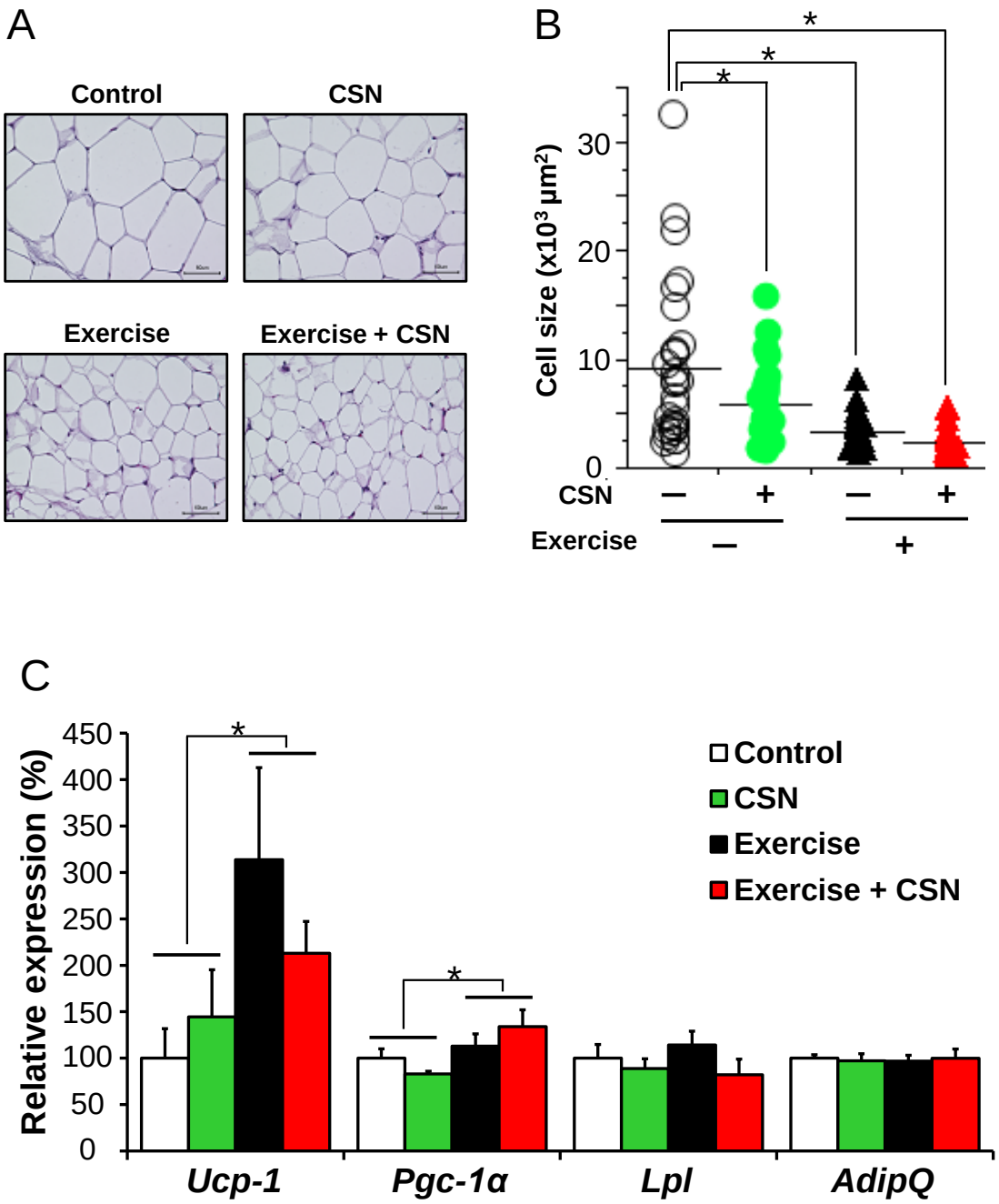

Fig. 4. CSNs supplementation with exercise decreased the cell size in the subcutaneous WAT.
A, HE staining of subcutaneous WAT; B, cell size of A (in x10^3 μm^2). The sizes of 100 randomly chosen cells in representative HE-staining slides (n = 5) were quantified by ImageJ (1.48v). Each dot represents a cell, and the horizontal bar is the group mean; and C, mRNA expression levels of uncoupling protein-1 (*Ucp-1*), peroxisome proliferator-activated receptor gamma coactivator-1α (*Pgc-1a*), lipoprotein lipase (*Lpl*), and adiponectin (*AdipQ*) in the subcutaneous WAT of C57BL/6J mice fed an HFD (Control), HFD supplemented with CSNs (CSN), HFD in addition to voluntary exercise (Exercise), and HFD supplemented with CSNs in addition to voluntary exercise (Exercise + CSN) for 56 days. The values represent the means ± S.E. (n=7-8). *, $p < 0.05$, **, $p < 0.01$, *** $p < 0.001$.

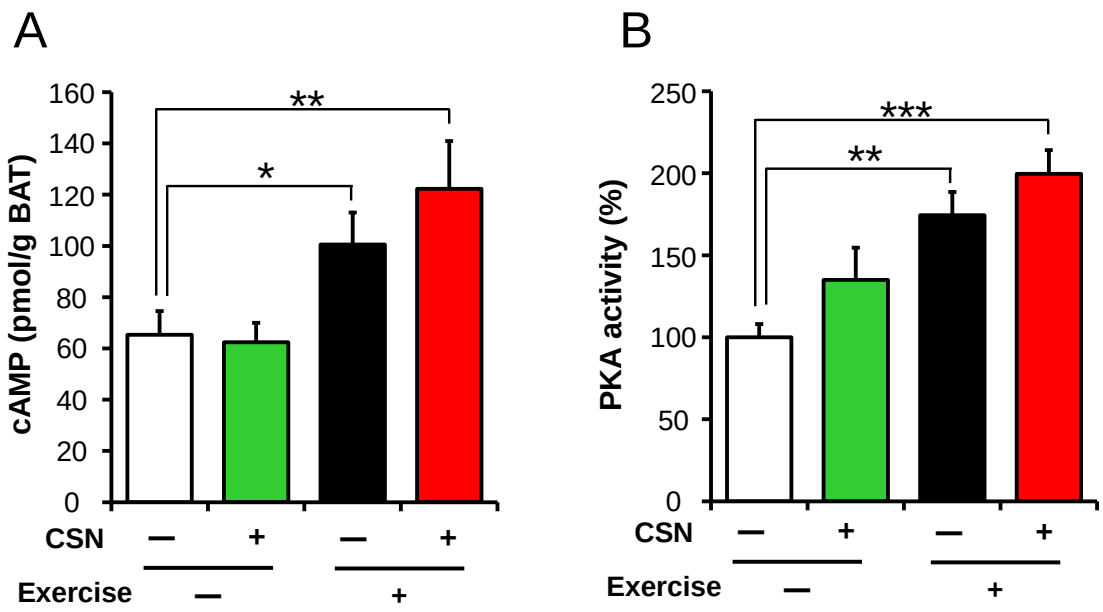

Fig.5 CSNs supplementation with exercise increased cAMP levels and PKA activity in the BAT.
A, The level of cyclic-AMP (cAMP); B, protein kinase A (PKA) activity in the BAT of C57BL/6J mice fed an HFD (Control), HFD supplemented with CSNs (CSN), HFD in addition to voluntary exercise (Exercise), and HFD supplemented with CSNs in addition to voluntary exercise (Exercise + CSN) for 56 days. The values represent the means ± S.E. (n=7-8). *, $p < 0.05$, **, $p < 0.01$, *** $p < 0.001$.

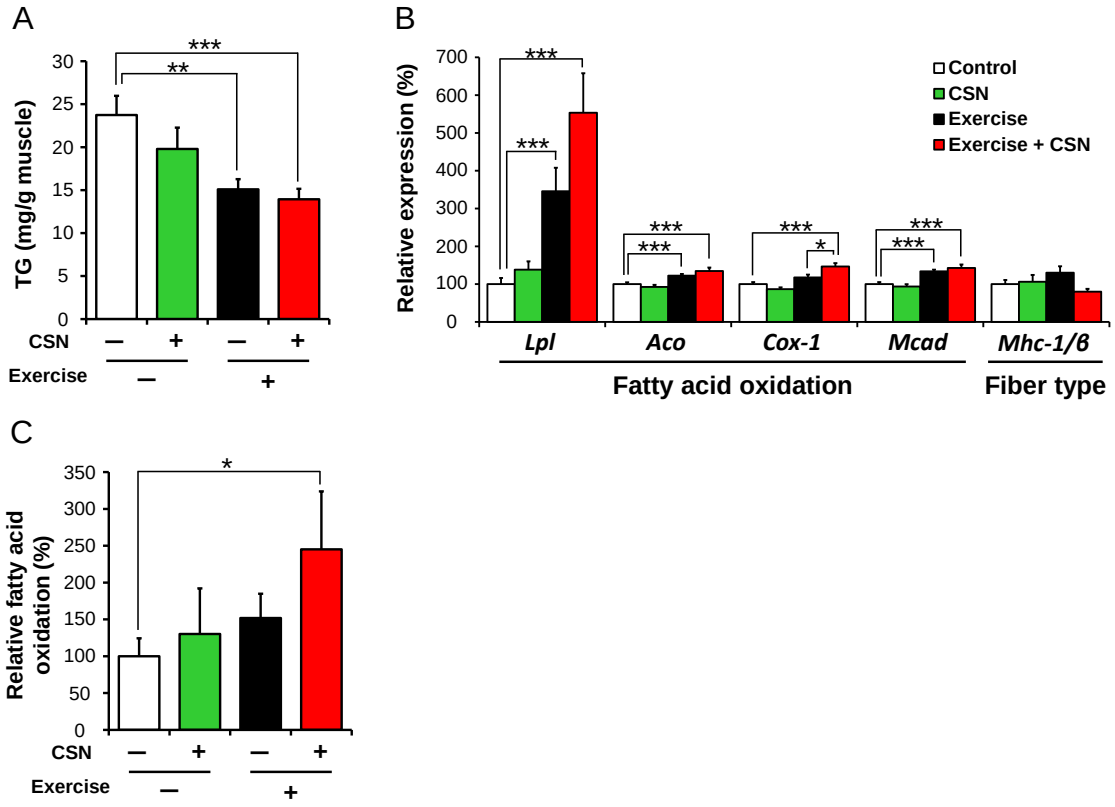

Fig. 6. CSNs supplementation with exercise increased fatty acid oxidation by activating the oxidative phosphorylation (OXPHOS) gene program in the gastrocnemius muscle.

A, The level of TGs in the gastrocnemius muscle; B, the mRNA expression levels of lipoprotein lipase (*Lpl*), acyl-CoA oxidase (*Aco*), cytochrome C oxidase-1 (*Cox-1*), medium-chain acyl dehydrogenase (*Mcad*) and myosin heavy chain-1/β (*Mhc-1/β*) in the gastrocnemius muscle; and C, fatty acid oxidation rate in the gastrocnemius muscle of C57BL/6J mice fed an HFD (Control), HFD supplemented with CSNs (CSN), HFD in addition to voluntary exercise (Exercise), and HFD supplemented with CSNs in addition to voluntary exercise (Exercise + CSN) for 56 days. The values represent the means ± S.E. (n=7-8). *, $p < 0.05$, **, $p < 0.01$, *** $p < 0.001$.

REFERENCES

1. Anthonsen MW, Ronnstrand L, Wernstedt C, Degerman E, and Holm C, Identification of novel phosphorylation sites in hormone-sensitive lipase that are phosphorylated in response to isoproterenol and govern activation properties in vitro. J Biol Chem. 273: 215-21, 1998.
2. Baar K, Wende AR, Jones TE, Marison M, Nolte LA, Chen M, Kelly DP, and Holloszy JO, Adaptations of skeletal muscle to exercise: rapid increase in the transcriptional coactivator PGC-1. FASEB J. 16: 1879-86, 2002.
3. Baraldi PG, Preti D, Materazzi S, and Geppetti P, Transient receptor potential ankyrin 1 (TRPA1) channel as emerging target for novel analgesics and anti-inflammatory agents. J Med Chem. 53: 5085-107, 2010.
4. Batsis JA, Nieto-Martinez RE, and Lopez-Jimenez F, Metabolic syndrome: from global epidemiology to individualized medicine. Clin Pharmacol Ther. 82: 509-24, 2007.
5. Bostrom P, Wu J, Jedrychowski MP, Korde A, Ye L, Lo JC, Rasbach KA, Bostrom EA, Choi JH, Long JZ, Kajimura S, Zingaretti MC, Vind BF, Tu H, Cinti S, Hojlund K, Gygi SP, and Spiegelman BM, A PGC1-alpha-dependent myokine that drives brown-fat-like development of white fat and thermogenesis. Nature. 481: 463-8, 2012.
6. Cannon B and Nedergaard J, Brown adipose tissue: function and physiological significance. Physiol Rev. 84: 277-359, 2004.
7. Carlson CL and Winder WW, Liver AMP-activated protein kinase and acetyl-CoA carboxylase during and after exercise. J Appl Physiol. 86: 669-74, 1999.
8. Degerman E, Smith CJ, Tornqvist H, Vasta V, Belfrage P, and Manganiello VC, Evidence that insulin and isoprenaline activate the cGMP-inhibited low-Km cAMP phosphodiesterase in rat fat cells by phosphorylation. Proc Natl Acad Sci U S A. 87: 533-7, 1990.
9. Fedorenko A, Lishko PV, and Kirichok Y, Mechanism of fatty-acid-dependent UCP1 uncoupling in brown fat mitochondria. Cell. 151: 400-13, 2012.
10. Folch J, Lees M, and Sloane Stanley GH, A simple method for the isolation and purification of total lipides from animal tissues. J Biol Chem. 226: 497-509, 1957.
11. Haramizu S, Mizunoya W, Masuda Y, Ohnuki K, Watanabe T, Yazawa S, and Fushiki T, Capsiate, a nonpungent capsaicin analog, increases endurance swimming capacity of mice by stimulation of vanilloid receptors. Biosci Biotechnol Biochem. 70: 774-81, 2006.
12. Holm C, Molecular mechanisms regulating hormone-sensitive lipase and lipolysis. Biochem Soc Trans. 31: 1120-4, 2003.
13. Horowitz JF and Klein S, Lipid metabolism during endurance exercise. Am J Clin Nutr. 72: 558S-63S, 2000.

14. Iida T, Moriyama T, Kobata K, Morita A, Murayama N, Hashizume S, Fushiki T, Yazawa S, Watanabe T, and Tominaga M, TRPV1 activation and induction of nociceptive response by a non-pungent capsaicin-like compound, capsiate. Neuropharmacology. 44: 958-67, 2003.

15. Inoue N, Matsunaga Y, Satoh H, and Takahashi M, Enhanced energy expenditure and fat oxidation in humans with high BMI scores by the ingestion of novel and non-pungent capsaicin analogues (capsinoids). Biosci Biotechnol Biochem. 71: 380-9, 2007.

16. Inoue N, Nogusa Y, Hara-Kimura Y, Okabe-Nogusa Y, Ohyama K, Tsukamoto-Yasui M, and Ono K, Capsinoids prevent diet-induced obesity and insulin resistance via activation of TRPV1. Int J Obes (Lond). submitted.

17. Jeukendrup AE, Saris WH, and Wagenmakers AJ, Fat metabolism during exercise: a review--part II: regulation of metabolism and the effects of training. Int J Sports Med. 19: 293-302, 1998.

18. Kang JH, Goto T, Han IS, Kawada T, Kim YM, and Yu R, Dietary capsaicin reduces obesity-induced insulin resistance and hepatic steatosis in obese mice fed a high-fat diet. Obesity (Silver Spring). 18: 780-7, 2010.

19. Kawabata F, Inoue N, Yazawa S, Kawada T, Inoue K, and Fushiki T, Effects of CH-19 sweet, a non-pungent cultivar of red pepper, in decreasing the body weight and suppressing body fat accumulation by sympathetic nerve activation in humans. Biosci Biotechnol Biochem. 70: 2824-35, 2006.

20. Kawada T, Hagihara K, and Iwai K, Effects of capsaicin on lipid metabolism in rats fed a high fat diet. J Nutr. 116: 1272-8, 1986.

21. Kawai N, Kawai T, and Kawai K, [Ultrasonic and laboratory studies on fatty liver in white-collar workers]. Nihon Shokakibyo Gakkai Zasshi. 92: 1058-65, 1995.

22. Klaus S, Pultz S, Thone-Reineke C, and Wolfram S, Epigallocatechin gallate attenuates diet-induced obesity in mice by decreasing energy absorption and increasing fat oxidation. Int J Obes (Lond). 29: 615-23, 2005.

23. Kobata K, Sutoh K, Todo T, Yazawa S, Iwai K, and Watanabe T, Nordihydrocapsiate, a new capsinoid from the fruits of a nonpungent pepper, capsicum annuum. J Nat Prod. 62: 335-6, 1999.

24. Kobata K, Todo T, Yazawa S, Iwai K, and Watanabe T, Novel Capsaicinoid-like Substances, Capsiate and Dihydrocapsiate, from the Fruits of a Nonpungent Cultivar, CH-19 Sweet, of Pepper (Capsicum annuum L.). Journal of Agricultural and Food Chemistry. 46: 1695-1697, 1998.

25. Kohrt WM, Bloomfield SA, Little KD, Nelson ME, and Yingling VR, American College of Sports Medicine Position Stand: physical activity and bone health. Med Sci Sports Exerc. 36: 1985-96, 2004.

26. Lavoie JM and Gauthier MS, Regulation of fat metabolism in the liver: link to non-alcoholic hepatic steatosis and impact of physical exercise. Cell Mol Life Sci. 63: 1393-409, 2006.

27. Lee IM, Physical activity and cancer prevention--data from epidemiologic studies. Med Sci

Sports Exerc. 35: 1823-7, 2003.

28. Lin J, Wu H, Tarr PT, Zhang CY, Wu Z, Boss O, Michael LF, Puigserver P, Isotani E, Olson EN, Lowell BB, Bassel-Duby R, and Spiegelman BM, Transcriptional co-activator PGC-1 alpha drives the formation of slow-twitch muscle fibres. Nature. 418: 797-801, 2002.

29. Lowell BB and Spiegelman BM, Towards a molecular understanding of adaptive thermogenesis. Nature. 404: 652-60, 2000.

30. Luo Z, Ma L, Zhao Z, He H, Yang D, Feng X, Ma S, Chen X, Zhu T, Cao T, Liu D, Nilius B, Huang Y, Yan Z, and Zhu Z, TRPV1 activation improves exercise endurance and energy metabolism through PGC-1alpha upregulation in mice. Cell Res. 22: 551-64, 2012.

31. Masuda Y, Haramizu S, Oki K, Ohnuki K, Watanabe T, Yazawa S, Kawada T, Hashizume S, and Fushiki T, Upregulation of uncoupling proteins by oral administration of capsiate, a nonpungent capsaicin analog. J Appl Physiol. 95: 2408-15, 2003.

32. Matsuzawa Y, The metabolic syndrome and adipocytokines. FEBS Lett. 580: 2917-21, 2006.

33. Murase T, Haramizu S, Shimotoyodome A, and Tokimitsu I, Reduction of diet-induced obesity by a combination of tea-catechin intake and regular swimming. Int J Obes (Lond). 30: 561-8, 2006.

34. Murase T, Nagasawa A, Suzuki J, Hase T, and Tokimitsu I, Beneficial effects of tea catechins on diet-induced obesity: stimulation of lipid catabolism in the liver. Int J Obes Relat Metab Disord. 26: 1459-64, 2002.

35. Nagao T, Komine Y, Soga S, Meguro S, Hase T, Tanaka Y, and Tokimitsu I, Ingestion of a tea rich in catechins leads to a reduction in body fat and malondialdehyde-modified LDL in men. Am J Clin Nutr. 81: 122-9, 2005.

36. Nedergaard J, Golozoubova V, Matthias A, Asadi A, Jacobsson A, and Cannon B, UCP1: the only protein able to mediate adaptive non-shivering thermogenesis and metabolic inefficiency. Biochim Biophys Acta. 1504: 82-106, 2001.

37. Oh-ishi S, Kizaki T, Toshinai K, Haga S, Fukuda K, Nagata N, and Ohno H, Swimming training improves brown-adipose-tissue activity in young and old mice. Mech Ageing Dev. 89: 67-78, 1996.

38. Oh KS, Kim EY, Yoon M, and Lee CM, Swim training improves leptin receptor deficiency-induced obesity and lipid disorder by activating uncoupling proteins. Exp Mol Med. 39: 385-94, 2007.

39. Ohnuki K, Haramizu S, Oki K, Watanabe T, Yazawa S, and Fushiki T, Administration of capsiate, a non-pungent capsaicin analog, promotes energy metabolism and suppresses body fat accumulation in mice. Biosci Biotechnol Biochem. 65: 2735-40, 2001.

40. Ohnuki K, Niwa S, Maeda S, Inoue N, Yazawa S, and Fushiki T, CH-19 sweet, a non-pungent cultivar of red pepper, increased body temperature and oxygen consumption in humans. Biosci Biotechnol Biochem. 65: 2033-6, 2001.

41. Ono K, Tsukamoto-Yasui M, Hara-Kimura Y, Inoue N, Nogusa Y, Okabe Y, Nagashima K, and Kato F, Intragastric administration of capsiate, a transient receptor potential channel agonist, triggers thermogenic sympathetic responses. J Appl Physiol. 110: 789-98, 2011.

42. Park H, Kaushik VK, Constant S, Prentki M, Przybytkowski E, Ruderman NB, and Saha AK, Coordinate regulation of malonyl-CoA decarboxylase, sn-glycerol-3-phosphate acyltransferase, and acetyl-CoA carboxylase by AMP-activated protein kinase in rat tissues in response to exercise. J Biol Chem. 277: 32571-7, 2002.

43. Patapoutian A, Peier AM, Story GM, and Viswanath V, ThermoTRP channels and beyond: mechanisms of temperature sensation. Nat Rev Neurosci. 4: 529-39, 2003.

44. Pilegaard H, Saltin B, and Neufer PD, Exercise induces transient transcriptional activation of the PGC-1alpha gene in human skeletal muscle. J Physiol. 546: 851-8, 2003.

45. Puigserver P and Spiegelman BM, Peroxisome proliferator-activated receptor-gamma coactivator 1 alpha (PGC-1 alpha): transcriptional coactivator and metabolic regulator. Endocr Rev. 24: 78-90, 2003.

46. Sallis JF, Haskell WL, Fortmann SP, Vranizan KM, Taylor CB, and Solomon DS, Predictors of adoption and maintenance of physical activity in a community sample. Prev Med. 15: 331-41, 1986.

47. Sasahara I, Furuhata Y, Iwasaki Y, Inoue N, Sato H, Watanabe T, and Takahashi M, Assessment of the biological similarity of three capsaicin analogs (Capsinoids) found in non-pungent chili pepper (CH-19 Sweet) fruits. Biosci Biotechnol Biochem. 74: 274-8, 2010.

48. Sherwood NE and Jeffery RW, The behavioral determinants of exercise: implications for physical activity interventions. Annu Rev Nutr. 20: 21-44, 2000.

49. Shintaku K, Uchida K, Suzuki Y, Zhou Y, Fushiki T, Watanabe T, Yazawa S, and Tominaga M, Activation of transient receptor potential A1 by a non-pungent capsaicin-like compound, capsiate. Br J Pharmacol. 165: 1476-86, 2012.

50. Snitker S, Fujishima Y, Shen H, Ott S, Pi-Sunyer X, Furuhata Y, Sato H, and Takahashi M, Effects of novel capsinoid treatment on fatness and energy metabolism in humans: possible pharmacogenetic implications. Am J Clin Nutr. 89: 45-50, 2009.

51. Spiegelman BM and Flier JS, Obesity and the regulation of energy balance. Cell. 104: 531-43, 2001.

52. Steyn NP, Mann J, Bennett PH, Temple N, Zimmet P, Tuomilehto J, Lindstrom J, and Louheranta A, Diet, nutrition and the prevention of type 2 diabetes. Public Health Nutr. 7: 147-65, 2004.

53. Tani Y, Fujioka T, Sumioka M, Furuichi Y, Hamada H, and Watanabe T, Effects of capsinoid on serum and liver lipids in hyperlipidemic rats. J Nutr Sci Vitaminol (Tokyo). 50: 351-5, 2004.

54. Trauner M, Arrese M, and Wagner M, Fatty liver and lipotoxicity. Biochim Biophys Acta. 1801: 299-310, 2010.

55. Urhausen A, Gabriel H, and Kindermann W, Blood hormones as markers of training stress and overtraining. Sports Med. 20: 251-76, 1995.

56. Weir JB, New methods for calculating metabolic rate with special reference to protein metabolism. J Physiol. 109: 1-9, 1949.

57. Wolfram S, Raederstorff D, Wang Y, Teixeira SR, Elste V, and Weber P, TEAVIGO (epigallocatechin gallate) supplementation prevents obesity in rodents by reducing adipose tissue mass. Ann Nutr Metab. 49: 54-63, 2005.

58. Xu X, Ying Z, Cai M, Xu Z, Li Y, Jiang SY, Tzan K, Wang A, Parthasarathy S, He G, Rajagopalan S, and Sun Q, Exercise ameliorates high-fat diet-induced metabolic and vascular dysfunction, and increases adipocyte progenitor cell population in brown adipose tissue. Am J Physiol Regul Integr Comp Physiol. 300: R1115-25, 2011.

59. Yan Z, Okutsu M, Akhtar YN, and Lira VA, Regulation of exercise-induced fiber type transformation, mitochondrial biogenesis, and angiogenesis in skeletal muscle. J Appl Physiol. 110: 264-74, 2011.

60. Yoneshiro T, Aita S, Kawai Y, Iwanaga T, and Saito M, Nonpungent capsaicin analogs (capsinoids) increase energy expenditure through the activation of brown adipose tissue in humans. Am J Clin Nutr. 95: 845-50, 2012.

61. Yoneshiro T, Aita S, Matsushita M, Kayahara T, Kameya T, Kawai Y, Iwanaga T, and Saito M, Recruited brown adipose tissue as an antiobesity agent in humans. J Clin Invest. 123: 3404-8, 2013.

CHAPTER. IV

Catechin-Rich Grape Seed Extract Supplementation Attenuates Diet-Induced Obesity in C57BL/6J Mice

Chapter. IV

Catechin-Rich Grape Seed Extract Supplementation Attenuates Diet-Induced Obesity in C57BL/6J Mice

INTRODUCTION

In recent years, there has been a rapid increase in the adult obese population in Western countries (1). This problem is characterized by an increase in the number and size of fat cells in the adipose tissue due to the imbalance between energy intake and energy expenditure. Obesity is a major risk factor for a number of chronic diseases, including diabetes, hypertension, and heart disease (2). To manage or prevent obesity, it is required to implement lifestyle changes such as increasing energy consumption and/or reducing calorie intake, as well as changing dietary habits. The red content of wine is produced not only from the juice of the grapes, but also from their skins and seeds, which are rich in polyphenols such as tannins and proanthocyanidins (3, 4). Grape seeds, although they make up a small percentage of the composition of grapes, contain two thirds of the extractable polyphenols (5). Proanthocyanidin polymers in grape seed extracts (GSEs) are reported to present health benefits in animal models, such as antioxidant activity in rats (6), anti-atherogenic activity in rabbits (7), and the amelioration of lipid metabolism in rats (8, 9) . Furthermore, it is reported that GSEs improved the disease presentation of type 2 diabetes in db/db mice (10). Overall, GSEs are thought to prevent and attenuate the symptoms of the metabolic syndrome in animal models.

The particular GSE we used in our study, catechin rich GSE (CGSE), is a product

manufactured using specially selected materials. In the preliminary analysis, CGSE was shown to be a 98% purified polyphenol product and was found to contain high concentrations of monomeric proanthocyanidins. Because most GSEs are reportedly rich in polymers in products such as Gravinol [proanthocyanidin (1 dimer) 89.3%] (11) and grape seed procyanidin extract [procyanidin (1 dimer) 79.77%] (12), this product might be very unique in this way. As previously mentioned, the anti-obesity activity of high-polymer-enriched GSEs has been investigated in previous studies (8, 9). However, the protective activities of monomeric polyphenol-enriched GSEs, such as CGSE, against obesity have never been studied. To clarify the anti-obesity effects of CGSE, we precisely analyzed the components of CGSE using liquid chromatography-mass spectrometry (LC-MS) and evaluated the effects using diet induced-obesity in a mouse model.

MATERIAL AND METHODS

Componential Analysis Using LC-MS

The commercial CGSE used in this study (OmniVin) was kindly provided by Ajinomoto Omnichem (Louvain-la-Neuve, Belgium). Constituents of CGSE were analyzed by LC-MS using Quattro micro TM API (Waters Co., Ltd.) interfaced to Mass-Lyncs TM (Waters Co., Ltd.). The flow was operated in an Inertsil ODS-3 (I.D. 4.6 x 250 mm, 5 μm, GL Sciences Co., Ltd.) column at 40 ^{o}C. CGSE (20 mg) was extracted with 10 ml of distilled water and filtered through a 0.45 μm filter. Five microliters of sample solution were injected at a flow rate of 0.3 ml/min and separated with 20% methanol with 0.05% trifluoroacetic acid for 20 min followed by a gradient of 20–50% methanol with trifluoroacetic acid for 60 min at a flow rate of 0.3 ml/min. The determination of catechin

and epicatechin contents (both Wako, Osaka, Japan) was performed using authentic samples of each compound.

Animals and Diets

C57BL/6J male mice were purchased from Charles River Japan, Inc. (Kanagawa, Japan) at 7 weeks of age. They were housed in a light-controlled environment (lights on from 14.00 to 2.00 h) at 25 ± 1 ^{o}C with food and water provided ad libitum. All animal experiments were approved by the Animal Committee of Ajinomoto Co., Inc. (Tokyo, Japan), and the animals received care in compliance with guidelines for the care and use of laboratory animals.

Experimental Setup

In the first experiment, the acute effect of orally administered CGSE was investigated in 14- to 15-week-old male C57BL/6J mice fed with a standard diet (CRF-1). In total, 16 mice were randomly divided into two groups. The vehicle group received oral doses of water only (n = 8) and the CGSE group received CGSE at 500 mg/kg dissolved in water (n = 8) for 3 days. All applications were performed between 13.00 and 14.00 h (1 h before onset of the dark period). Oxygen consumption, respiratory quotient (RQ = V CO_2 /V O_2) and spontaneous activity were measured continuously for 3 days. In the second experiment, we investigated the effect of dietary supplied CGSE on dietary-induced obesity in C57BL/6J mice. In total, 48 male C57BL/6J mice aged 9 weeks were divided into 4 groups (n = 12/group) and fed one of the following diets for 12 weeks: standard diet (STD), high-fat diet (HFD), or HFD supplemented with 0.5% (w/w) or 1% (w/w) CGSE. CGSE was mixed into a chow supplied in powder form (table 1). Food and

water were always supplied ad libitum. Body weight and food intake were monitored twice a week. At the end of the experiment, mice were anesthetized with ether. Blood samples were centrifuged at 3,000 g for 10 min at 4 ^{o}C, and the plasma was separated and stored at –20 ^{o}C. Organs [liver, mesenteric white adipose tissue (WAT), perirenal WAT, epididymal WAT, and subcutaneous WAT] were immediately frozen in liquid nitrogen and stored at –80 ^{o}C.

Blood Analysis

The plasma levels of blood glucose and glutamate pyruvate transaminase (GPT) were determined using Fuji Dri-Chem (Fujifilm, Tokyo, Japan). Plasma insulin and leptin levels were determined by mouse enzyme-linked immunosorbent assay kits (Morinaga, Kanagawa, Japan). Plasma levels of cholesterol and triglyceride (TG) were determined by the cholesterol and TG test Wako kits (both Wako), respectively.

Liver Lipid Analysis

Liver lipid was extracted by Folch partition (13), with slight modifications as follows; a portion (300 mg) of the liver tissue was homogenized in 2.5 ml of methanol, and 5 ml of chloroform was added. The mixture was horizontally shaken for 10 min and placed at 4 ^{o}C overnight for lipid extraction. The extracted samples were filtered (Kiriyama-rohto; Kiriyama, Tokyo, Japan) and filled to 8 ml by aliquots of methanol:chloroform (2: 1, v/v). Saline (1.6 ml) was then added. The mixture was horizontally shaken for 10 min and centrifuged at 2,000 rpm for 5 min at 4 ^{o}C. The supernatant was eliminated and the lower chloroform phase was filled to 6 ml by chloroform. The lipid fraction (2.5 ml) in this phase was dried and weighed. The dried

lipid was dissolved in 1 ml of 10% Triton/ isopropanol, and TG levels were determined using the TG test Wako kit.

Quantitative Real-Time PCR

Total RNA was isolated from the liver using Isogen (Nippon Gene, Tokyo, Japan). cDNAs were synthesized from 1 μg of RNA using PrimeScript TM RT Enzyme (Takara, Shiga, Japan). After cDNA synthesis, quantitative real-time PCR was performed in 25 μl of SYBR Premix Ex Taq Mix (Takara) using a fluorometric thermal cycler (Thermal Cycler Dice® Real Time System; Takara). Reaction mixtures were incubated for an initial denaturation at 95 ºC for 10 s, followed by 45 cycles at 95 ºC for 5 s and 60 ºC for 20 s. The sequences of the sense and antisense primers are listed in table 2. To account for possible variation related to cDNA input or the presence of PCR inhibitors, the endogenous reference gene 18S was simultaneously amplified for each sample and data were normalized accordingly.

Respiratory Gas Analysis and Measurement Activity

Utilizing a respiratory gas analysis system consisting of an acrylic metabolic chamber, gas analyzers, and a switching system (ARCO2000-RAT/ANI System; Arco, Chiba, Japan), gas was sampled from each metabolic chamber and measured as described previously (14). Briefly, room air was constantly pumped through the chamber, and expired air was dried in a thin cotton column and then introduced into a gas analyzer. RQ was calculated according to the report by Weir (15). Spontaneous activities were measured by an activity sensor (NS-AS01; Neuroscience, Tokyo, Japan). All measurements were performed in 4.5-min intervals.

Statistical Analysis

Results are given as means 8 SEM. Data analyses between the groups were conducted by the unpaired Student's t test (first experiment) or the Tukey-Kramer test (second experiment) using statistical software (Statview 5.0 for Windows, SAS Institute Inc., Cary, N.C., USA). Differences at $p<0.05$ were considered statistically significant.

RESULTS

Componential Analysis of CGSE

To confirm the content of CGSE, we evaluated the componential analysis of CGSE using LC-MS. LC-MS analysis confirmed the presence of catechin and epicatechin (**fig. 1**). The contents of catechin and epicatechin in CGSE were 220 and 180 mg/g, respectively.

Acute Effects of Orally Administered CGSE on Parameters of Energy Metabolism

It is reported that tea catechins upregulate energy metabolism (16, 17). Therefore, we considered the potential effect of CGSE on energy metabolism due to its high catechin contents. We evaluated the acute effects of CGSE on energy homeostasis and substrate oxidation. Figure 2 shows the daily patterns of oxygen consumption (**fig. 2a**), RQ (**fig. 2b**), and spontaneous activity (**fig. 2c**) during the 3-day oral administration. There was no effect of CGSE on the pattern of oxygen consumption or spontaneous activity. However, although it was not statistically significant, RQ tended to decrease following repeated treatment with 500 mg/kg CGSE compared with control (**table 3**).

Long-Term CGSE Supplementation in Mice with HFD-Induced Obesity

Long-term dietary supplementation of CGSE significantly affected body weight development (**fig. 3a**). CGSE suppressed weight gain by feeding HFD in a dose-dependent manner. The difference in body weights between the 1% CGSE group and the HFD control group was statistically significant during the experimental period. Neither daily nor total food intake during the period of supplementation was affected. The reduction in body fat and liver by CGSE was also observed and correlated with the suppressed body weight gain by CGSE (**table 4**). The weight of subcutaneous, epididymal, mesenteric, and perirenal WAT and liver in 1% CGSE-supplemented mice was reduced by 50, 36, 58, 43, and 21%, respectively, compared with the HFD control group. Quadriceps muscle weight was not affected by CGSE supplementation.

To investigate the effect of CGSE on the metabolic blood parameters and circulating adipocytokines, we measured blood glucose and plasma insulin, leptin, GPT, cholesterol, and TG concentrations. With HFD supplementation, blood glucose, plasma leptin, and cholesterol concentrations were significantly increased compared to the STD. Plasma insulin increased more than twice in the HFD compared with the STD group, but because of its high variance, it was not statistically significant. CGSE decreased blood glucose and plasma insulin, leptin, GPT, and cholesterol concentrations compared to the HFD group (**table 5**). Supplementation with 1% CGSE decreased blood glucose, plasma insulin, leptin, GPT, and cholesterol by 14, 60, 83, 57, and 21%, respectively, compared with the HFD controls. There was no statistical difference in plasma TG between the groups.

Total lipid and TG contents in the liver were decreased by 48 and 64%, respectively,

in the 1% CGSE-supplemented mice compared with the HFD mice (**fig. 3b, c**). We determined the expression of genes relevant to fatty acid metabolism, such as acyl-CoA oxidase (ACO) and carnitine palmitoyltransferase I (CPT-1). The mRNA levels of ACO were significantly increased by CGSE supplementation (**fig. 3d**). The mRNA levels of CPT-1 tended to increase as a result of 0.5% CGSE supplementation (**fig. 3e**).

Parameters of Energy Metabolism in Chronic CGSE Supplementation

To investigate the effect of CGSE on energy homeostasis, we examined energy expenditure after a 12-week CGSE supplementation with HFD. We determined expired gas, RQ, and spontaneous activity over the last 4 days of the supplementation period. CGSE supplementation (1%) tended to increase expired gas and spontaneous activity, and decrease RQ, but they were not statistically significant (data not shown).

DISCUSSION

GSEs have been reported to have beneficial effects on health as antioxidants, anti-thrombotics, and cardioprotectants (18-20). Furthermore, it has been reported that GSEs display anti-obesity activity. The anti-metabolic activities of GSEs have been determined using high-fat, high-fructose diet-induced obesity models in mice and rats (9, 21). Because most commercialized GSEs are rich in proanthocyanidins, we speculated that most of those activities were attributed to proanthocyanidins.

On the other hand, CGSEs are rich in monomeric catechins. The LC-MS analysis revealed that CGSE included 220 mg/g catechin and 180 mg/g epicatechin. These CGSE components are completely contrary to those of typical GSEs. For example,

representative GSE such as Gravinol S included only 25 mg/g catechin and 22 mg/g epicatechin, representing only a small component of the total GSE (11). Therefore, we aimed to determine how the componential differences in CGSEs would affect physiological functions.

We assumed that the main action behind the anti-obesity effect of CGSE was based on the high concentration of the very bioavailable compounds: catechin and epicatechin. Some reports describe the activities of catechin and epicatechin in in vitro experiments using differentiation of 3T3-L1 preadipocytes to adipocytes, in which catechin and epicatechin suppressed intracellular lipid accumulation (22). Another report using 3T3-L1 cells to evaluate anti-mitogenic effects revealed that epicatechin suppressed cell differentiation in the cells (23). Thus, catechin and epicatechin have been shown to have effects related to antiobesity in vitro, and the absorption and bioavailability ofthe compounds are high. Therefore, it is reasonably concluded that catechin and epicatechin in CGSEs are the main contributors to the anti-obesity effect. However, there is still a possibility that unidentified components in CGSEs other than catechin and epicatechin might contribute to the anti-obesity effect. CGSE is a 98% purified polyphenol product, so components other than monomeric catechins are thought to be oligomers and polymers, for example flavonol polymers and tannins. It is reported that GSE, which contains higher percentages of oligomers and polymers than CGSE, possesses stronger lipase inhibitor activity (24, 25). Since lipase inhibitors suppress the absorption of lipids, their supplementation combined with HFD conditions results in suppression of body weight gain and an increase in fecal lipid excretion. In the present study, lipid content in the feces that were collected for 7 days after 8 weeks of CGSE supplementation under HFD conditions did not differ compared with the HFD controls (data not shown). Consequently,

suppression of weight gain due to CGSE supplementation was not effected by inhibition of lipid absorption, suggesting oligomer and polymer fractions may play only a small role in the anti-obesity effect of CGSE compared to the effects of catechin and epicatechin.

Throughout the long-term CGSE supplementation experimental period, food calorie and water intake in CGSE-supplemented groups was equal to that in their non-supplemented counterparts. Nevertheless, the body weight gain and adipose tissue weight gain in CGSE-supplemented groups were significantly suppressed in a dose-dependent manner. The reduced body weight gain induced by CGSE was exclusively due to the reduction in body fat. Acute and chronic CGSE administration indicated a tendency to reduced RQ. In chronic CGSE administration, the mRNA expression level of ACO and CPT-1 in the liver increased. The reduction in RQ implies changes in substrate utilization from glucose to fat, and ACO and CPT-1 are the genes relevant to fatty acid metabolism (26, 27). These data suggest that the body fat reduction following CGSE supplementation may be due to the increased fatty acid oxidation. However, the reduction in RQ by acute or chronic CGSE administration was not significant; the effect of CGSE on energy metabolism has to be evaluated in more detail in future studies.

Previous studies have reported that excessive TG accumulation in the liver by HFD induces disorders such as fatty liver, or can progress to liver cirrhosis and even hepatocellular cancer (28). CGSE supplementation decreased the total lipid and TG content of the liver, in particular 1% CGSE supplementation resulted in marked decreases in the STD group. Plasma cholesterol levels were significantly lower in the CGSE-supplemented groups, too. Plasma GPT, a sensitive parameter in the diagnosis of fatty liver in humans (29), also decreased dramatically in the CGSE groups. Taken together, CGSE seems to have a high potential to control lipid metabolism in mice. Park et al. (21)

reported that HFDs with GSE supplementation reduced plasma and liver TG as well as cholesterol levels in mice by inducing carnitine fraction levels in the liver and, as a result, increased β-oxidation in the liver. Upregulation of ACO gene expression in the liver implies that CGSE supplementation markedly improves HFD induced fatty liver pathology by increasing β-oxidation.

The reduction in serum leptin levels was higher with 1% than 0.5% CGSE supplementation. Because serum leptin levels are highly correlated with fat mass (30), this decrease could be a simple consequence of the reduced subcutaneous, epididymal, mesenteric, and perirenal WAT depots. Obese animals were shown to have higher leptin levels, indicating that these forms of animal obesity are associated with leptin resistance (31). High leptin levels in the HFD control group indicated that the mice in this experiment had developed leptin resistance. On the other hand, the leptin levels in CGSE-supplemented mice decreased significantly in the 1% CGSE groups, reaching levels of the STD group, indicating that CGSE suppresses leptin resistance induced by HFD.

In conclusion, our results indicate that CGSE supplementation significantly improves HFD-induced metabolic impairments, such as hyperlipidemia, hyperleptinemia, and fat accumulation in adipose tissue and liver. These findings suggest that monomeric catechins and epicatechins, and/or perhaps other factors of CGSE, ameliorate the pathological conditions of the metabolic syndrome in HFD-induced obesity models.

Table 1. Composition of the experimental diets (%)

	STD	HFD	HFD + 0.5% CGSE	HFD + 1% CGSE
Casein	20.00	20.00	20.00	20.00
Sucrose	10.00	10.00	10.00	10.00
Corn starch	39.75	22.48	22.11	21.73
α-Corn starch	13.20	7.47	7.34	7.22
L-Cysteine	0.30	0.30	0.30	0.30
Cellulose	5.00	5.00	5.00	5.00
Lard	7.00	30.00	30.00	30.00
Mineral mix	3.50	3.50	3.50	3.50
Vitamin mix	1.00	1.00	1.00	1.00
Choline bitartrate	0.25	0.25	0.25	0.25
TBHQ	0.0014	0.0014	0.0014	0.0014
CGSE	–	–	0.50	1.00

Table 2. Primers used for real-time PCR analysis

Gene	Sense	Antisense	ID No.
18S	GTGGAGCGATTTGTCTGGTT	AACGCCACTTGTCCCTCTAA	NR_003278
ACO	CATTGGCATCGTGAGAACAG	AGCAAATCTGATGGCTTTGA	NM_015729
CPT-1	AACCCAGTGCCTTAACGATG	GAACTGGTGGCCAATGAGAT	NM_013549

Table 3. Acute effects of orally administrated CGSE (3-day treatment) on parameters of energy metabolism in C57BL/6J mice

Parameters	Vehicle	CGSE (500 mg/kg)
Initial body weight, g	25.67 ± 0.35	25.72 ± 0.19
Final body weight, g	24.69 ± 0.32	24.66 ± 0.50
Total food intake during 3 days of treatment, g	9.48 ± 0.12	9.35 ± 0.53
Expired gas on day 3 of treatment, ml/min/$g^{0.75}$	1.077 ± 0.012	0.984 ± 0.052
RQ on day 3 of treatment	0.913 ± 0.005	0.863 ± 0.024
Spontaneous activity on day 3 of treatment, counts/min	73.29 ± 2.60	53.63 ± 10.05

Means ± SE (n = 8).

Table 4. Effects of CGSE on body and tissue weights in C57BL/6J mice fed the different diets for 84 days

Parameters	STD	HFD	HFD + 0.5% CGSE	HFD + 1% CGSE
Body weight, g	33.17 ± 0.83^{c}	41.76 ± 0.69^{a}	39.89 ± 1.47$^{a, b}$	35.95 ± 1.14$^{b, c}$
Food intake, kcal/day	13.79 ± 0.46	13.69 ± 0.25	13.85 ± 0.41	13.56 ± 0.30
Tissue weight, g				
Subcutaneous WAT	1.05 ± 0.14^{b}	2.32 ± 0.11^{a}	1.98 ± 0.21^{a}	1.15 ± 0.19^{b}
Epididymal WAT	1.17 ± 0.15^{b}	2.19 ± 0.08^{a}	2.06 ± 0.19^{a}	1.40 ± 0.15^{b}
Mesenteric WAT	0.43 ± 0.06^{b}	1.25 ± 0.11^{a}	0.95 ± 0.12^{a}	0.52 ± 0.11^{b}
Perirenal WAT	0.44 ± 0.06^{b}	0.96 ± 0.04^{a}	0.84 ± 0.08^{a}	0.55 ± 0.07^{b}
Total abdominal WAT	2.04 ± 0.27^{b}	4.41 ± 0.14^{a}	3.85 ± 0.35^{a}	2.47 ± 0.33^{b}
Liver	1.21 ± 0.04^{b}	1.59 ± 0.10^{a}	1.47 ± 0.12$^{a, b}$	1.26 ± 0.07$^{a, b}$
Quadriceps muscle	0.24 ± 0.004	0.23 ± 0.004	0.24 ± 0.004	0.25 ± 0.007

Means ± SE (n = 11–12). The values with different superscripts are significantly different ($p < 0.05$).

Table 5. Effects of CGSE on blood metabolites in C57BL/6J mice fed the different diets for 84 days

Parameters	STD	HFD	HFD + 0.5% CGSE	HFD + 1% CGSE
Blood glucose, mg/dl	202.25 ± 10.64^{b}	249.91 ± 8.56^{a}	220.25 ± 10.63^{b}	214.33 ± 15.67^{b}
Insulin, ng/ml	1.17 ± 0.27	2.84 ± 0.62	1.80 ± 0.51	1.13 ± 0.35
Leptin, ng/ml	3.50 ± 1.90^{b}	23.03 ± 3.11^{a}	17.46 ± 4.41$^{a, b}$	3.90 ± 3.67^{b}
GPT, U/l	32.33 ± 4.66$^{a, b}$	57.45 ± 11.56^{a}	34.83 ± 9.05$^{a, b}$	24.75 ± 4.39^{b}
Cholesterol, mg/dl	184.66 ± 9.07^{b}	234.62 ± 11.70^{a}	222.30 ± 10.86$^{a, b}$	184.90 ± 7.91^{b}
TG, mg/dl	72.99 ± 4.76	66.23 ± 2.78	66.70 ± 2.15	68.54 ± 3.06

Means ± SE (n = 11–12). The values with different superscripts are significantly different ($p < 0.05$).

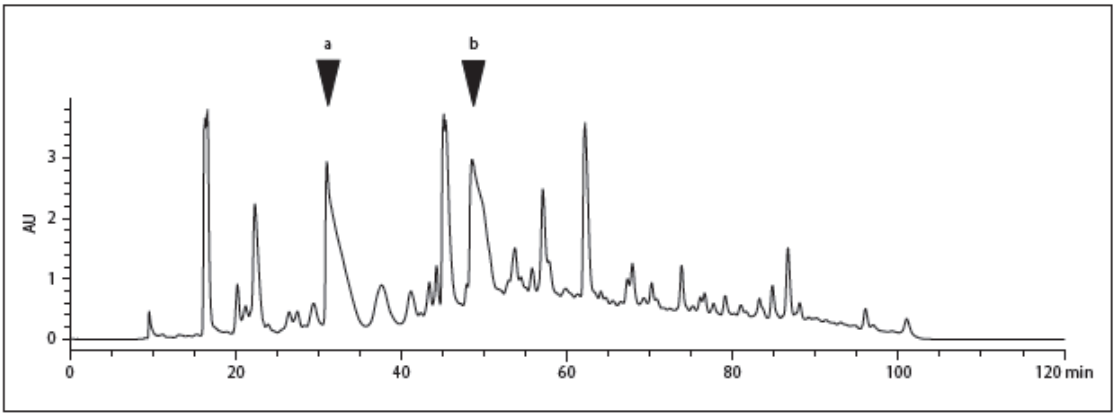

Fig. 1. LC-MS chromatogram of CGSE. Peak a corresponds to catechin and peak b to epicatechin.

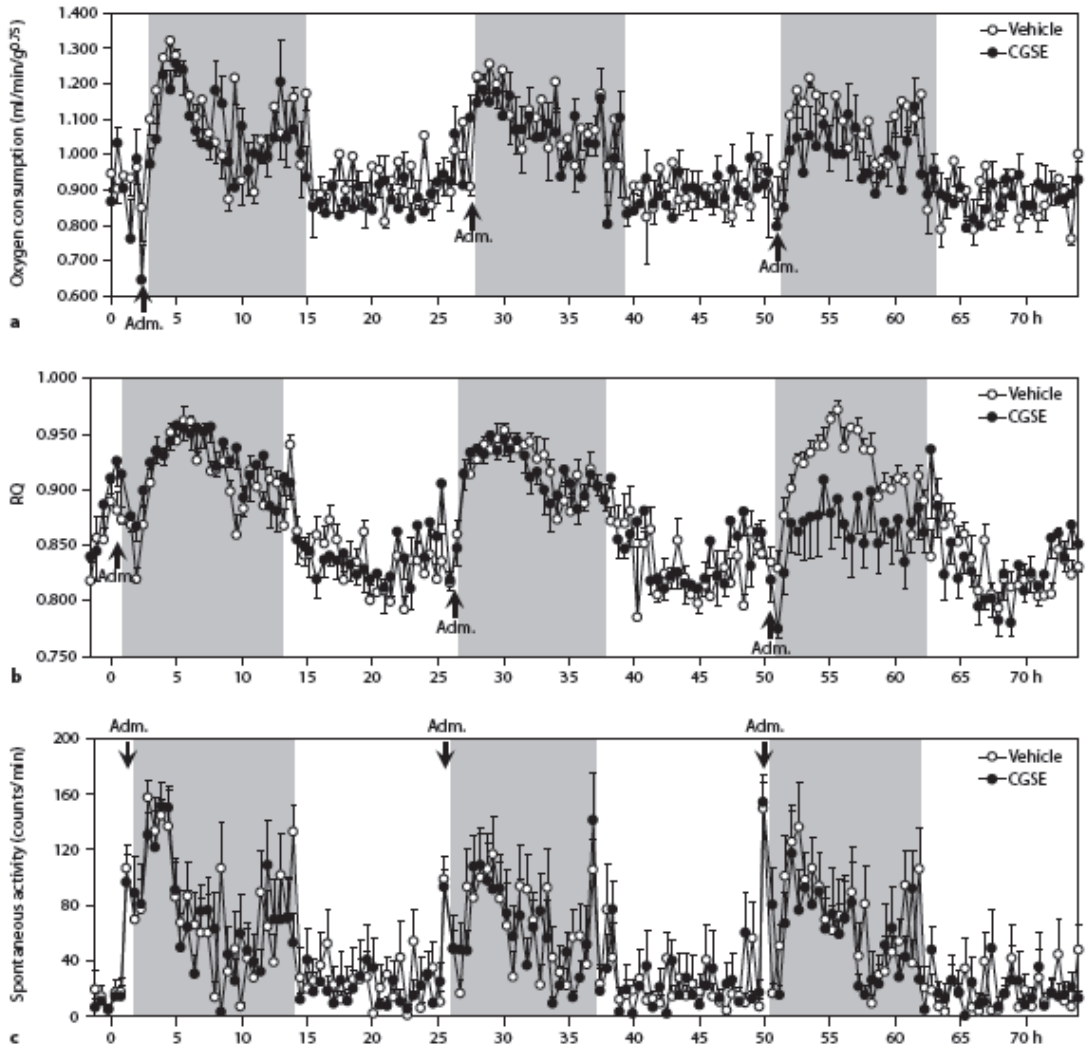

Fig. 2. CGSE acutely downregulated RQ in C57BL/6J mice (b). Means 8 SE of oxygen consumption (a), RQ (b), and spontaneous activity (c) for 3 days of C57BL/6J mice administered vehicle (dH_2O) or 500 mg/kg body weight CGSE (n = 8). Adm. = Administration of vehicle or CGSE.

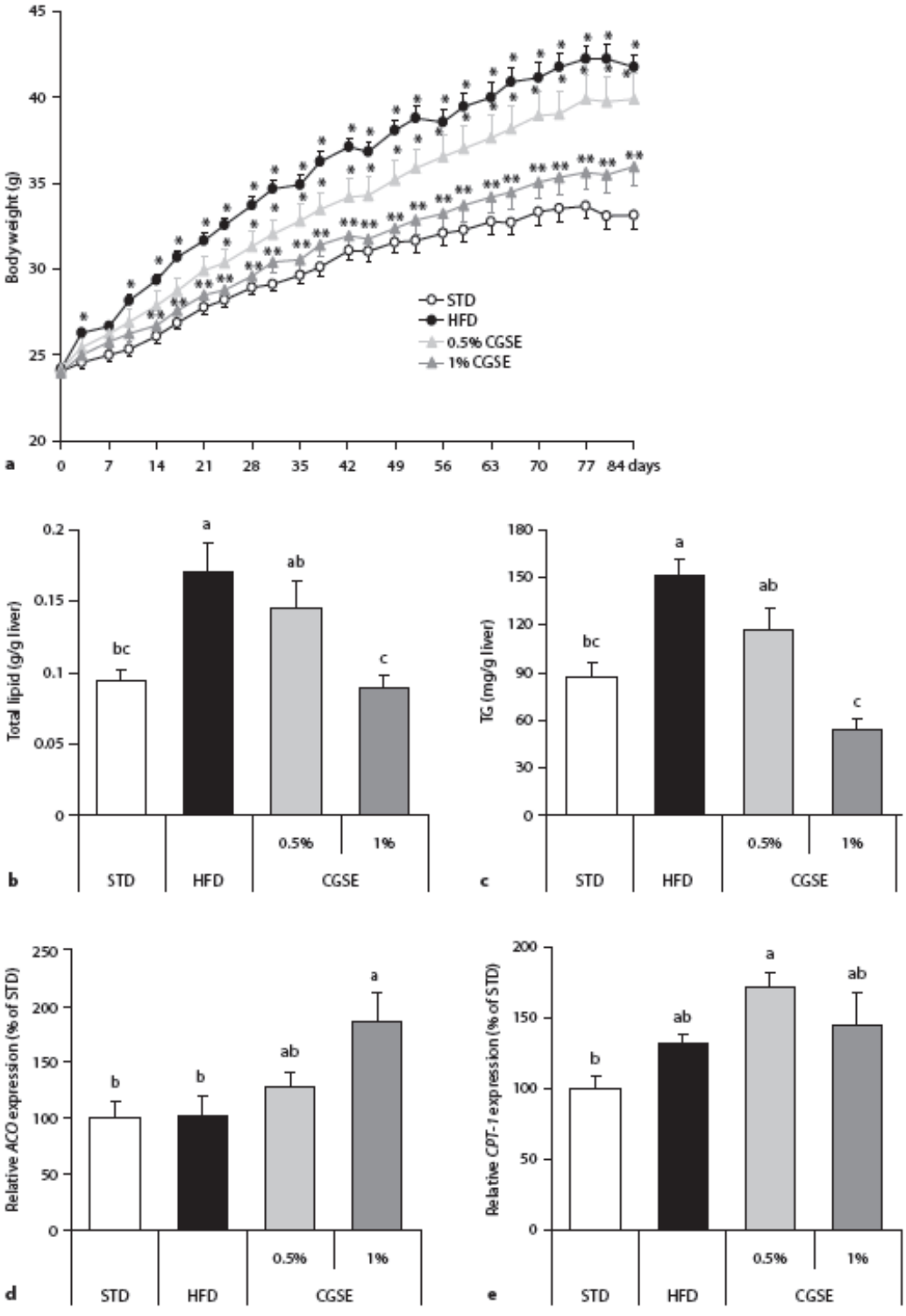

Fig. 3. CGSE suppressed body weight gain and decreased liver lipid content and increased mRNA expression related fatty acid oxidation in diet-induced obesity in a mouse model. Body weight development (a), total lipid (b) and TG contents (c) in the liver, and the mRNA expression of ACO (d) and CPT-1 (e) in the liver of C57BL/6J mice fed STD, HFD, and HFD supplemented with CGSE (0.5 or 1%) for 84 days. Means 8 SE (n = 11–12). * $p<0.05$ vs. STD, * * $p<0.05$ vs. HFD. The values with different superscripts are significantly different ($p<0.05$).

REFERENCES

1. Lamarche, B., et al., Visceral obesity and the risk of ischaemic heart disease: insights from the Quebec Cardiovascular Study. Growth Horm IGF Res, 1998. 8(suppl B): 1-8.
2. Matsuzawa, Y., The metabolic syndrome and adipocytokines. FEBS Lett, 2006. 580(12): p. 2917-21.
3. Monagas, M., et al., Monomeric, oligomeric, and polymeric flavan-3-ol composition of wines and grapes from Vitis vinifera L. Cv. Graciano, Tempranillo, and Cabernet Sauvignon. J Agric Food Chem, 2003. 51(22): p. 6475-81.
4. Soleas, G.J., E.P. Diamandis, and D.M. Goldberg, Wine as a biological fluid: history, production, and role in disease prevention. J Clin Lab Anal, 1997. 11(5): p. 287-313.
5. Tsai Su, C. and V. Singleton, Identification of three flavan-3-ols from grapes. Phytochemistry, 1969. 8(8): p. 1553-1558.
6. Koga, T., et al., Increase of antioxidative potential of rat plasma by oral administration of proanthocyanidin-rich extract from grape seeds. J Agric Food Chem, 1999. 47(5): p. 1892-7.
7. Yamakoshi, J., et al., Proanthocyanidin-rich extract from grape seeds attenuates the development of aortic atherosclerosis in cholesterol-fed rabbits. Atherosclerosis, 1999. 142(1): p. 139-49.
8. Quesada, H., et al., Grape seed proanthocyanidins correct dyslipidemia associated with a high-fat diet in rats and repress genes controlling lipogenesis and VLDL assembling in liver. Int J Obes (Lond), 2009. 33(9): p. 1007-12.
9. Yokozawa, T., H.J. Kim, and E.J. Cho, Gravinol ameliorates high-fructose-induced metabolic syndrome through regulation of lipid metabolism and proinflammatory state in rats. J Agric Food Chem, 2008. 56(13): p. 5026-32.
10. Lee, Y.A., E.J. Cho, and T. Yokozawa, Effects of proanthocyanidin preparations on hyperlipidemia and other biomarkers in mouse model of type 2 diabetes. J Agric Food Chem, 2008. 56(17): p. 7781-9.
11. Iwasaki, Y., T. Matsui, and Y. Arakawa, The protective and hormonal effects of proanthocyanidin against gastric mucosal injury in Wistar rats. J Gastroenterol, 2004. 39(9): p. 831-7.
12. Del Bas, J.M., et al., Dietary procyanidins lower triglyceride levels signaling through the nuclear receptor small heterodimer partner. Mol Nutr Food Res, 2008. 52(10): p. 1172-81.
13. Folch, J., M. Lees, and G.H. Sloane Stanley, A simple method for the isolation and purification of total lipides from animal tissues. J Biol Chem, 1957. 226(1): p. 497-509.

14. Ohnuki, K., et al., Administration of capsiate, a non-pungent capsaicin analog, promotes energy metabolism and suppresses body fat accumulation in mice. Biosci Biotechnol Biochem, 2001. 65(12): p. 2735-40.
15. Weir, J.B., New methods for calculating metabolic rate with special reference to protein metabolism. J Physiol, 1949. 109(1-2): p. 1-9.
16. Klaus, S., et al., Epigallocatechin gallate attenuates diet-induced obesity in mice by decreasing energy absorption and increasing fat oxidation. Int J Obes (Lond), 2005. 29(6): p. 615-23.
17. Murase, T., et al., Beneficial effects of tea catechins on diet-induced obesity: stimulation of lipid catabolism in the liver. Int J Obes Relat Metab Disord, 2002. 26(11): p. 1459-64.
18. Pataki, T., et al., Grape seed proanthocyanidins improved cardiac recovery during reperfusion after ischemia in isolated rat hearts. Am J Clin Nutr, 2002. 75(5): p. 894-9.
19. Sano, T., et al., Anti-thrombotic effect of proanthocyanidin, a purified ingredient of grape seed. Thromb Res, 2005. 115(1-2): p. 115-21.
20. Jang, J. and J. Han, The antioxidant ability of grape seed extracts. Korean J Food Sci Technol, 2002. 34: p. 524-528.
21. Park, S.H., T.S. Park, and Y.S. Cha, Grape seed extract (Vitis vinifera) partially reverses high fat diet-induced obesity in C57BL/6J mice. Nutr Res Pract, 2008. 2(4): p. 227-33.
22. Furuyashiki, T., et al., Tea catechin suppresses adipocyte differentiation accompanied by down-regulation of PPARgamma2 and C/EBPalpha in 3T3-L1 cells. Biosci Biotechnol Biochem, 2004. 68(11): p. 2353-9.
23. Hung, P.F., et al., Antimitogenic effect of green tea (-)-epigallocatechin gallate on 3T3-L1 preadipocytes depends on the ERK and Cdk2 pathways. Am J Physiol Cell Physiol, 2005. 288(5): p. C1094-108.
24. Goncalves, R., N. Mateus, and V. de Freitas, Study of the interaction of pancreatic lipase with procyanidins by optical and enzymatic methods. J Agric Food Chem, 2010. 58(22): p. 11901-6.
25. Moreno, D.A., et al., Inhibitory effects of grape seed extract on lipases. Nutrition, 2003. 19(10): p. 876-9.
26. Osumi, T. and T. Hashimoto, Acyl-CoA oxidase of rat liver: a new enzyme for fatty acid oxidation. Biochem Biophys Res Commun, 1978. 83(2): p. 479-85.
27. Shepherd, D., D.W. Yates, and P.B. Garland, The rate-limiting step in the oxidation of palmitate or palmitoyl-coenzyme A by rat-liver mitochondria. Biochem J, 1966. 98(1): p. 3C-4C.
28. Trauner, M., M. Arrese, and M. Wagner, Fatty liver and lipotoxicity. Biochim Biophys Acta, 2010. 1801(3): p. 299-310.
29. Kawai, N., T. Kawai, and K. Kawai, [Ultrasonic and laboratory studies on fatty liver in white-collar workers]. Nihon Shokakibyo Gakkai Zasshi, 1995. 92(7): p. 1058-65.

30. Maffei, M., et al., Leptin levels in human and rodent: measurement of plasma leptin and ob RNA in obese and weight-reduced subjects. Nat Med, 1995. 1(11): p. 1155-61.
31. Frederich, R.C., et al., Leptin levels reflect body lipid content in mice: evidence for diet-induced resistance to leptin action. Nat Med, 1995. 1(12): p. 1311-4.

SUMMARY

Chapter 1

We have identified EHMT1 as an essential BAT-enriched methyltransferase that controls brown adipose cell fate, adaptive thermogenesis and glucose homeostasis *in vivo.* Delineating the causal link between EHMT1 mutations and BAT thermogenesis will provide a new perspective in understanding the molecular control of energy homeostasis through the epigenetic pathways, which may lead to effective therapeutic interventions for obesity and metabolic diseases.

Chapter 2

We found that combination of capsinoids and mild cold environment synergistically suppressed obesity. Its suppression derived from beige adipocyte development by PRDM16 stabilization through β2 adrenoceptor activation. These observations document a previously unappreciated molecular circuit that controls beige adipocyte biogenesis and suggest a plausible approach to increase whole body energy expenditure by combining dietary components and environmental cues.

Chapter 3

Capsinoids efficiently promote the anti-obesity effect of exercise. Combination of exercise and capsinoids additively increased whole body fat oxidation. The mechanism of up-regulated energy expenditure was increasing lipolysis in BAT and increasing fatty

acid oxidation in muscle. It is indicated that combining exercise with capsinoids could be a powerful and plausible tool for fighting obesity.

Chapter 4

Catechin rich grape seed extracts (CGSE) supplementation in the high fat diet induced obesity model suppressed the increase of body weight and fat pad. It also improved metabolic parameter abnormalities. Furthermore, it increased fatty acid oxidation related genes in liver. These data suggested CGSE ameliorates obesity, in part by increasing fatty acid oxidation in liver.

ACKNOWLEDGEMENT

The author would like to express his sincere gratitude to Dr. Teruo Kawada, Professor of Graduate School of Agriculture, Kyoto University, for his valuable guidance.

The author would like to be grateful to Dr. Shingo Kajimura, Assistant professor of UCSF, for his helpful support and continuous guidance. Thanks to him, the author could work at UCSF and write papers.

The author would like to thank Dr. Makoto Bannai and Mr. Takashi Kayahara for their great help to work at UCSF.

The author would like to thank A. Tarakhovsky, E. D. Rosen, Y. Shinkai and E. Hara for providing mice and plasmids.

The author would like to thank my colleagues in the University of California, San Francisco, including Y. Qiu, A. Chawla, C. Paillart, S. Koliwad, M. Robblee, D. Scheel, S. Ohata, L. Mera, D. Lowe, S. Sonne, S. Keylin, I. Luijten, H. Hong and E. Tomoda for their assistance.

The author would like to thank my colleagues in Ajinomoto Co., Inc, including S. Takahashi, N. Nishikawa, H. Ishizaki, A. Morita, K. Uchino and R. Iritani for their support in caring for the mice and their experimental technical assistance.

The author would like to thank W. V. Brussel for providing CGSE samples.

The author has a lot to be grateful to K. Shinoda for his great support and helpful suggestion.

The author would like to thank members of the Nutrition group in Ajinomoto Co., Inc. and the members of Kajimura lab, for helpful support, assistance, and cheer.

Finally, the author gratefully appreciate my friends and family for their support and cheer.

Kana Ohyama

LIST OF PUBLICATIONS

- **Ohyama K**, Furuta C, Nogusa Y, Nomura K, Miwa T, Suzuki K. Catechin-rich grape seed extract supplementation attenuates diet-induced obesity in C57BL/6J mice. ***Ann Nutr Metab.*** 58(3), 250-8. (2011)

- Ohno H(*), Shinoda K(*), **Ohyama K(*)**, Sharp LZ, Kajimura S. EHMT1 controls brown adipose cell fate and thermogenesis through the PRDM16 complex. ***Nature.*** 504(7478), 163-7. (2013) (* co-first author)

- **Ohyama K**, Nogusa Y, Suzuki K, Shinoda K, Kajimura S, Bannai M. A combination of exercise and capsinoid supplementation additively suppresses diet-induced obesity by increasing energy expenditure in mice. ***Am J Physiol Endocrinol Metab.*** 308(4), E315-23. (2015)

- **Ohyama K**, Nogusa Y, Shinoda K, Suzuki K, Bannai M, Kajimura S. A synergistic anti-obesity effect by a combination of capsinoids and cold temperature through promoting beige adipocyte biogenesis. ***Diabetes.*** 65(5), 1410-23. (2016)

Related Papers

- Kuroyanagi K, Kang MS, Goto T, Hirai S, **Ohyama K**, Kusudo T, Yu R, Yano M, Sasaki T, Takahashi N, Kawada T. Citrus auraptene acts as an agonist for PPARs and enhances adiponectin production and MCP-1 reduction in 3T3-L1 adipocytes. ***Biochem Biophys Res Commun.*** 366(1), 219-25. (2008)

- Takahashi N, Kang MS, Kuroyanagi K, Goto T, Hirai S, **Ohyama K**, Lee JY, Yu R, Yano M, Sasaki T, Murakami S, Kawada T. Auraptene, a citrus fruit compound, regulates gene expression as a PPARalpha agonist in HepG2 hepatocytes. ***Biofactors.*** 33(1), 25-32. (2008)

- Kang MS, Hirai S, Goto T, Kuroyanagi K, Kim YI, **Ohyama K**, Uemura T, Lee JY, Sakamoto T, Ezaki Y, Yu R, Takahashi N, Kawada T. Dehydroabietic acid, a diterpene, improves diabetes and hyperlipidemia in obese diabetic KK-Ay mice. ***Biofactors.*** 35(5), 442-8. (2009)

- Goto T, Teraminami A, Lee JY, **Ohyama K**, Funakoshi K, Kim YI, Hirai S, Uemura T, Yu R, Takahashi N, Kawada T. Tiliroside, a glycosidic flavonoid, ameliorates obesity-induced metabolic disorders via activation of adiponectin signaling followed by enhancement of fatty acid oxidation in liver and skeletal muscle in obese-diabetic mice. ***J Nutr Biochem.*** 23(7), 768-76. (2012)

- Nogusa Y, Mizugaki A, Hirabayashi-Osada Y, Furuta C, **Ohyama K**, Suzuki K, Kobayashi H. Combined supplementation of carbohydrate, alanine, and proline is effective in maintaining blood glucose and increasing endurance performance during long-term exercise in mice. ***J Nutr Sci Vitaminol (Tokyo).*** 60(3), 188-93. (2014)

- Okamatsu-Ogura Y, Tsubota A, **Ohyama K**, Nogusa Y, Saito M, Kimura K. Capsinoids suppress diet-induced obesity through uncoupling protein 1-dependent mechanism in mice. . ***Journal of Functional Foods.*** 19, 1-9. (2015)

- Shinoda K, **Ohyama K**, Hasegawa Y, Chang HY, Ogura M, Sato A, Hong H, Hosono T, Sharp LZ, Scheel DW, Graham M, Ishihama Y, Kajimura S. Phosphoproteomics Identifies CK2 as a Negative Regulator of Beige Adipocyte Thermogenesis and Energy Expenditure. ***Cell Metab.*** 22(6), 997-1008. (2015)